Preparation and surface-functionalization of dye-doped bioconjugated poly(styrene-*co*-maleimide) nanoparticles

By Andri Swanepoel

Dissertation presented in partial fulfilment of the requirements for the degree of Master of Science (Chemistry)

Supervisor: Prof Bert Klumperman

Co-supervisor: Dr Avashnee Chetty

Stellenbosch University:

Department of Chemistry and Polymer Science

December 2014

Declaration

By submitting this thesis electronically, I declare the entirety of the work contained therein is my own, original work, that I am the owner of the copyright thereof (unless to the extent explicitly otherwise stated) and that I have not previously in its entirety or in part submitted it for obtaining any qualification.

Andri Swanepoel September 2014

Contents

Abstract

Standard methods used for detection of microbial contamination in water and food are based on culturing of samples to increase the number of bacteria present to a detectable level. These tests are however time-consuming (requiring one to two days for results to be generated) and labour intensive. The study described in this dissertation aims to develop dye-doped poly(styrene-*co*-maleimide) nanoparticles conjugated to antibodies for the rapid (within a few hours) detection of *E. coli* in water via clustering of the nanoparticles around bacteria to create a concentrated and localised fluorescent signal.

Pristine and dye-doped nanoparticles were synthesised according to a one-step (published) method, and surface-functionalised with formaldehyde and three different diamine compounds. The percentage dye added to the particles was also varied in the study.

The functionalised nanoparticles were characterised via FTIR, TEM, DSC, and Zetasizer. The emission properties of the dye-loaded NPs were measured with a spectrofluorometer.

The functionalised nanoparticles were bioconjugated with avidin and antibodies. The extent of avidin attachment was quantified via the use of a biotin(5-fluorescein) conjugate and via an avidin titration assay. The functionality of the bioconjugated nanoparticles was tested via a sandwich assay and a centrifuge based assay with *E. coli* cultures. Fluorescence microscopy was also utilised to demonstrate the utility of the particles in creating localised fluorescent signals indicating the presence of *E. coli* cells.

Acknowledgements

"Not that we are sufficient in ourselves to claim anything as coming from us, but our sufficiency is from God"

2 Corinthians 3:5 (English Standard Version)

I would like to thank the following individuals and groups for their contributions to this project:

My supervisor, **Prof Bert Klumperman**, for allowing me the opportunity to be part of your research group, and for all your assistance and patience.

My co-supervisor, **Dr Avashnee Chetty**, for your guidance and many inputs on the project, and for always making time to listen.

Thank you to **Dr Ilse du Preez** for your invaluable help with especially the microbiology and biochemistry aspects of the project, and for your constant support and motivation, both professionally and personally.

A big thank you to my sisi, **Ms Thembisile Mahlangu**, for all the support and camaraderie, both in and out of the laboratory.

Thank you to **Dr Yolandy Lemmer** for allowing me to work in your laboratory and for always being willing to help out where you can.

I would like to say a big thank you to the following people for their help on several of the aspects of the project: **Mr Khotso Mpitso** (PSMI synthesis and surface-functionalization), **Dr Francois Cummings** (TEM imaging), **Dr Arjun Maity** (chemistry),**Ms Nusrat Sheikh** (PSMI synthesis), **Mr Lonji Kalombo** (Zeta-potential theory), **Dr Philip Labuschagne** (DSC theory and sample processing), **Dr Vincent Khumalo** (DSC sample processing), **Dr Mohammed Balogun** (pKa theory), **Dr James Wesley-Smith** (TEM imaging), and **Dr David Motaung** (Spectrofluorimetry).

I would also like to thank the **Polymers and Composites Competency Area** of the CSIR for all their support, as well as the Klumperman research group in Stellenbosch.

Thank you to the **CSIR** for providing the project with financial support.

On a personal note I would like to thank the following people:

My family and friends, for your continued love and support throughout my entire academic career thus far. A special thank you to **my grandmother Wena,** your support and 'positive thoughts' have sustained me during my undergraduate and post graduate years.

My friend and colleague, **Lara Kotzé-Jacobs,** for all your advice, mentorship and support.

My husband, Dewald (and our 'son', Oreo,), for all your love and support.

List of Figures

List of Tables

Definitions and Abbreviations

ATP	adenosine triphosphate
ATR-FTIR	Attenuated Total Reflectance Fourier Transform Infrared Spectroscopy
BSA	bovine serum albumin
B5F	biotin(5-fluorescein)
DSC	Differential Scanning Calorimetry
DNA	deoxyribonucleic acid
E. coli	*escherichia coli*
EDC	1-ethyl-3-(3-dimethlyaminopropyl) carbodiimide
ELISA	enzyme-linked immunosorbent assay
FC	faecal coliforms
Fc	constant fragment
FISH	fluorescently-labelled *in situ* hybridization
Fv	variable fragment
IEA	immuno-enzyme assay
IFA	immunofluorescence assay
IMS	immunomagnetic separation
IR	infrared
ISH	*in situ* hybridisation
MF	membrane filter technique

MNPs	magnetic nanoparticles
MTF	multiple tube fermentation
M_w	molecular weight
MWCO	molecular weight cut off
NASBA	nucleic acid sequence based amplification
NHS	*N*-hydroxysuccinimide
NP(s)	nanoparticle(s)
PBS	phosphate buffer
PCL	poly(ε-caprolactone)
PCR	polymerase chain reaction
PEG	poly(ethylene glycol)
PLA	poly(lactic acid)
PLGA	poly(lactic-*co*-glycolic acid)
PS	poly(styrene)
PSMA	poly(styrene-*co*-maleic anhydride)
PSMI	poly(styrene-*co*-maleimide)
QD(s)	quantum dot(s)
Q-PCR	quantitative polymerase chain reaction
RNA	ribonucleic acids
RT-PCR	reverse transcriptive polymerase chain reaction

RuBdy	tris(2,2’ bipyridyl) dichlororuthenium(II) hexahydrate
S. typhimurium	*salmonella typhimurium*
TB	tuberculosis
TC	total coliforms
TEM	Transmission Electron Microscopy
T_g	glass transition temperature
Tris-HCl	trisma hydrochloride

Chapter 1: Introduction

1.1 Background

Contamination of water sources with faecal matter is a constant concern in South Africa; a country with one of the lowest annual rainfall averages in the world. Added to this are rapid urbanisation, inequalities of the past, poverty, failing infrastructure, lack of skilled engineers, and a large population of people susceptive to diseases (including symptoms such as diarrhea, etc.) because of the high prevalence of HIV/AIDS, all contributing towards South Africa facing extreme challenges in securing safe drinking water for the whole population.

In order for very low but still dangerous concentrations of pathogens to be detected in food and water, culturing methods are used to increase the number of bacteria present in a sample to a detectable level. These methods however are time-consuming and require specific infrastructure and trained personnel. In case of contamination, it will thus take one to two days before results are available and also before any action can be taken or warnings are issued to the public.

In recent years, extensive research has been performed on rapid detection of pathogens by the use of more sophisticated methods (than tedious culturing techniques) such as the polymerase chain reaction (PCR), enzyme-linked immunosorbent assays (ELISA), and enzymatic methods to amplify the signal given by low concentrations of pathogens. For a developing and resource-limited country such as South Africa, these methods are however too expensive and the skills required to perform such techniques are lacking. Additionally, the majority of the commercially available methods are still dependent on an incubation period, which means that real-time monitoring of water sources for pathogens is still not possible.

Consequently, there exists a definite need, especially in South Africa, to develop a device, material or technique that can address the problem of detecting very low concentrations of

pathogens (1 bacterium in 100 mL of potable water) in water samples rapidly *i.e*. faster than conventional methods, while still being relatively cheap and easy to use for minimally skilled operators.

Nanoparticles (NPs) have emerged as a very important tool in several scientific fields including chemistry and biology due to their exceptional surface area to volume ratios and ability to penetrate through biological barriers to name but a few. NPs have become a popular tool for capture of organisms by surface-functionalising the particles with receptor groups that either interact electrostatically with organisms or via interaction with receptors on the organisms' cell walls. According to Vikesland & Wigginton, antibodies are the most widely used receptor or recognition element used in conjunction with NPs for pathogen detection (Vikesland & Wigginton, 2010). Well established methods exist for the conjugation of the antibodies to particle surfaces and specificity can be tailored according to the application through the use of monoclonal or polyclonal antibodies. Several commercial products exist that comprise of micro- or nanoparticles (often magnetic or paramagnetic) that are either functionalised with antibodies or are surface-modified to be easily bound to antibodies for biological assays such as pathogen capture, purification and cell culture.

In 2004, Zhao and colleagues published an article whereby dye-doped silica (SiO_2) NPs functionalised with antibodies were utilised to immediately detect the presence of a single *escherichia coli* (*E. coli)* bacterium (Zhao *et al.,* 2004). The difference in size between NPs (smaller than 200 nm) and bacteria (a few microns in length) was utilised through the clustering of many antibody-containing NPs around a bacterium. This clustering of fluorescently labelled particles thus caused a notable signal indicating the presence of a pathogen to which the antibodies in question showed affinity (Zhao *et al.,* 2004). The authors reported the validity of single cell detection using a spectrofluorometer, successful multiple-sample analyses with a plate reader fluorometer and single cell detection of bacteria-nanoparticle clusters using a laboratory-made flow cytometer (Zhao *et al.,* 2004). In recent

years, the literature has been inundated with several articles pertaining to bacteria detection using dye-doped SiO_2 NPs.

In addition to SiO_2 and popular magnetic materials, NPs are also fabricated from polymers such as poly(styrene) (PS), poly(lactic acid) (PLA), poly(lactic-*co*-glycolic acid) (PLGA), poly(ε-caprolactone) (PCL), and chitosan. The copolymer poly(styrene-*co*-maleic anhydride) (PSMA) is an interesting polymer for immobilisation of various biological compounds due to the reactive nature of the maleic anhydride groups. This is due to the ease with which the anhydride groups of a PSMA copolymer can react with low molecular compounds such as water, alcohols and amines (Donati *et al.,* 2002). In 2010, a Belgian group published a simple one-step method detailing the manufacture of poly(styrene-*co*-maleimide) (PSMI) nanoparticles (with a hydrodynamic diameter of less than 100 nm) from PSMA via an imidisation process (Samyn *et al.,* 2010). However to the author's knowledge, to date, no study has been conducted regarding the use of PSMI NPs for bacteria detection.

The aim of this project is to utilise the reactive nature of PSMA to synthesise PSMI NPs (produced via the published method of Samyn and colleagues (Samyn *et al.,* 2010)) that are doped with a fluorescent dye, and to attach antibodies specific for *E. coli* onto the surfaces of the NPs. Signal amplification will be investigated as reported by Zhao and coworkers (2004) by tracking attachment of the antibody-polymer particles to *E. coli* using fluorescence (Zhao *et al.,* 2004). Detection of bacteria at a concentration of 1 CFU/mL is not an explicit target for this project, the aim is to initially contact dye-doped NPs with higher concentrations of bacteria in order to refine the technique and to determine, if possible, quantitative detection limits for the NPs.

1.2. Aim

As stated in the previous section, the rapid detection (ideally < 1 hour, up to a maximum of 1 working day) of target micro-organisms in water samples is greatly needed for authorities to quickly identify and react to contamination of large water sources. The aim of this project is

to address this need through the synthesis and characterisation of dye–doped PSMI NPs functionalised with amine groups, and bioconjugated to avidin and biotinylated anti-*E. coli* antibodies for rapid detection of *E. coli* in water. The small size of the NPs when compared to a single bacterium will theoretically lead to attachment of many particles around a single bacterium due to the affinity interaction between the bacterium and the selected antibodies functionalised onto the NP surfaces. This clustering of particles (loaded with fluorescent molecules) around a bacterium will then cause an amplification of the signal given off by ideally only one bacterium due to a spike in the fluorescent signal detected.

This project is limited to the development and characterisation of a material (NPs with dye encapsulated and antibodies attached) for the application of rapid detection of pathogens in water. Preliminary testing of the material against samples containing *E. coli* will be performed to determine the efficiency of antibody-*E. coli* binding, and possibly determine detection limits of the NPs.

1.3 Structure

The structure of this dissertation will be as follows:

1. Chapter 1: an introduction to the background and the problem statement of the project.
2. Chapter 2: a comprehensive literature review on the existing knowledge with regards to the subject of bacteria detection via dye-doped NPs.
3. Chapter 3: a discussion of the methods and results of the synthesis and amine surface-functionalisation, as well as characterisation of the PSMI NPs.
4. Chapter 4: a discussion of the methods and results obtained for the bioconjugation of the PSMI NPs with avidin and biotinylated antibodies, as well as preliminary testing against *E. coli* bacteria as proof of principle.
5. Chapter 5: a summary of the conclusions made for the project as a whole.
6. Chapter 6: possible future work to be done.

A list of references and an appendix with sample calculations and raw data will also be supplied.

Chapter 2: Literature review

The development of rapid and accurate methods to test for pathogenic bacteria in food and water samples is a challenge faced by the entire international community. In recent years advances have been made with respect to development of new techniques (other than the standard culturing methods) for water and food monitoring as well as analysis of biological samples that are both rapid and highly sensitive, as reported in a large number of publications found on the subject.

In this literature review, the traditional methods for pathogen detection as well as some of the most cutting edge detection techniques based on conventional bio-technology will be described (Section *2.1 Current methods for pathogen detection*), followed by a review of the literature available on the use of polymer nanotechnology for pre-concentration and detection of pathogens and other analytes (Section *2.2 Concentration and detection of pathogens via nanoparticles*). Finally in Section 2.3, conclusions and recommendations will be presented for this study.

2.1 Current methods for pathogen detection

The following section gives a brief overview of the current standard culture-based methods used to test water samples for pathogens as well as newer and more advanced techniques.

The conventional techniques approved by the relevant governing bodies of many countries for the detection of coliforms in water are the membrane filter technique (MF), the multiple tube fermentation (MTF) technique and the presence/absence test (Rompré *et al.,* 2002). The conventional techniques rely on culturing of bacterial colonies in order to measure either metabolic endpoints or to determine the growth of an organism after a certain incubation time. New molecular and enzymatic methods are also available that do not require

incubation time and that can detect organisms ranging from bacteria to viruses (Noble & Weisberg, 2005).

The disadvantages of the conventional methods include lengthy incubation periods, antagonistic organism interference, non-specificity and weak levels of detection of slow-growing or stressed coliforms as a result of water treatment (such as chlorination). The conventional methods become highly inaccurate if a large part of a bacterial population is non-culturable, which is sometimes the case. As a result, contamination levels are often underestimated with these techniques as they are not sensitive to the detection of stressed or starved bacterial cells (USA Environmental Protection Agency, 1978). Detailed descriptions of each of these techniques are given below.

2.1.1 Culture-based methods

2.1.1.1 Multiple tube fermentation technique

The multiple tube fermentation technique has been used for over 80 years and requires inoculating a series of different concentrations of a water sample in a series of tubes. The production of gas, acid and growth of cells after 48 hours at 35 °C is taken as a positive preliminary indication of bacteria present in the sample. The tubes that test positive are then subjected to further confirmation tests. The technique is not highly precise and underestimations can occur due to interference of large numbers of non-coliform organisms and inhibitory effects of the media used (Rompré *et al.,* 2002).

2.1.1.2 Membrane filtration technique

The membrane filtration technique, which is currently the gold standard, requires filtering water through a 0.45 µm pore size filter. The filter retains any bacteria present, which are subsequently incubated in a selective medium. Selectivity is a problem as some of the colonies that form show the attributes (colour, sheen, etc.) of typical coliform colonies even when they are not, and vice versa. It is then recommended that further coliform verification

tests be performed. This technique is susceptible to interference by other types of organisms leading to over- or underestimations, and it cannot recover stressed or injured coliforms (USA Environmental Protection Agency, 1978). Optimisation of media according to different geographical environments and physiological states of bacteria (influenced by water treatment methods such as chlorination) is required to obtain accurate results (Grabow & Du Preez, 1979), and even then the insufficient specificity of the technique might require extra confirmation tests taking up to an additional 24 hours (USA Environmental Protection Agency, 1978).

The conventional culture-based techniques, despite requiring long incubation periods, however remain the preferred methods for detection due to their relatively high selectivity and sensitivity (Lazcka *et al.,* 2007).

2.1.2 Enzymatic techniques

An alternative to these conventional methods is the use of enzymatic techniques to indirectly test for the presence of pathogenic bacteria. The enzymatic techniques operate according to varying microbial enzyme profiles and can be specific to group, genus or species, depending on the enzyme that is being targeted.

It has been found that activity of the Glucuronidase enzyme is mostly limited to *E. coli* (Kilian & Bulow, 1976). Chromogenic and fluorogenically modified substrates are often utilised to detect *E. coli* as they emit either colour or fluorescence respectively when coming into contact with the glucuronidase enzyme. Studies have shown that chromogenic/fluorogenic substrates provide faster detection and improved accuracy in a universal medium than conventional techniques (Bascomb, 1987; Manafi *et al*., 1991). The tests are easy to perform, highly specific and sensitive and require only basic laboratory equipment. They are however more expensive than the classical techniques, but they require shorter incubation

periods (typically 24 hours). They are thus also not capable of providing ‘same day’ results (Rompré *et al.,* 2002).

Enzymatic methods are also utilised in conjunction with the MTF and MF techniques in the so-called “presence/absence” test. The use of a specific substrate that only supplies nutrients to target organisms i.e. total coliforms (TC) and *E. coli* that releases a chromogen or fluorochrome upon utilisation indicates the presence of the target organism, but cannot provide quantitative results. A maximum response time of 24 hours is achievable and the technique has been applied in commercial applications such as Colilert® (and the extended Quanti-Tray test for quantification of results), Colisure® and Coliquick (Rompré *et al.,* 2002). The defined substrate methods are easy to use, provide more rapid and realistic results, but are more expensive than MTF and MF when these methods (MF and MTF) do not require confirmation steps. However, in all cases the defined substrates techniques require less manpower.

Major water utilities in South Africa such as Johannesburg Water currently use Colilert® as the standard test for all water samples. Samples of 100 mL are collected in clear, autoclaved plastic bottles, and the Colilert® substrate (in powder form) is added to the sample. The mixture is subsequently cultured for 18-22 hours. A positive result indicating the presence of coliforms is indicated by a colour change from clear to yellow.

A further quantification can then be performed by using the Quanti Tray method whereby the incubated sample is transferred into a specialised tray (shown in Figure 1) and viewed under UV light. With the help of correlation tables the result of the UV light test can be used to quantify the number of *E. coli* present. Colilert® is currently the best practise in the UK, but in SA it is utilised only by large metropolitan municipalities, while the majority of other smaller municipalities in South Africa still rely on the membrane filtration technique due to shortage of funds.

Other detection methods used in conjunction with enzymatic methods include fluorimetry and solid phase cytometry. The Colifast system, an automated analyser, can rapidly (in less than 2 hours) detect TC and faecal coliforms (FC) via an increase in fluorescence due to substrate hydrolysis, but only in samples with relatively high bacterial counts that can provide a strong enough fluorescence signal (Rompré *et al.,* 2002).

Figure 1: Colilert tray containing a sample that tested positive for the presence of coliforms (yellow colour)

The use of solid phase cytometry combined with enzymatic fluorescence can detect metabolically active but non-culturable cells in less than 3.5 hours (Rompré *et al.,* 2002).

Adenosine triphosphate (ATP) bioluminescence is a well-known method for the non-specific indication of microbial presence. All living cells contain ATP as it is used as a source of energy. The presence of ATP is thus an indication of living microorganisms being present in a sample. When reacted with the enzyme-substrate complex luciferase-luciferin energy transfer from ATP to the complex leads to an oxidisation reaction with light emitted as a by-product. The amount of light that is emitted is proportional to the amount of ATP present in

the sample, and with the correct bioluminescence reader the amount of microorganisms in the sample can be calculated in relation to the intensity of the light emitted. The ATP bioluminescence method however requires extraction of ATP from cells which can add to the complexity of the method when compared to the detection of whole cells. Additionally this method cannot be used on its own as a confirmatory test for a specific organism, since ATP is present in all living cells. The ATP method hence must be used in conjunction with a recognition element specific to the target organism(s) to be detected in order to achieve sample specificity. For *E. coli* detection in water samples, ATP bioluminescence is often reported in conjunction with immunomagnetic separation (Lee & Deininger 2004; Bushon *et al.,* 2009; Lee *et al.,* 2010) or synthetic samples (Cheng *et al.,* 2009).

2.1.3 Molecular methods

Molecular whole cell and surface recognition comprises of capturing and/or labelling of target organisms by binding to molecular ligands on either the exterior or the interior of the cell (Noble & Weisberg, 2005). High sensitivity and specificity can be achieved without the need for complex cultivation and additional conformational steps. Results are obtained in a matter of hours rather than days (Rompré *et al.,* 2002).

2.1.3.1 Immunological methods

Immunological methods rely on specific recognition between antibodies and antigens. Antibodies can be used for molecular recognition specific to a single antigenic strain, or for a single species or an entire group or family, although the last two approaches are more complicated (Noble & Weisberg, 2005). (More detailed information on antibodies can be found in Section 4.1 *Introduction: Bioconjugation to PSMI nanoparticle surfaces*). The antibody-antigen compound can be used for immunological capture of cells or antigens by enzyme-linked immunosorbent assays (ELISA or IMS) as well as detection of targeted cells by immunofluorescence assay (IFA) or immuno-enzyme assay (IEA) (Rompré *et al.,* 2002).

However, one of the challenges with this technique is possible cross-reactions with non-targeted cells.

ELISA is a rapid, simple and relatively sensitive test. Antigens from a sample are attached to a surface, with an antigen-specific antibody solution then added to bind to the antigen. This primary antibody is either linked to an enzyme, or a secondary enzyme linked antibody is added to the assay to bind specifically to the primary antibody. Finally an enzymatic substrate that provides a signal when it reacts with the enzyme is added (see Figure 2). Thorough washing after each step ensures that non-specifically bound molecules that can cause false positive results are removed.

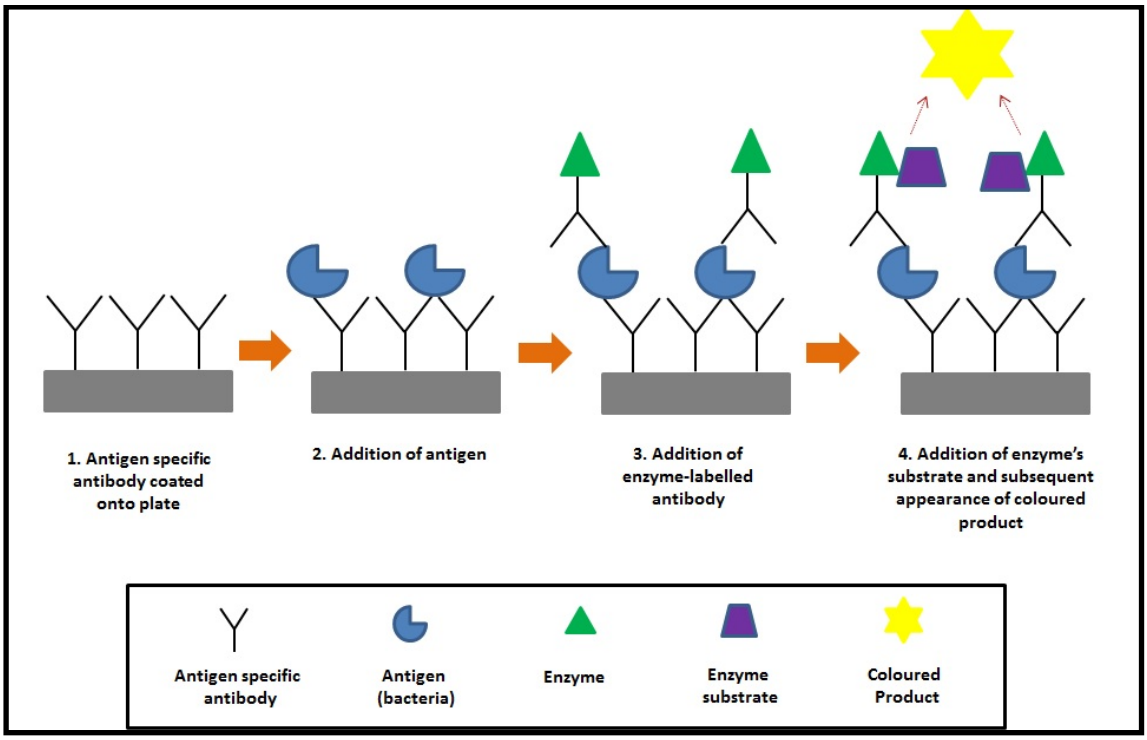

Figure 2: Schematic representation of an ELISA test for the presence of bacteria.

ELISA tests are however limited by specificity of the antibody used, the concentration of both the antibody and the antigen and the type of reaction solution used. Immunofluorescent assays allow the identification and enumeration of a specific cell in a natural sample. The antibody can be directly conjugated with a fluorochrome or the antibody can be allowed to

bind to the antigen where after a fluorochrome labelled-antibody can be introduced directed against the first antibody. These secondary fluorochrome-conjugated antibodies can easily be obtained commercially and enumeration can then be achieved using fluorescence microscopy, solid phase cytometry or via flow cytometry. IFA does not however provide information on the physiological status of cells or whether cells are dead or alive.

The attachment of antibodies to NPs for capture and detection of *E. coli* in water samples has also been widely investigated (Zhao *et al.,* 2004; Lee & Deininger 2004; Qin *et al.,* 2007; Qin *et al.,* 2008; Bushon *et al.,* 2009; Cheng *et al.,* 2009; Ravindranath *et al.,* 2009; Cowles *et al.,* 2011; Huang *et al.,* 2013). This subject will be expanded on in Section 2.2.1 *Surface-functionalisation with receptor molecules*.

2.1.3.2 Nucleic acid-based methods

Nucleic acid amplification was developed in the mid-1980s and is widely used in bacterial detection (Lazcka *et al.,* 2007). Nucleic-acid based methods operate on the mechanism of molecular hybridisation, which involves the complementary sequence recognition between a nucleic probe and a nucleic target. These methods can distinguish between classes, genera, species or subspecies of organisms. Some of these methods do not require pre-enrichment and can provide results within hours. The most commonly used ones are polymerase chain reaction (PCR) (which includes normal PCR, reverse transcriptive PCR (RT-PCR) and quantitative PCR (Q-PCR)), nucleic acid sequence based amplification (NASBA) and the *in situ* hybridisation (ISH) techniques.

Polymerase chain reaction (PCR) methods

PCR allows for the amplification of a target fragment of deoxyribonucleic acid (DNA) by cycling replication *in vitro* or *in situ*. The two strands of the DNA double helix are physically separated at high temperatures, followed by the introduction of primers and DNA polymerase at lower temperatures, which leads to the replication of the initial DNA strands. The newly generated DNA serves as a template for further replication, and exponential

amplification of the initial DNA sample is achieved. This amplification increases the chance of detecting very low concentrations of target organisms in a sample (Bej *et al*., 1990; Burtscher *et al*., 1999). NASBA is similar to PCR except that it is an isothermal process utilising an enzyme mixture instead of the thermostable DNA polymerase to amplify ribonucleic acid (RNA).

Exponential amplification of the target DNA is achieved,.

In order for PCR to be used on water samples where low levels of pathogens are present, concentration of the sample must first be performed via e.g. filtration. The extraction of DNA needed for amplification can be performed by lysing bacteria captured by the membrane filter. Even though PCR is a highly specific method for the detection and identification of organisms, it provides no information on the psychological state of the cells as it extracts DNA from living, injured or dead cells alike (Rompré *et al.,* 2002). RT-PCR however is capable of distinguishing between viable and non-viable cells by synthesising genes present during the bacteria's growth phase (Lazcka *et al.,* 2007). The presence of humic substances and colloidal matter in drinking water samples can interfere with the PCR process by decreasing the PCR yield and by obscuring the amplified products. The technique also requires highly skilled staff and dedicated laboratory space, as well as specific reagents to prevent cross-contamination with other DNA (Rompré *et al.,* 2002).

In situ hybridisation techniques (ISH)

In situ hybridisation (ISH) techniques utilise oligonucleotide probes to detect complementary nucleic acid sequences (DNA or RNA). The technique is based on the ability of nucleic acids to bind to one another in very specific complementary ways to form hybrids (Rompré *et al.,* 2002).

These probes are highly specific as they are either made of the nucleic acids of the target organisms or are complementary to a specific nucleic acid sequence of the target molecule. Probes specific to ribosomal RNA (rRNA) have become the standard in identifying

organisms. The use of fluorescently-labelled probes to detect rRNA hybridisation (the so-called “FISH” technique) is a very popular ISH method. FISH is a sensitive, easy to use and rapid technique that yields stable hybridisation products when compared to radioactive labelling. Hybridised cells are detected by epifluorescence microscopy and a counterstain or the use of orange acridine to determine the total number of cells. Detection can also be performed via flow or solid phase cytometry.

Different probes aimed at the *E. coli* family rather than TC have been developed as the TC category varies too much genetically for a single probe to suffice. FISH is highly specific at cellular level, but is limited when used for drinking water samples due to low ribosomal content of starved cells which then only gives off a weak fluorescent signal (Rompré *et al.,* 2002). Even though the rRNA content is directly correlated with the growth rate of the bacterial cells, it is not an absolute indication of the physiological state of the cells, as studies have found that RNA detection methods still showed bacterial presence for up to 48 hours after chlorination or heat inactivation while no cells were detected with plate count or enzymatic methods (Rompré *et al.,* 2002).

The majority of techniques related to detection of nucleic acids require sophisticated equipment as well as highly skilled operators. These techniques also require the lysing of microorganism cells in order to obtain genetic material needed for testing, adding another level of complexity to the detection process. Whole cell detection of pathogens via membrane filtration and defined substrate enzyme techniques (Colilert®) currently represents the approved standard tests for detection of pathogens in water. This project will thus aim to detect whole cell microorganisms in order to ensure good correlation with these approved methods.

2.2 Concentration and detection of pathogens via nanoparticles

A large amount of literature is available on the use of functionalised NPs for use as bio- or nanosensors. Various types of NPs are used in preconcentration, detection and/or labelling of microorganisms in food and water samples. Magnetic nanoparticles (MNPs) have been studied extensively to easily concentrate and separate microorganisms from (relatively) large volumes by the application of an external magnetic field. Other types of NPs include gold and other metals, SiO_2 NPs and polymer-based NPs. The addition of fluorescent dyes to SiO_2 NPs has been utilised for the detection and/or labelling of microorganisms (Zhao *et al.,* 2004; Qin *et al.,* 2007; He *et al.,* 2011; Cai *et al.,* 2012) and cells (Chen *et al.,* 2012). Polymer-dye NPs have also been applied in the detection and labelling of cells or organisms (Holzapfel *et al.,* 2005; Napp *et al.,* 2011), detection of nucleic acids (Taylor *et al.,* 2000; Ho *et al.,* 2005), and for sensing of analytes in solution (Childress *et al.,* 2012).

In order for binding to occur between NPs and target microorganisms, the attachment of receptor molecules to particle surfaces must be achieved, either via passive adsorption or via directed surface chemistry. Nanoparticles are typically one to two orders of magnitude smaller than bacteria, ensuring that multiple particles can attach to a single bacterial cell, given that sufficient receptor sites are available on the surface of the bacterium. When these NPs are magnetic in nature, a large enough magnetic force can be generated to separate out the particles along with the bacterial cell(s) (El-Boubbou *et al.,* 2007). The particle-pathogen agglomerate can then be re-suspended in a smaller volume better suited to the chosen method of detection. If the nanoparticles are fluorescently labelled or contain encapsulated fluorescent dye, the clustering of the NPs and the subsequent increased local fluorescent signal can be utilised to image and/or detect the bacteria.

2.2.1 Surface-functionalisation with receptor molecules

Various types of receptor molecules/recognition elements can be utilised to target specific epitopes on the cell surfaces of microorganisms. Receptor molecules vary with respect to the complexity of the functionalisation process required to immobilise the molecule(s) onto NP surfaces, and the level of selectivity achievable with the specific receptor or probe. For the whole-cell detection of microorganisms, receptor molecules such as antibodies (Lee & Deininger 2004; Qin *et al.,* 2008; Zhao *et al.,* 2008; Bushon *et al.,* 2009; Cheng *et al.,* 2009; Ravindranath *et al.,* 2009; Cowles *et al.,* 2011; Yilun Luo *et al.,* 2012; Huang *et al.,* 2013;), carbohydrates (El-Boubbou *et al.,* 2007; He *et al.,* 2011;; Tseng *et al.,* 2011), aptamers (Cai *et al.,* 2012) and phages (Goodridge *et al.,* 1999; Mosier-Boss *et al.,* 2003; Edgar *et al.,* 2006) have been utilised to detect bacteria.

Of all the receptor molecules/mechanisms available, the use of antibodies is by far the most popular method for selective capture of microorganisms. The use of antibodies with MNPs is according to literature “the most widely used tool for the selective capture and labelling of microorganisms” (Vikesland & Wigginton, 2010). Antibodies have been extensively utilised in the so-called immunomagnetic separation (IMS) of biological organisms for various applications (Lee & Deininger 2004; Bushon *et al.,* 2009; Cheng *et al.,* 2009; Ravindranath *et al.,* 2009). IMS involves the use of magnetic particles (in the micron and nanometer size range) manufactured from various superparamagnetic materials and surface-functionalised with antibodies with affinity for a specific type of microorganism(s) to capture and concentrate bacteria present in food, water or biological samples. The pre-concentrated bacteria can then be further processed according to the detection technique of choice.

In 2004, Lee and Deininger tested beach water samples for the presence of *E. coli* via IMS with ATP bioluminescence as detection method (Lee & Deininger, 2004). One liter samples were collected and pre-filtered with a 20 µm nylon filter membrane to remove organic debris, after which filtration through a 0.45 µm filter was performed to pre-concentrate the sample. Superparamagnetic PS beads coated with antibodies were used to selectively capture and

remove any *E. coli* present by the application of a magnetic field. ATP was extracted from viable cells and measured. The results correlated well with conventional culture-based techniques (Lee & Deininger, 2004). The entire procedure took less than an hour and could be performed on site. This method has since been expanded and used in similar studies for bacterial detection in environmental water samples (Bushon *et al.,* 2009; Lee *et al.,* 2010).

Cheng and colleagues (2009) used the combination of IMS with ATP bioluminescence to rapidly detect *E. coli* in spiked samples of pasteurised milk (Cheng *et al.,* 2009). Amine surface-functionalisation of Fe_3O_4 NPs allowed the immobilisation of polyclonal anti *E. coli* antibodies onto the particle surfaces. Two different binding strategies were pursued; in the first strategy the antibodies were directly immobilised onto the particle surface by crosslinking free carboxylic acid groups present on the antibodies with the amine groups on the particles, while the second strategy comprised of linking avidin to the particles before immobilising biotinylated antibodies onto the avidin-NP conjugates. The authors found that at low concentrations of bacteria, 90% of the bacteria could be removed when using the avidin-antibody NP conjugates versus a 75% removal of bacteria when using the NPs with randomly attached antibodies. The more efficient capture of bacteria via the use of the NP-avidin-bioconjugates was explained by the authors as a result of the high affinity between avidin and biotin, thus enforcing orientation of the antibody recognition sites away from the particles, ensuring availability for binding. By comparison the random nature of antibody attachment resultant of the first strategy led to blocking of some of the antibody receptor sites due to non-orientated binding (Cheng *et al.,* 2009). (A more detailed explanation regarding the avidin-biotin linkage and orientated antibody binding can be found in Section 4.1 *Introduction: Bioconjugation to PSMI nanoparticle surfaces*.) Detection could be achieved in approximately an hour with a detection limit of 20 CFU/mL via the ATP bioluminescence detection method.

Detection of *E. coli* and *S. typhimurium* from a bacterial mixture and from food matrixes were attempted by Ravrindranath and colleagues via MNPs functionalised with target specific antibodies (Ravindranath *et al.,* 2009). A portable IR spectrometer was used to identify bacteria via their unique spectroscopic fingerprint. It was postulated that the binding of the bacteria to the surfaces of magnetic NPs would result in a change in the spectral fingerprint of the biofunctionalised NPs. The specific phosphate moieties in the nucleic acids of pathogens in the mid-IR range could then be used to identify specific bacterial strains. Specific capture of *E. coli* and *S. typhimurium* was achieved via antibody coating and detected in less than 30 minutes (Ravindranath *et al.,* 2009).

ZnS NPs were bioconjugated with avidin and biotinylated antibodies for the detection of *E. coli* O157:H7 (Cowles *et al.,* 2011), while SiO_2 NPs bioconjugated with antibodies have been utilised to detect tuberculosis (TB) cells (Qin *et al.,* 2007; Qin *et al.,* 2008), *E. coli* (Zhao *et al.,* 2004), cancer cells (Chen *et al.,* 2012), and enroflaxin residues (Huang *et al.,* 2013).

Bacteria targeting and binding is however not limited to the use of antibodies. Studies using MNPs functionalised with cationic or anionic polymers or NPs manufactured from biopolymers (Huang *et al.,* 2010; Larsen *et al.,* 2009; Shan *et al.,* 2010) have successfully shown bacterial attachment via a mechanism of electrostatic attraction. This is possible as a result of the inherently negative charge of bacterial cell walls within the pH range of 5-9 (Huang *et al.,* 2010). Positively charged amine-functionalised MNPs were utilised to cluster and remove 97% of bacteria in solution due to electrostatic interaction and the agglomeration of the MNPs when a magnetic field was applied (Huang *et al.,* 2010). Carboxyl-modified pH sensitive MNPs were used to assist in the isolation of plasmid DNA from *E. coli* culture (Shan *et al.,* 2010). The carboxyl groups were introduced to the Fe_3O_4 MNPs' surfaces via emulsion polymerisation with a methacrylic acid monomer. These types of methods offer the advantage of using a cheaper and more robust ligand compared to antibodies, however they are hampered by non-specific electrostatic interactions with other organisms and ionic molecules.

Larsen and colleagues (2009) proposed the use of chitosan, a naturally occurring linear cationic polysaccharide, to prepare NPs in order to aggregate *E. coli* in samples containing low concentrations of bacteria (Larsen *et al.,* 2009). Due to the inherent positive surface charge of the chitosan NPs electrostatic interaction was utilised to non-specifically attract bacteria from a prepared sample. Immediate flocculation of over 90% of the bacteria-NP complexes occurred when adding chitosan NPs with a highly positive (51.1 mV) surface charge (Larsen *et al.,* 2009). Chitosan can also be used as a functional polymer to modify iron oxide NP surfaces in order for molecules such as antibodies, proteins and targeting ligands to be attached to the particles (Bahadur *et al.,* 2009).

The electrostatic interaction between chitosan and micro-organisms is however non-specific in nature and thus not suited for the specific capture of *E. coli* from water samples.

The mechanism whereby bacteria use carbohydrates on the walls of mammalian cells for attachment has also been exploited for bacterial capture by functionalising sugar moieties onto NPs (El-Boubbou *et al.,* 2007; He *et al.,* 2011; Tseng *et al.,* 2011). El-Boubbou and colleagues (El-Boubbou *et al.,* 2007) achieved 65% removal of the target bacteria after 5 minutes of contact with MNPs functionalised with mannose. Gold nanodots functionalised with mannose were used to detect *E. coli* (Tseng *et al.,* 2011), while He and colleagues (2011) utilised MNPs functionalised with mannose for pre-concentration of *E. coli* O157:H7 from a sample volume of 10 mL (He *et al.,* 2011).

Efforts have also been made in attaching vancomycin, an antibiotic glycopeptide effective against Gram-positive bacteria, to MNPs to act as receptor molecule for the capture of target organisms (Lin *et al.,* 2005; Kell *et al.,* 2008). Vancomycin as a receptor molecule is however only effective when targeting a wide range of bacteria, and is thus not suitable for the specific detection of *E. coli*.

In 1999, Goodridge and colleagues developed an assay for the detection of *E. coli* O157:H7 using immunomagnetic separation and fluorescently labelled bacteriophages (Goodridge *et*

al., 1999). Bacteriophages are viruses that attach to specific receptor molecules on host cells, and subsequently inject the host cell with bacteriophage nucleic acid. The binding between bacteriophage and the host cell is extremely specific (Mosier Boss *et al*., 2003). By either labelling the phage with fluorescent markers such as fluorescent nucleic acid dye (Goodridge *et al.,* 1999; Mosier-Boss *et al.,* 2003) or with quantum dots (QDs) (Edgar *et al.,* 2006), infected host cells such as *E. coli* (Goodridge *et al.,* 1999; Edgar *et al.,* 2006) and *Salmonella* (Mosier-Boss *et al.,* 2003) could be detected via a fluorescent signal. Phages are highly selective, robust, and the phage capsid serves as an encapsulating barrier between fluorescent stains and the environment, when compared to exposed fluorophores used to label antibodies (Mosier-Boss *et al.,* 2003).

Aptamers can also be used as receptor molecules for selective detection. These small nucleic acid sequences can fold into three dimensional configurations and bind very specifically to target molecules/analytes. Aptamers (biotin-labelled) have been utilised to image cancer cells by conjugation to dye-doped SiO_2 NPs functionalised with avidin (Cai *et al.,* 2012). Aptamer technology however is currently not as established a technology as antibodies, and will therefore not be considered for use in this study.

2.2.2 Dye-doped or dye-labelled nanoparticles

MNPs with attached receptor molecules or specific functional groups have mostly been used for the capture of target organisms from samples in order to concentrate low concentrations of bacteria into small sample volumes. The actual detection of the captured pathogens is however mainly conducted via the addition of chromophores, fluorophores, enzymes and fluorescently labelled antibodies to the concentrated bacteria that can generate a signal to be detected by specialised equipment based on fluorescent and optical microscopy, microluminometry, flow cytometry and fluorimetry (filter fluorimetry or spectrofluorimetry).

The direct labelling of antibodies with fluorophores is a well-established technique used in cellular imaging, cell sorting and in the operation of flow cytometry. Fluorescently labelled antibodies have been utilised for the detection of *E. coli* by immobilisation onto microwires (Kim *et al.,* 2011b), fiber optic wave guides (Leskinen *et al.,* 2009; Geng *et al.,* 2006) and biochips (Dyer *et al.,* 2009), as well as utilised in flow cytometry for *E. coli* detection (Yang *et al.,* 2009). The encapsulation of (fluorescent) dyes into NPs however leads to increased local dye concentrations when compared to labelling with free dye molecules (Sauer *et al.,* 2012). The encapsulated dye is also protected from the environment and more resistant to photobleaching (Taylor *et al.,* 2000). The use of NPs encapsulating thousands of dye molecules as marker molecules compared to labelling antibodies with a few fluorescent molecules should thus lead to greatly enhanced signal amplification. The NP shells also offer surfaces for modification that allows for easier conjugation to biomolecules.

It must be noted that there are many publications available on the use of QDs functionalised with antibodies for signal amplification and detection of microorganisms (Edgar *et al.,* 2006; Zhao *et al.,* 2008; Kuo *et al.,* 2008; Xue *et al.,* 2009; Kim & Son 2010; Mazumder *et al.,* 2010, Kim *et al.,* 2011a; Wang *et al.,* 2011). QDs are fluorescent nanocrystals of 2 to 10 nm that display high quantum yields. QDs however require laborious and intricate preparation procedures (when compared to the simple NP synthesis method proposed by Samyn *et al.* (2010)), they are known to be toxic due to possible leaching of heavy metal ions from the particles, and they are susceptible to fluctuations in photoluminescence over time (De Dios & Díaz-García, 2010).

Recent review publications are available regarding the use of SiO_2 and Au NPs in bio-imaging and labelling (Bitar *et al.,* 2012 and Saha *et al.,* 2012 respectively). The concept of amplified signal detection that this project is based on was published by Zhao and colleagues (2004), where the dye tris(2,2' bipyridyl) dichlororuthenium(II) hexahydrate (more commonly known as RuBpy dye) was encapsulated into SiO_2 NPs (Zhao *et al.,* 2004).

The inclusion of dyes into polymer NPs is well documented. Dyes are typically physically entrapped during particle preparation or swelling and soaking the prepared particles in a dye solution (Sauer *et al.,* 2012). Covalent attachment of dye to particles can occur either through the covalent attachment of dye molecules to particle surfaces or via copolymerisation with a dye with a copolymerisation function (Sauer *et al.,* 2012). A method often used for this is miniemulsion copolymerisation, whereby oil-soluble fluorescent dyes can be embedded into polymer matrices. Figure 3 shows the different methods used for dye inclusion into/onto NPs.

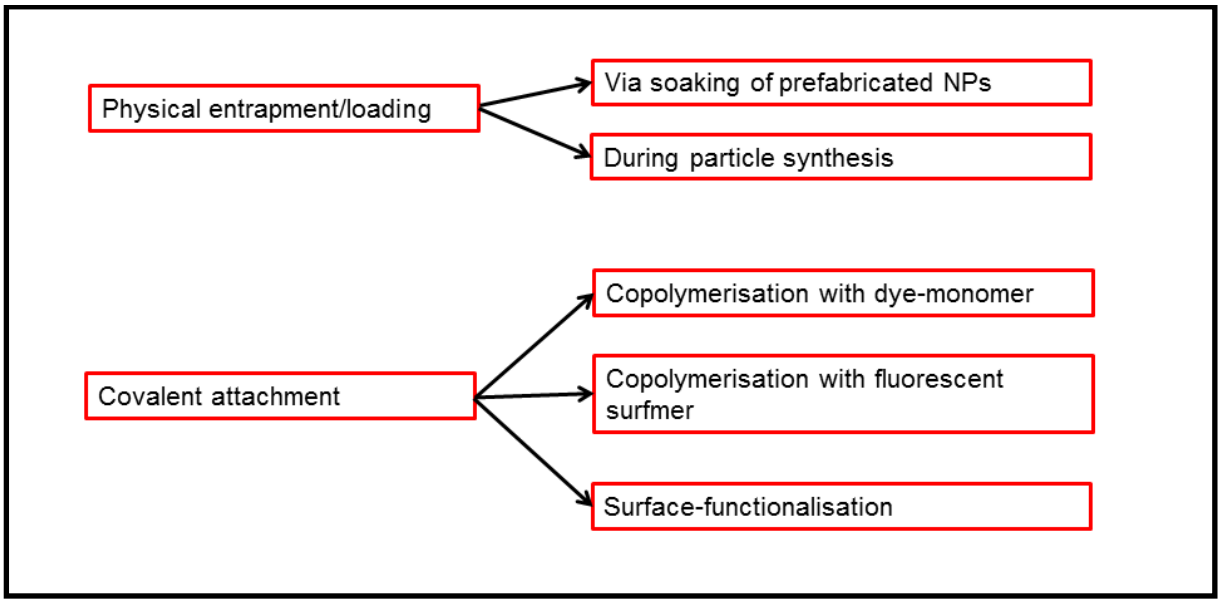

Figure 3: Different methods of dye addition to NPs.

Fluorescent PS particles with well-defined carboxylated and aminated surfaces were prepared via miniemulsion polymerisation (Holzapfel *et al.,* 2005). The dye-labelled NPs were used to image and track the uptake of NPs in HeLa cells.

Sun *et al.* (2006) covalently linked 2 dyes to a polyacrylamide matrix via microemulsion copolymerisation (Sun *et al.,* 2006). One dye acted as reference dye while the second dye, a fluoresceinamine derivative, was used as a pH sensor. The dye molecules were modified and converted into functional monomers which were then copolymerised with acrylamide

and methylenebis(acrylamide) in a reverse water-in-oil microemulsion to form polyacrylamide NPs. The authors also synthesised similar NPs, but with dye physically embedded. The rate of dye leaching from the particles where the dye had been covalently embedded was compared to that of the particles with physically entrapped dye. It was found that 70-80% of the physically embedded dyes had leached out of the particles during the first 6 hours, compared to only 9% of dye lost in the same period from the particles where the dyes had been covalently entrapped (Sun *et al.,* 2006) (see Figure 4). The fact that the covalently entrapped dye leached from the particles at all could, according to the authors, also possibly be attributed to the presence of unreacted monomers still present in the particles (Sun *et al.,* 2006).

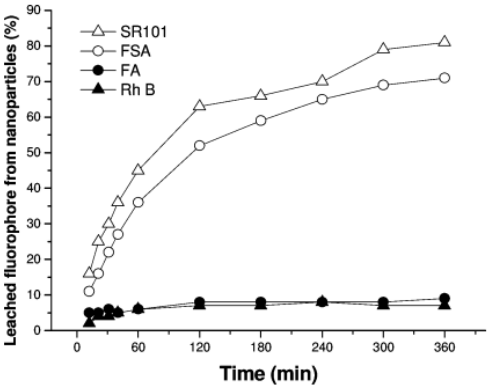

Figure 2. Leaching rate of dyes out of NP sensors., Less than 9% of the dyes *N*-fluoresceinylacrylamide (●) and *N*-acrylamide-*N*′-rhodamine B thiourea (▲) leached out of particles with a covalent bond between the dye and the matrix during the first 6 h, whereas more than 70% of the dyes fluorescein-5 (and -6) sulfonic acid (○) and sulforhodamine 101 (△) leached from particles with physical blend between the dye and the matrix.

Figure 4: Differences in rate of leaching from NPs of physically entrapped dyes (empty symbols) versus covalently embedded dyes (filled symbols). Reprinted with permission from (SUN, H., SCHARFF-POULSEN, A.M., GU, H. and ALMDAL, K., 2006. Synthesis and Characterisation of Ratiometric, pH Sensing Nanoparticles with Covalently Attached Fluorescent Dyes. *Chemistry of Materials*, 18(15), pp. 3381-3384). Copyright (2006) American Chemical Society.)

Surface attachment of dye molecules can be complicated by the phenomenon of quenching, as the dye molecules are exposed to the environment (Sun *et al.,* 2006). The dye molecules

attached to particle surfaces must also be sufficiently spaced to avoid quenching (Soto *et al.,* 2006). A study was conducted whereby an engineered virus was utilised as a particle (Soto *et al.,* 2006). Dye molecules were attached to thiol groups on the virus capsid that were appropriately spaced to avoid quenching using a maleimide-activated avidin-biotin binding protein.

Sauer and colleagues used miniemulsion copolymerisation to prepare PS NPs with fluorescent interfaces (Sauer *et al.,* 2012). Their technique allowed them to prepare NPs (via a direct one-pot procedure) that were selectively fluorescently labelled at the particle-solution interface. These particles could then be used as sensors based on fluorescence quenching or fluorescence resonance energy transfer effects. The interactions between the dye and the environment (and the resultant quenching effects) are thus utilised in a constructive manner.

Core shell type fluorescent NPs were manufactured via dispersion radical polymerisation in the presence of styrene and an ethylene glycol macromonomer in such a manner that the particle surfaces were covered with NH_2-capped poly(ethylene glycol) (PEG) tethered chains (Matsuya *et al.,* 2003). Fluorescent molecules were incorporated inside the particles through physical entrapment. The reactive amine groups at the ends of the PEG chains were converted to maleimide groups using a hetero crosslinker and these maleimide groups were then covalently bound to thiol containing proteins under mild reaction conditions.

PS NPs doped with dye have also been used as nanosensors for oxygen sensing (Napp *et al.,* 2011). Commercially available amino-functionalised beads were loaded with two different dyes, via soaking and swelling of the particles in the respective dye solutions. The authors were able to achieve dye loading efficiencies of 81% and 30% for the two dyes respectively, without altering the size or the morphology of the particles (Napp *et al.,* 2011). Particle surfaces were functionalised with PEG and monoclonal antibodies were conjugated to the particles to ensure specific targeting of tumour cells.

The inherent fluorescent nature of the conjugated polymer poly[9,9-dioctylfluorenyl-2,7-diyl)-co-1,4-benzo-{2,1 ′ -3}-thiadiazole)] (PFBT) was combined with a rhodamine fluorescent dye during particle preparation to prepare sensors for the detection of mercury in water (Childress *et al.,* 2012).

By comparison, the preparation of PSMI NPs via imidisation of PSMA is a relatively simple method for the preparation of small (< 100 nm on average) polymer NPs. Even though literature would suggest that the covalent distribution of dye molecules throughout a NP structure is the most efficient method of dye encapsulation in terms of reduced leaching and improved stability, the method published by Samyn *et al.* (2010) lends itself to physical entrapment of a hydrophobic dye within a hydrophobic polymer matrix, during the ring-opening and ring-closing reactions that occur during synthesis of PSMI NPs. The addition of a hydrophobic dye to the reaction mixture provides a simple method of encapsulation without completely altering the proven particle preparation method. Exalite 613, a highly stable and hydrophobic red laser dye, can be used to load the PSMI NPs during synthesis. Due to its hydrophobic nature it should remain entrapped inside the hydrophobic particles due to hydrophobic-hydrophobic interaction when they are utilised in an aqueous environment.

2.2.3 Dye-doped nanoparticles in field-based devices

Even though many studies have shown detection of low numbers of *E. coli* in water samples, the majority of the techniques proposed are still strictly laboratory bound. The question regarding the ultimate goal, namely the development of a reliable, sensitive, specific, quantitative and rapid test that can be used directly at a sampling point in the field, remains unanswered.

Huang *et al.* prepared dye-doped SiO_2 NPs and incorporated the NPs into a lateral flow device for the detection of residues of enroflaxin (a fluoroquinolone used to protect livestock against veterinary diseases) in chicken meat (Huang *et al.,* 2013). The fluorescent signal

given off by the lateral flow device was read with a prototype portable fluorescent strip reader, and a detection limit of 0.02 ng/mL of enroflaxin residue in chicken extract was achieved. There thus exist definite possibilities for the incorporation of dye-doped NPs into devices that could potentially be utilised on-site for the detection of very low concentrations of pathogens.

Regardless of the detection material and method used, the accurate detection of small amounts of microorganisms in water will always be highly dependent on proper sample preparation, especially with regard to the reduction of sample volume from the required minimum of 100 mL (according to standards) to volumes of millilitres or microliters required for most detection methods discussed in this review. Even though the subject of pre-concentration must thus always be considered when discussing detection of low concentrations of microorganisms (especially in water samples), it is not included in the scope of this dissertation.

2.3 Conclusion and recommendations

The following conclusions and recommendations could be made from the literature review conducted:

- When comparing the different receptor molecules available, it was found that antibodies would be the most suitable for this project, considering the high level of specificity they provide, as well as the many existing techniques available for the immobilisation of antibodies onto NPs.
- The strong affinity between avidin and biotin would ensure orientated attachment of biotinylated antibodies onto NPs coated with avidin.
- Dye labelling of the immobilised antibodies and the subsequent exposure of the dye molecules to the environment would be avoided by the encapsulation of a fluorescent dye into the NPs.

- The use of dye-doped PSMI NPs is an interesting approach for *E. coli* detection. This polymer offers ease of surface-functionalisation for antibody attachment, and its use of bacteria detection has not yet been reported in the literature.

Chapter 3: Preparation of poly(styrene-*co*-maleimide) nanoparticles and surface-functionalisation with formaldehyde and diamine compounds

3.1 Introduction

Poly(styrene-*co*-maleic anhydride) (PSMA) is a useful thermoplastic with many possible industrial applications (Lee & Ahn, 1998). The reactive anhydride ring provides PSMA with good miscibility while the polymer's transparency and high heat resistance makes it very useful in the improvement of other polymers' heat resistance. The highly reactive anhydride ring in the copolymer is however susceptible to hydrolysis and thus degradation (Samyn *et al*., 2010, Lee & Ahn, 1998, Liu *et al*., 2005). It was found that the replacement of the anhydride ring with the more thermally stable imide group creates a structurally more desirable maleimide derivative, poly(styrene-*co*-maleimide) (PSMI) with improved thermal properties (Liu *et al*., 2005) (See Figure 5).

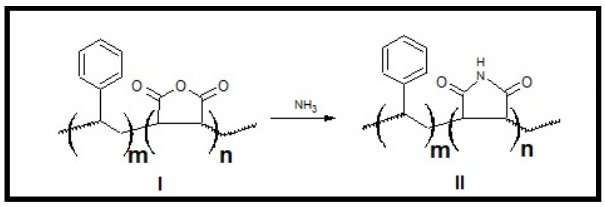

Figure 5: Imidisation of (I) PSMA to form PSMI (II).

PSMI can either be synthesised via the direct copolymerisation of the styrene and maleimide monomers or via the imidisation of PSMA (Liu *et al*., 2005, Samyn *et al*., 2010). Direct copolymerisation is a simple process, but the synthesis of the maleimide monomer however is complex and very expensive (Liu *et al*., 2005). Imidisation has thus been established as the preferred synthesis route (Samyn *et al*., 2010).

Samyn and colleagues (2010) developed a method for the synthesis of PSMI NPs in aqueous media via the imidisation of PSMA with ammonium hydroxide under high pressure and temperature using an oil-heated autoclave reactor (Samyn *et al*., 2010). It is known that during imidisation with ammonium hydroxide the maleic anhydride ring structure opens to form an amic acid moiety (Samyn *et al*., 2010). High temperatures are then required for the ring closing reaction to proceed, leading to formation of the imide structure (Liu *et al*., 2005). The mechanism is shown in Figure 6. The PSMI is then able to form nanostructured materials through self-association (under mild pH conditions) (Samyn *et al*., 2010).

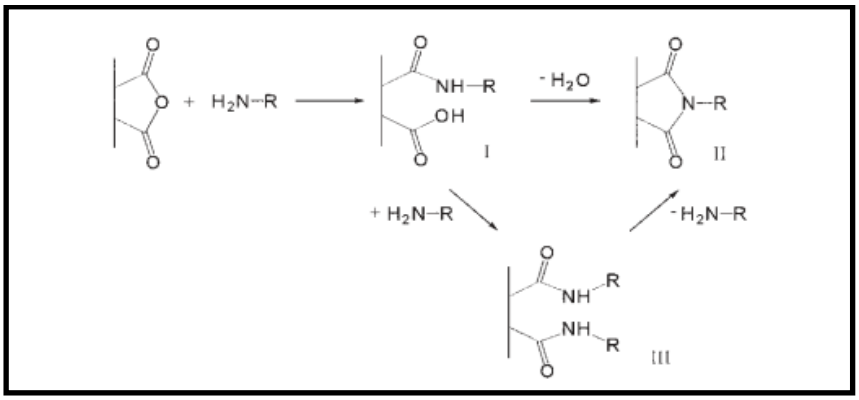

Figure 6: A schematic representation showing the two step ring-opening (I & III) and ring-closing reaction (II) of PSMA with a primary amine. Reprinted with permission from (LIU, H., CAO, K., HUANG, Y., YAO, Z., LI, B. and HU, G., 2006. Kinetics and simulation of the imidisation of poly (styrene-*co*-maleic anhydride) with amines. *Journal of Applied Polymer Science*, 100(4), pp. 2744-2749).

3.2 Experimental

3.2.1 Materials and equipment

The synthesis of the PSMI NPs required the use of PSMA with a 26 wt% maleic anhydride content and a weight average molar mass (M_w) of 80 000 g/mol (Polyscope, NL), a pre-prepared ammonium hydroxide solution of 25% (Fluka), and a red laser dye, Exalite 613 (Exciton, USA). Surface-functionalisation was performed with a 38% formaldehyde solution (Sigma), as well as ethylene diamine (EDA or 2C diamine) (Sigma), 1,4-diaminobutane (4C

diamine) (Sigma) and 1,6-diaminohexane (6C diamine) (Sigma). The reactor used for imidisation is a 250 mL picoclave reactor (Büchi, Switzerland).

3.2.2 Synthesis of PSMI nanoparticles

The PSMI NPs were manufactured via the imidisation of PSMA as proposed by Samyn and colleagues (Samyn *et al*., 2010). Particles were synthesised and loaded with dye in one step. A double walled oil-heated stirring reactor was loaded with the standard formulation as given below:

Standard particle formulation:

- 20 g poly(styrene-*co*-maleic anhydride) (26% MA content, M_w = 80 000 g/mol)
- 100 mL of distilled water
- 5 mL of 25% ammonium hydroxide solution
- 5 mg of Exalite 613 (Perylene Red) (for dye-doped NPs)

Imidisation was allowed to proceed at a bath temperature of 180 °C, with stirring at 1000 rpm, for 6 hours. After reaction completion and cooling of the latex, some or all of the mixture was dialysed with a 10 000 molecular weight cut off (MWCO) snake skin dialysis tube to remove unreacted molecules. The conversion of PSMA to PSMI was monitored via fourier transfer infrared spectroscopy (FTIR) analyses.

Initially, particles without dye were also synthesised and characterised to determine whether the method as proposed by Samyn *et al*. (2010) could successfully be repeated. These particles then also served as reference point to determine the effects (if any) that encapsulation of dye into the particles had on the particle characteristics.

In subsequent experiments, the amount of dye added to the formulation was also increased from 5 mg to 7.5 mg and 10 mg to determine the maximum dye loading.

3.2.3 Surface-functionalisation with amine functional groups

After imidisation of PSMA, and the preparation of PSMI NPs as described in the previous section, the particles were surface-functionalised with amine groups in 2 steps. The first step involved the reaction of the particles with an excess of formaldehyde to introduce methylol moieties on the particle surfaces. The particles were then reacted with an excess of either ethylene diamine, 1,4-diaminobutane or 1,6-diaminohexane. The proposed reaction mechanism for preparation of the surface-functionalised particles is given in Figure 7.

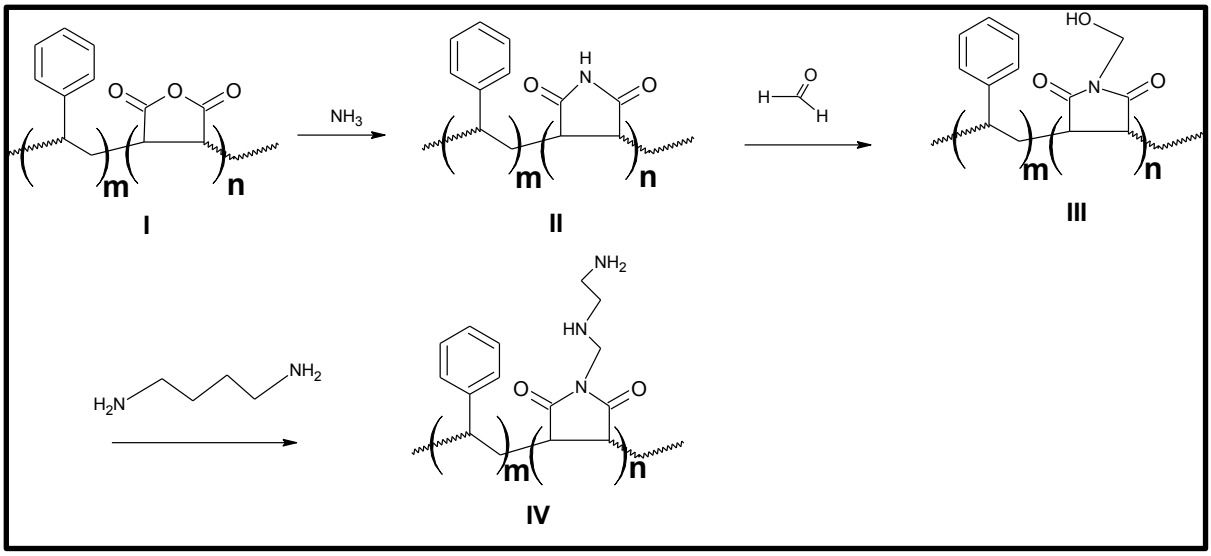

Figure 7: Reaction scheme for the synthesis and surface-functionalisation of poly(styrene-*co*-maleimide) NPs with excesses of formaldehyde and 1,4-diaminobutane.

After completion of each reaction step, the reaction mixture was dialysed in a 10 000 MWCO snake skin dialysis tube in deionised water to remove unreacted molecules. The experimental setup is shown in Figure 8.

The amounts of excess formaldehyde and diamine compounds used for surface-functionalization were varied. The amounts of formaldehyde and diamine added to the NPs were calculated based on assumptions made regarding the conversion of PSMA to PSMI as

well as the availability of maleimide groups for reaction with formaldehyde and diamine on the NP surfaces.

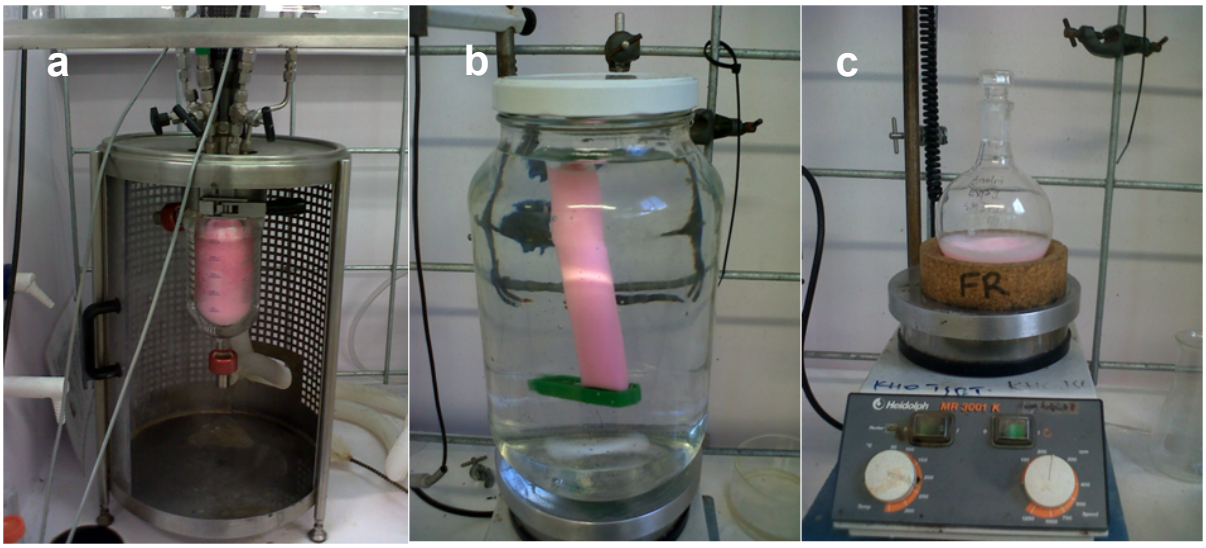

Figure 8: Experimental setup for the a) manufacture, b) dialysis and c) surface-functionalisation of PSMI NPs.

These assumptions and the method for determining the amounts of formaldehyde and diamine required for surface functionalisation can be found in the appendix. Experiments with longer chain diamine compounds were performed in order to determine whether attachment of these larger structures on the NP surfaces could enhance surface-functionalisation. Two alternative linear diamine compounds were experimented with, namely 1,4-diaminobutane (referred to as '4C diamine') and 1,6-diaminohexane (referred to as '6C diamine'), to introduce linear 4-carbon and linear 6-carbon amine-capped chains onto particle surfaces respectively.

3.3 Characterisation

3.3.1 Attenuated Total Reflectance Fourier Transform Infrared Spectroscopy (ATR-FTIR)

ATR-FTIR was used to determine whether NP formation had occurred successfully. Samples were analysed on a PerkinElmer Spectrum 100 at a resolution of 4 cm^{-1} and with 16 scans per sample.

FTIR was also utilised to track the surface-functionalisation process and whether modification of the particle surfaces had been successful. Samples were freeze-dried or oven dried in order to be tested.

3.3.2 Transmission Electron Microscopy (TEM)

Particle characterisation of the pure and functionalised PSMI NPs was performed via transmission electron microscopy (TEM). The NPs were diluted with water and stained with uranyl acetate to improve contrast. Imaging was performed at an acceleration voltage of 200 kV with a TecniaTM G 2 20 (FEI-Eindhoven) transmission electron microscope.

3.3.3 PSMI suspension pH

The pH values of the PSMI NP suspensions were measured with an Orion (Thermo Scientific) pH device calibrated with citrate/HCl buffer solutions at pH=4.0, 7.0 and 9.0 (Orion Application Solution). Where applicable, pH adjustments were performed with a 0.5 M HCl solution.

3.3.4 Photon Correlation Spectroscopy/Zetasizer

The surface charge of the particles was monitored via a Malvern Zetasizer Nano-ZS. PSMI NP suspensions were diluted with deionised water and initially analysed without adjusting pH of the final dilutions. NP suspensions of 50 to 200 µL were diluted in 5 mL of water, and sonicated for a minimum of 5 minutes. Every sample was analysed in 3 runs, each with a

number of measurements ranging from 20 to 50, to obtain statistically relevant results. Diamine surface-functionalised NPs were diluted in PBS and the pH adjusted with 0.5 M HCl for surface charge measurements.

3.3.5 Differential Scanning Calorimetry (DSC)

Thermal analyses of the samples were performed via a differential scanning calorimeter (DSC) (DSC Q2000, TA Instruments, USA), calibrated with indium and zinc. A heating rate of 10 °C/min was used in a nitrogen atmosphere, with a flow rate of 25 mL/min, over a temperature range of 20 to 250 °C. Aluminium sample pans were used. The sample masses, which were accurately determined on an analytical balance, ranged between 1.5 and 5 mg.

3.3.6 Characterisation of fluorescent properties

Absorbance of free Exalite 613 dye as well as dye-doped NPs was measured via a UV-Vis spectrophotometer (PerkinElmer Lambda 35) to determine the wavelength at which maximum absorbance occurred. Fluorescent emission properties were characterised using room temperature photoluminescence (Jobin-Yvon NanoLog spectrometer) at an excitation wavelength of 400 nm and 569 nm.

Serial dilutions of free Exalie 613 dye were prepared in acetone while serial dilutions of PSMI NPs with varying dye-loadings were prepared in deionised water.

3.4 Results and Discussion

3.4.1 FTIR results

3.4.1.1 Pure PSMA, pure PSMI & dye-doped PSMI

The functional groups (with corresponding characteristic peaks) that, according to Samyn *et al* (2010), are indicative of the successful formation of PSMI NPs from PSMA are shown in Table 1.

Table 1: Summary of characteristic functional groups used to identify PSMA and PSMI NPs (as given by (Samyn *et al*., 2010)).

Wavelength (cm^{-1})	Functional Group	Compound wherein functional group is present
3600 to 3100	NH stretching vibrations	PSMI
3100 to 2990	styrene, CH aromatic stretching	PSMA & PSMI
2924, 2854	CH_2 in backbone chain	PSMA & PSMI
1950	styrene	PSMA & PSMI
1860, 1775	C=O anhydride ring	PSMA (1860), PSMA & PSMI
1780	symmetric C=O, imide I	PSMI
1710	asymmetric C=O or N-C=O stretch, imide I	PSMI
1601, 1584	styrene C=C stretch	PSMA & PSMI
1493, 1453	styrene, aromatic C-C stretch	PSMA & PSMI
1370, 1325	styrene, C-H aromatic vibration	PSMA & PSMI
1345	imide II, C-N-C axial	PSMI
1220, 1076	cyclic C-O-C and carbonyl, anhydride	PSMA
1179	imide II, C-N-C transverse	PSMI
1071, 1029, 907, 847, 757, 695	styrene, aromatic C-H	PSMA & PSMI
946 to 920	C-H vibration in cyclic carbonyl compounds, anhydride	PSMA

The FTIR spectrum of pure PSMA used to synthesise the PSMI NPs is given in Figure 9. The most prominent peaks corresponded with the characteristic peaks of PSMA reported by Samyn *et al.* (2010). The presence of styrene groups are indicated by the peaks at 3063 cm-

[1] and 3028 cm^{-1}, as well as peaks at 1602 cm^{-1}, 1494 cm^{-1}, 1453 cm^{-1}, 1070 cm^{-1}, 913 cm^{-1}, 756 cm^{-1} and 698 cm^{-1}.

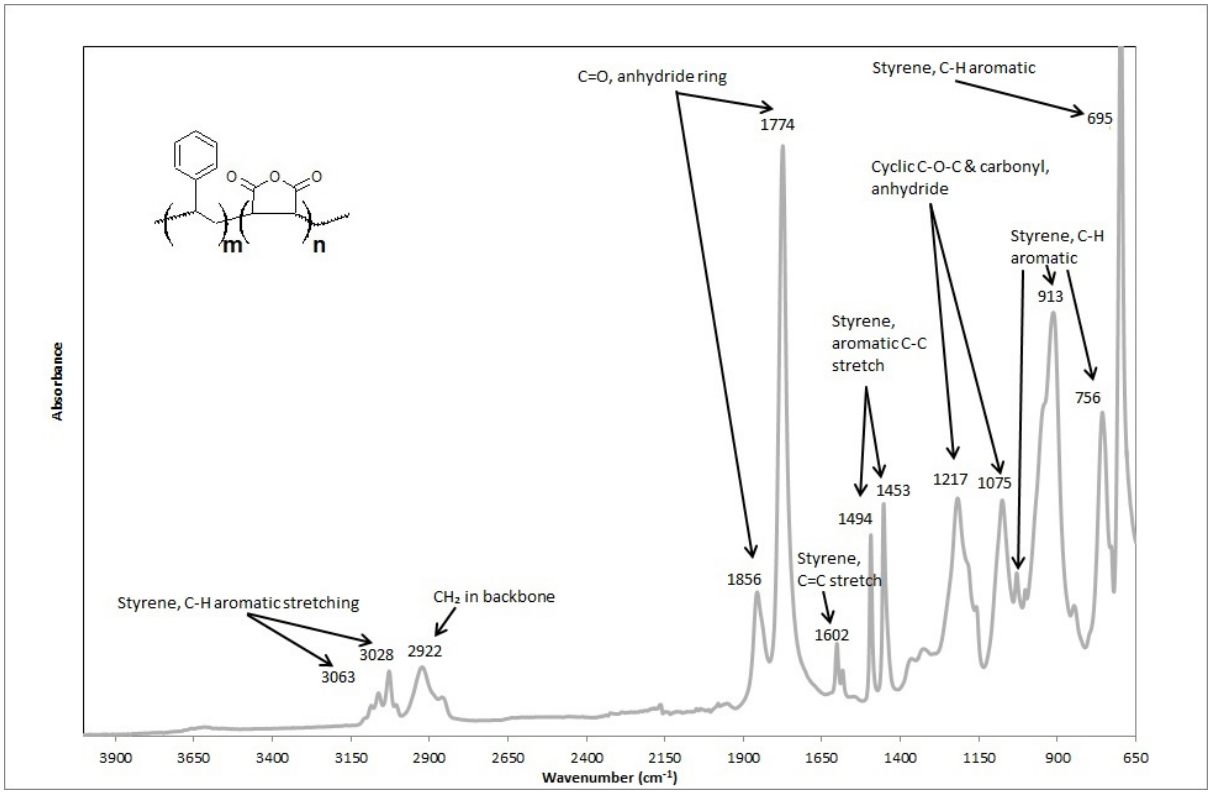

Figure 9: FTIR spectrum of the PSMA (26% maleic anhydride) polymer.

According to Samyn *et al.* (2010), the 1493 cm^{-1} and 1453 cm^{-1} peaks serve as "internal references" due to the non-participation of the aromatic moieties in the imidisation process, while the peaks from 1070 cm^{-1} to 847 cm^{-1} are typical of amorphous PS (Samyn *et al*., 2010). All PSMI spectra used for comparative purposes were normalised with reference to the 1493 cm^{-1} peak in order to compare peak intensities between spectra. The peak at 2922 cm^{-1} represents the CH_2 group in the polymer backbone. The anhydride ring is indicated by the peak at 1856 cm^{-1} (symmetrical C=O stretch in the cyclic maleic anhydride) and the very prominent peak at 1774 cm^{-1} (asymmetrical stretch in the cyclic maleic anhydride). The characteristic peaks at 1217 cm^{-1} and at 1075 cm^{-1} represent the cyclic C-O-C and the carbonyl groups of the anhydride structure.

A detailed FTIR spectrum of the pure PSMI NPs synthesised (without encapsulated dye) from the PSMA shown in Figure 9 is given in Figure 10. The carbon backbone linking the styrene and maleimide groups is again indicated by the CH_2 characteristic peak at 2920 cm^{-1}. The styrene 'fingerprint' area below 1070 cm^{-1} remained relatively unchanged, and the styrene peaks at 1602 cm^{-1}, 1493 cm^{-1} and 1452 cm^{-1} were also unaltered by the imidisation, as was expected seeing as imidisation only alters the anhydride structure of the PSMA and not the styrene structure.

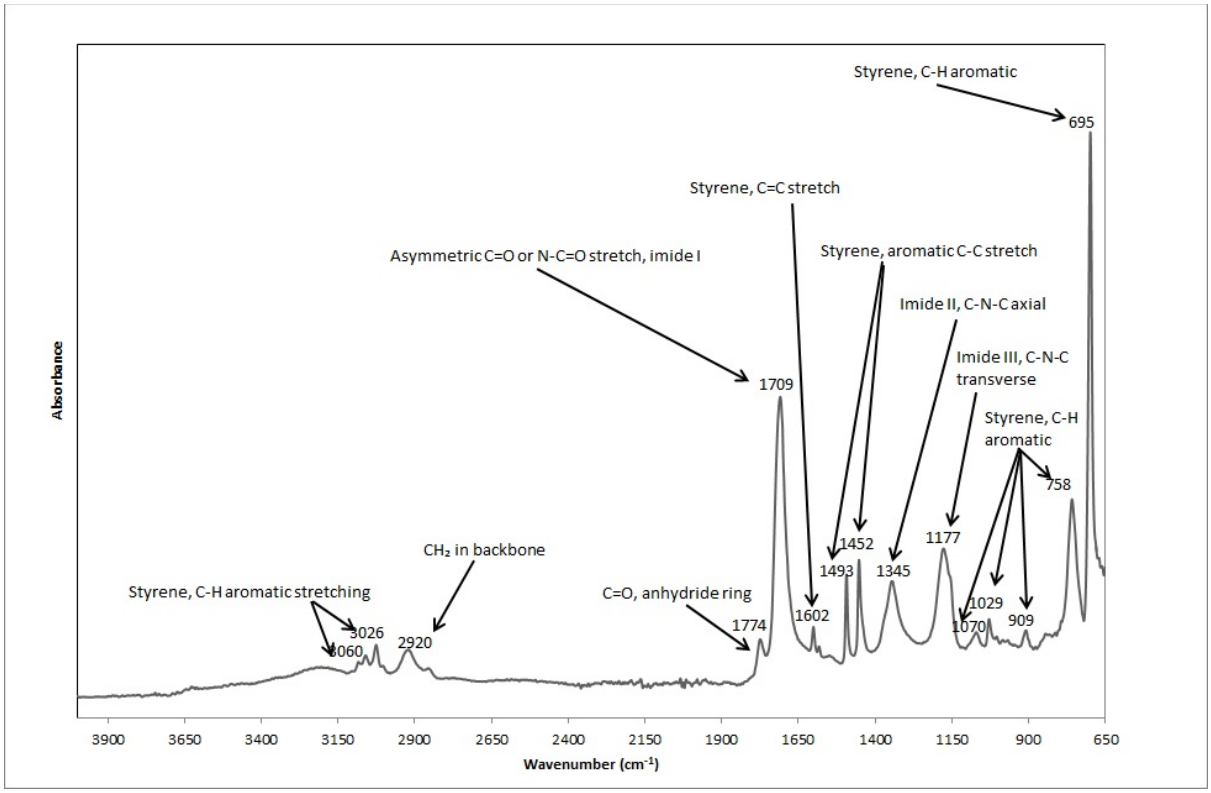

Figure 10: FTIR spectrum of standard pure PSMI nanoparticles synthesised by imidisation of PSMA.

The major changes to the FTIR spectrum caused by imidisation were seen in the reduction of the anhydride peak at 1774 cm^{-1} and the disappearance of the 1856 cm^{-1} anhydride peak. Successful imidisation was indicated by the appearance of a prominent peak at 1709 cm^{-1}, typical of the asymmetric C=O or N-C=O stretch of the imide I group, as shown in Table 1. The presence of the small peak at 1774 cm^{-1}, indicative of the C=O bond in an anhydride ring, can be taken as indication of residual maleic anhydride or as a 'side peak' of the 1709

cm^{-1} maleimide peak. Alternatively it could be assumed to be indicative of in-phase C=O stretching of the imide I group which has been reported previously at 1780 cm^{-1} (Samyn *et al*., 2010). The low intensity of the 1774 cm^{-1} peak relative to the peak at 1709 cm^{-1} is typical of ring closing reactions and indicates formation of cyclic imides (Samyn *et al*., 2010). Further evidence of successful imidisation could be seen by the appearance of characteristic peaks at 1345 cm^{-1} and 1177 cm^{-1}, indicating the presence of imide II and imide III bending respectively. The appearance of a broad, flat peak in the region of 3600 cm^{-1} to 3100 cm^{-1} was taken to be characteristic of N-H stretching vibrations as a result of the introduction of the N-H group to the 5-membered ring structure when anhydride was converted to imide.

The detailed FTIR spectrum of the red perylene dye, Exalite 613, used for dye-doping is given in Figure 11 along with the molecular structure of the dye as provided by the manufacturer.

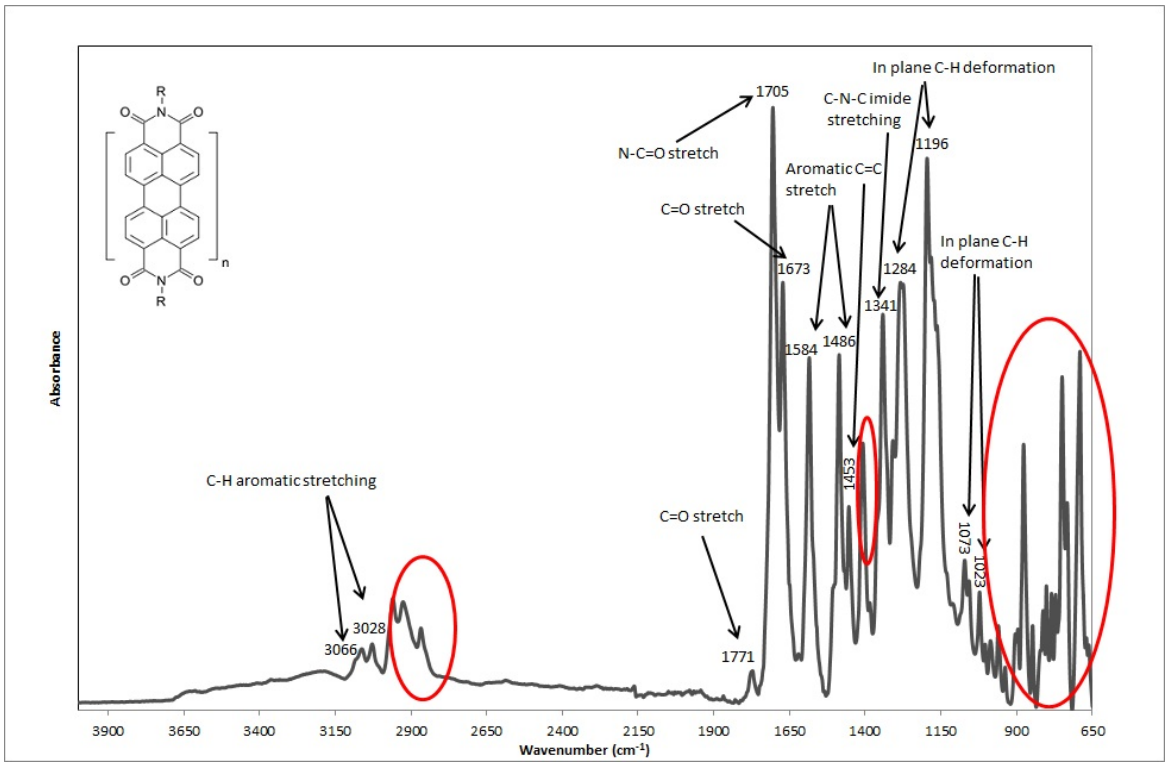

Figure 11: FTIR spectrum and molecular structure of Exalite 613 perylene dye used for dye-doping.

The FTIR spectrum of Exalite 613 shows characteristic peaks at 3028 cm^{-1} (aromatic C-H stretching vibrations), 1771 cm^{-1} (C=O stretch), 1705 cm^{-1} (N-C=O stretch), 1673 cm^{-1} (C=O stretch of an aldehyde conjugated to a phenyl group),1584 cm^{-1}, 1486 cm^{-1} and 1453 cm^{-1} (aromatic C=C stretch), 1341 cm^{-1} (C-N-C absorption of the imide structure), and between 1300-1000 cm^{-1} (in-plane C-H deformation) (Socrates, 2001). The populated absorption region between 960 cm^{-1} and 650 cm^{-1} (encircled) is characteristic of aromatic compounds experiencing out of plane C-H vibrations.

Due to matters of confidentiality the manufacturer of the dye was not willing to disclose the nature of the R group shown in the molecular structure of the dye, and thus it could only be speculated as to the nature of this group. It was assumed that the remaining unidentified areas encircled in Figure 11 between 3000 cm^{-1} and 2800 cm^{-1} and at 1409 cm^{-1} were indicative of functional groups present in this unidentified R group. The peaks in the absorption region between 3000 cm^{-1} and 2800 cm^{-1} could be attributed to C-H stretching vibrations of a linear carbon chain, similar to the linear backbone present in the PSMA and PSMI compounds, while the peak at 1409 cm^{-1} could then be attributed to the corresponding CH_2 bending deformation that occurs between 1470 cm^{-1} and 1350 cm^{-1}.

The spectra of the PSMI NPs without and with dye encapsulated were compared to determine whether dye inclusion had altered the composition of the NPs. This comparison is shown in Figure 12.

When comparing the spectra in Figure 12 it was observed that no new characteristic peaks were introduced upon dye-doping of the PSMI NPs with Exalite 613. The differences between the dye-loaded and pristine NPs were limited to similar characteristic peaks with differing intensities, most notably in the area between 3000 cm^{-1} and 3600 cm^{-1}, and between 1560 cm^{-1} and 1510 cm^{-1}, as well as the characteristic peaks at 1709 cm^{-1}, 1347 cm^{-1} and the peak at 1179 cm^{-1}.

As shown in Figure 11, the characteristic peaks at 1709 and 1347 cm^{-1} are also present in the Exalite 613 structure. Increases in the intensities of these peaks upon dye-loading could support a hypothesis whereby the dye was absorbed onto the NP surfaces instead of/as well as being encapsulated inside the NPs. The intensity of these peaks however decreased upon dye-loading.

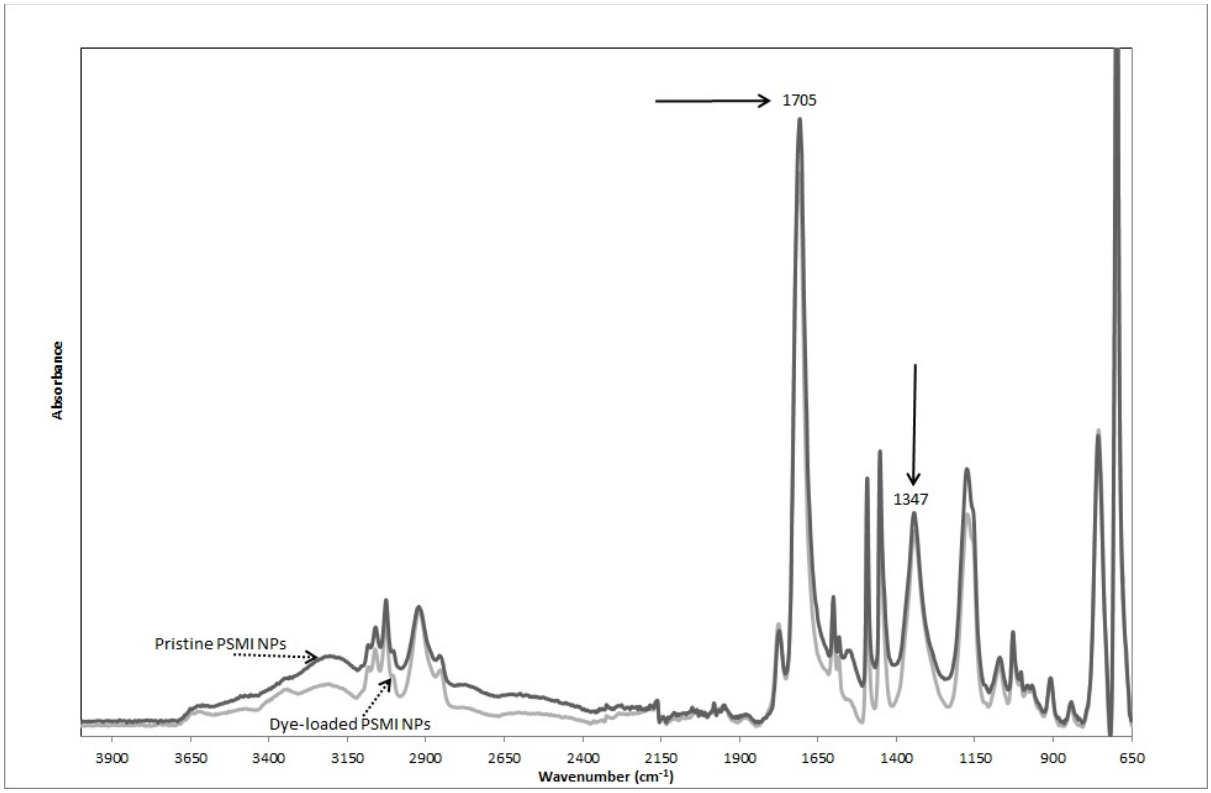

Figure 12: FTIR spectra of pristine and dye-loaded PSMI NPs.

The differences in intensities between the characteristic peaks mentioned above will be shown (in Section 3.4.1.3 *Dye-loading variation and varying degrees of imidisation*) to be more indicative of variations in the degree of imidisation (the degree of transformation of anhydride into imide groups during imidisation of PSMA) between NP batches rather than providing significant information on the effects of dye-loading on the FTIR spectra of the dye-doped NPs.

3.4.1.2 Functionalisation of PSMI

Surface-functionalisation was performed by first reacting the NP suspension with an excess of formaldehyde followed by reaction with an excess of a diamine compound (initially EDA or 2C diamine). It was postulated that the addition of excess EDA would create bridge-like structures on the surfaces of the particles with an amine group exposed. This amine group could then be utilised as a binding site for antibody attachment via carbodiimide chemistry.

In Figure 13 the FTIR spectrum of the PSMI NPs (no dye added) is compared to that of the NPs after addition of formaldehyde, and after surface-functionalisation with EDA.

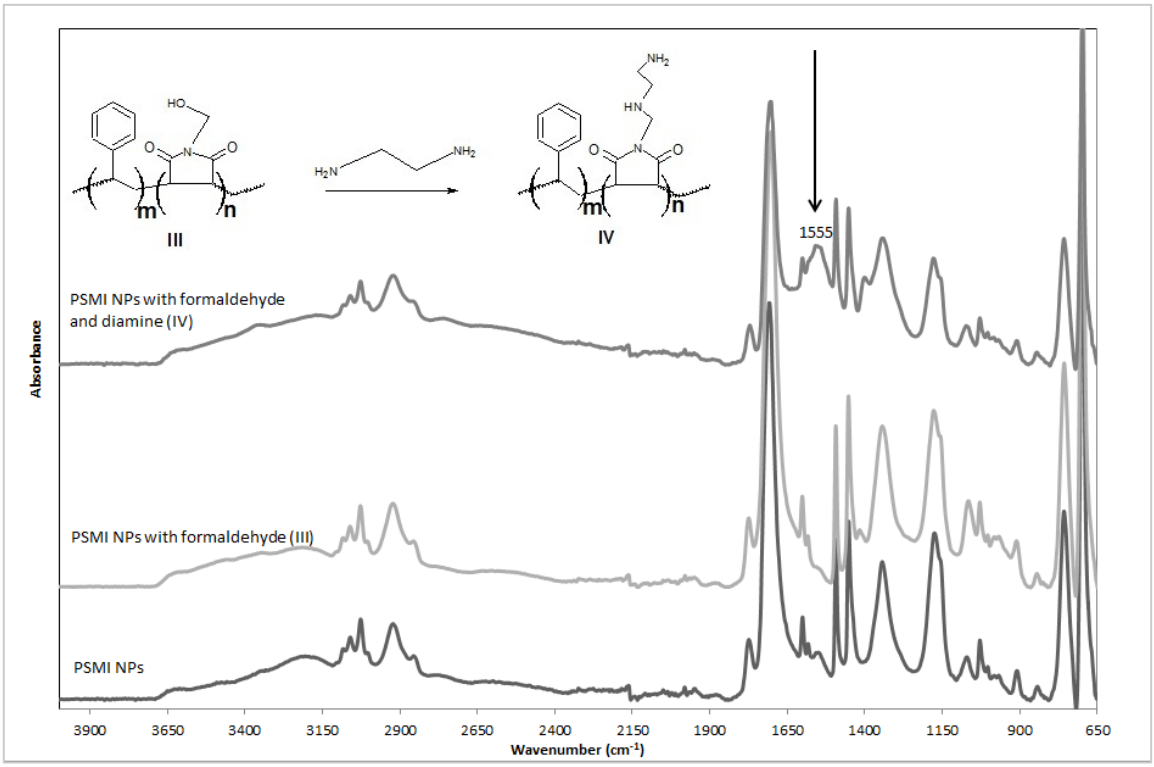

Figure 13: FTIR spectra of PSMI NPs (without dye) after particle synthesis (labelled as "PSMI NPs"), after formaldehyde addition ("PSMI NPs with formaldehyde and III) and after addition of EDA ("PSMI NPs with formaldehyde and diamine" and IV).

After functionalisation with formaldehyde a very slight peak appears at 1400 cm^{-1}, and this peak increases in intensity after the addition of EDA. The appearance of this peak was attributed to the additional CH_2 linkages introduced onto the NPs after formaldehyde and

diamine surface-functionalisation. The corresponding stretching vibrations fall within the range of 3000 cm^{-1} to 2850 cm^{-1}, an area already populated by a peak characteristic of the CH_2 groups in the backbone between the styrene and maleimide repeating units of the copolymer. The most noticeable difference between the spectra in Figure 13 was the appearance of a significant peak at 1555 cm^{-1} after surface-functionalisation with ethylene diamine was performed. As primary N-H bending is characterised by peaks in the range between 1650 cm^{-1} and 1580 cm^{-1}, it was concluded that the new peak was an indication of amine groups successfully functionalised onto the particle surfaces.

Primary N-H stretching is characterised by peaks between 3400-3300 cm^{-1} and 3330-3250 cm^{-1}, while O-H stretching vibrations are indicated by a broad peak in the region between 3500-3000 cm^{-1}. Comparison of the specific area between 4000 cm^{-1} and 2500 cm^{-1} for the three spectra given in Figure 13 is shown in Figure 14.

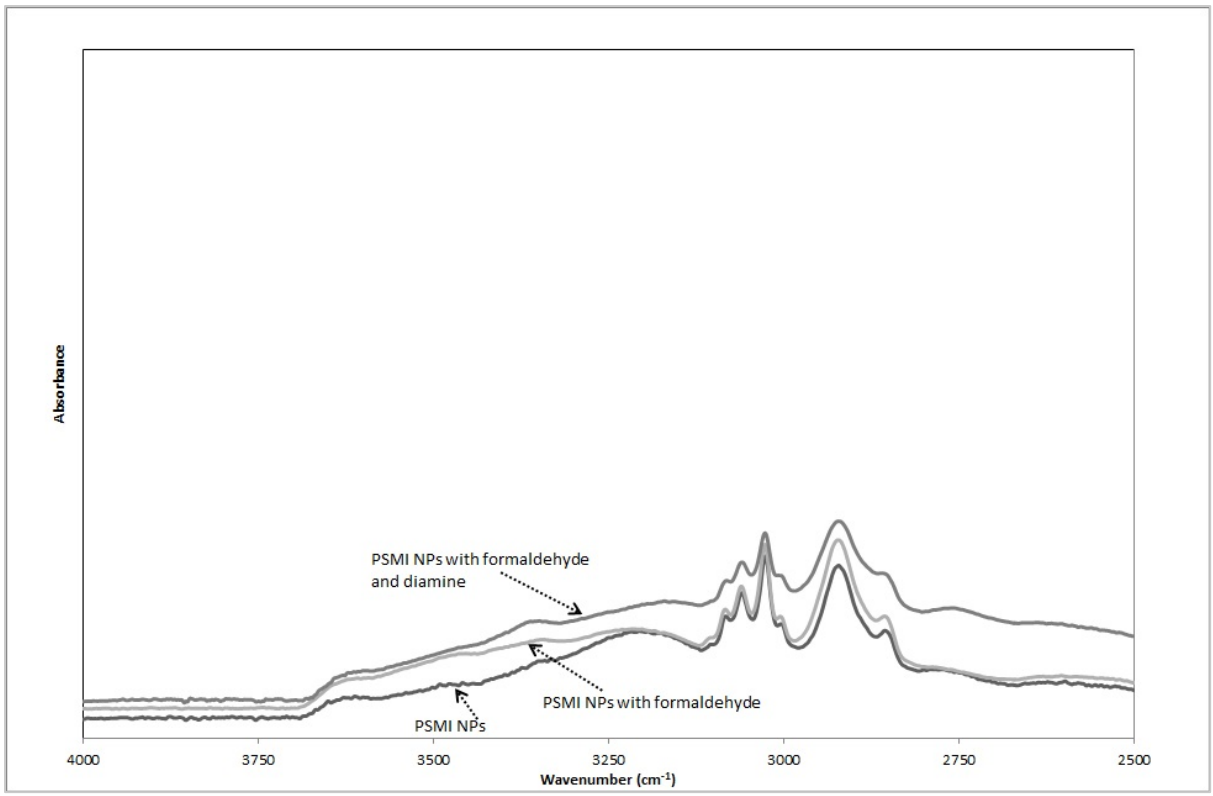

Figure 14: Comparison of the spectra of PSMI NPs and functionalised NPs in the absorption region of 4000 cm^{-1} to 2500 cm^{-1} for PSMI NPs, PSMI NPs with formaldehyde and PSMI NPs with formaldehyde and diamine (from bottom to top).

On close inspection, the broad peak between 3700 cm^{-1} and 3100 cm^{-1} present in the PSMI spectrum increases in intensity when the PSMI NPs are functionalised with formaldehyde, indicative of the stretching vibrations caused by the addition of the hydroxyl groups onto the NP surfaces. A further broadening of this peak in the area between 3400 and 3100 cm^{-1} upon functionalisation with the diamine compound could be attributed to primary amine stretching as a result of the NH_2 groups functionalised onto the NP surfaces.

The surface-functionalisation of dye-loaded PSMI NPs via FTIR is shown in Figure 15.

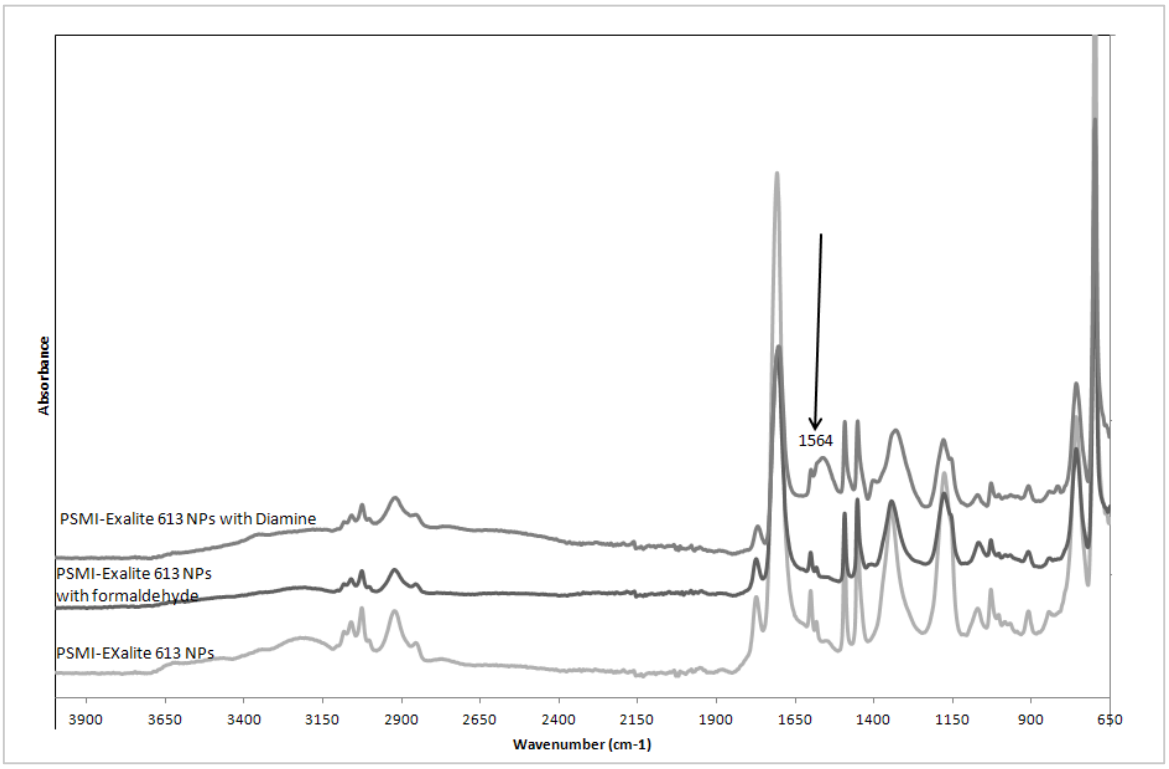

Figure 15: FTIR spectra of PSMI NPs (with dye) after particle synthesis (labelled as "PSMI-Exalite 613 NPs"), after formaldehyde addition ("PSMI-Exalite 613 NPs with formaldehyde) and after addition of ethylene diamine ("PSMI-Exalite 613 NPs with diamine").

As with the pure PSMI NPs a new characteristic peak in the region between 1650 cm^{-1} and 1500 cm^{-1} was detected after the addition of both excess formaldehyde and excess EDA, and the presence of this peak was used to conclude that surface-functionalisation with amine groups have been achieved. The slight shift of this peak to 1564 cm^{-1} compared to

1555 cm^{-1} for amine functionalised PSMI NP's without dye could possibly be attributed to the interaction of the added Exalite dye with the amine groups of the functionalised NPs.

As with the pure PSMI NPs, surface-functionalisation again leads to the formation and gradual increase of a new peak at 1400 cm^{-1}, indicating the presence of the CH_2 groups in the methylol and amine linkages introduced onto the NP surfaces after functionalisation.

Formaldehyde and Diamine Optimisation

The extent of molar excess of formaldehyde added during the first step of the surface-functionalisation process was varied in order to try and determine the optimal amount of formaldehyde needed and to determine whether changes in the molar excess of formaldehyde could increase the hydroxyl content introduced onto the PSMI NPs. The corresponding FTIR spectra are shown in Figure 16.

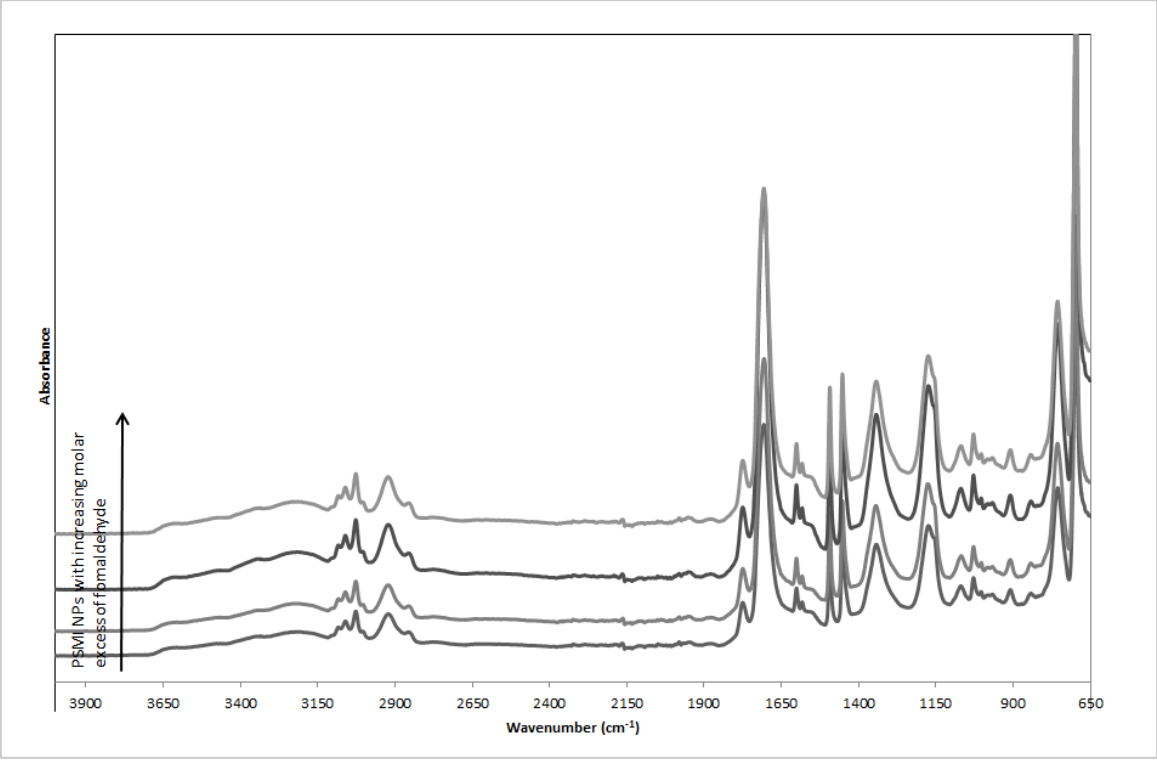

Figure 16: FTIR spectra of PSMI NPs functionalised with increasing molar excess of formaldehyde.

Figure 16 shows no significant difference in intensity of the characteristic peaks between samples functionalised with increasing excess of formaldehyde. This was confirmed on closer inspection of the absorption region between 4000 cm^{-1} and 3000 cm^{-1} for the spectra of the PSMI NPs functionalised with the lowest and highest molar excess of formaldehyde respectively (Figure 17).

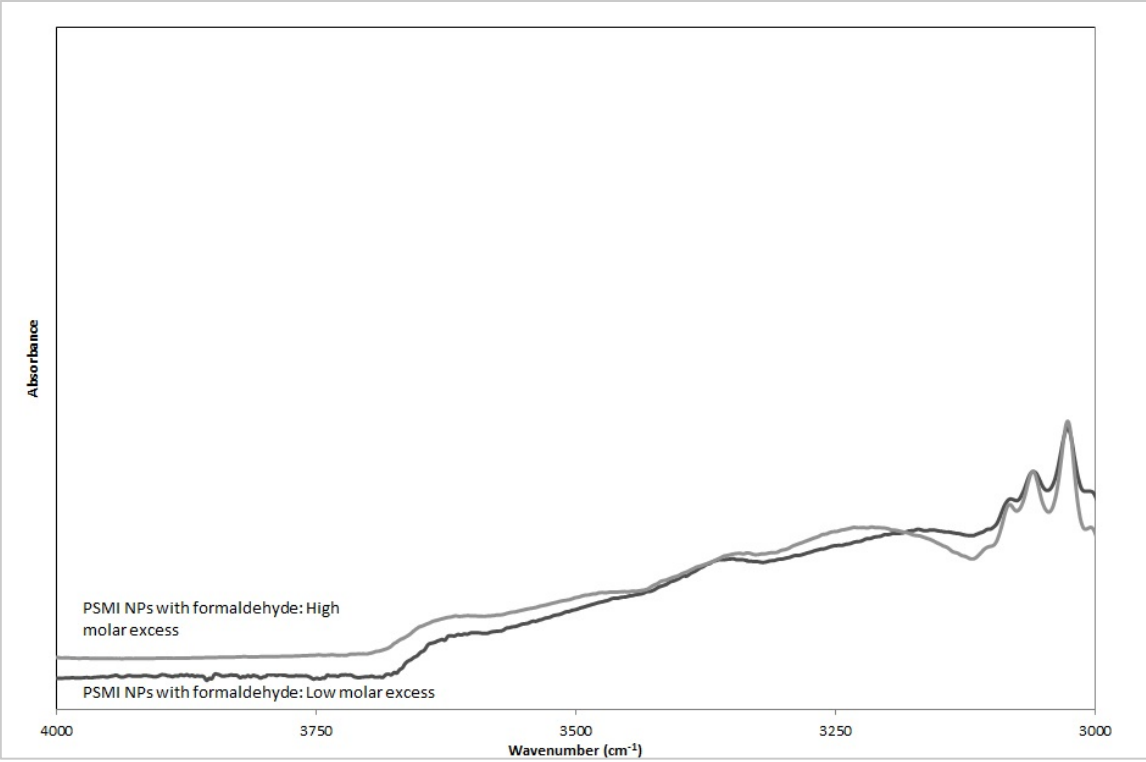

Figure 17: Comparison of the FTIR spectra of formaldehyde-PSMI NPs functionalised with the lowest (bottom) and highest (top) molar excesses shown in Figure 16.

It was postulated that if addition of an increased molar excess of formaldehyde to the PSMI led to an increased number of methylol groups introduced onto NP surfaces (that could not be clearly distinguished via FTIR) more amine groups could potentially bind to these particles compared to the NPs functionalised with a smaller excess of formaldehyde. Two batches of formaldehyde-functionalised NPs were thus prepared, with increasing formaldehyde molar excess. The two batches were then reacted with the same molar excess of 2C diamine and the FTIR spectra were compared (Figure 18).

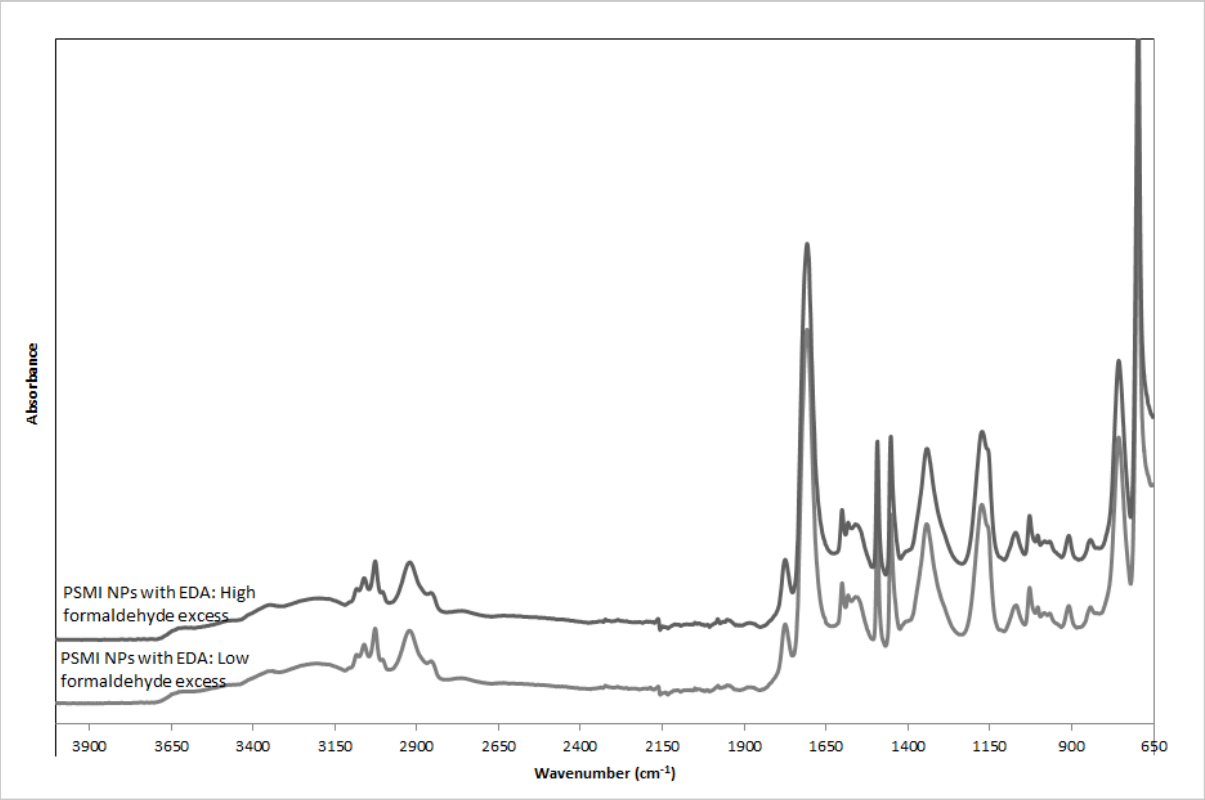

Figure 18: Comparison of FTIR spectra of diamine-functionalised PSMI NPs initially functionalised with two different molar excesses of formaldehyde.

There were no clear differences between the surface-functionalisation achieved with the lower and higher molar excess of formaldehyde added to PSMI as starting material for the diamine surface-functionalisation.

Diamine-functionalisation was further investigated by replacing the 2C diamine used in the final functionalisation step with its 4 carbon and 6 carbon chain length equivalents, referred to as '4C diamine' and '6C diamine' respectively. For both the 4C diamine and the 6C diamine, amine surface-functionalisation was successfully performed based on the appearance of a new characteristic peak in the absorption region between 1558 cm^{-1} and 1555 cm^{-1} (similar to 2C diamine functionalisation), as indicated by the FTIR spectra in Figure 19.

When comparing the intensity of the amine peaks of the 3 different diamine-functionalised NPs (indicated by the arrow) as given in Figure 19 it seemed at first inspection that the intensity of amine peaks increased as the chain length of the diamine compound used for surface-functionalisation increased.

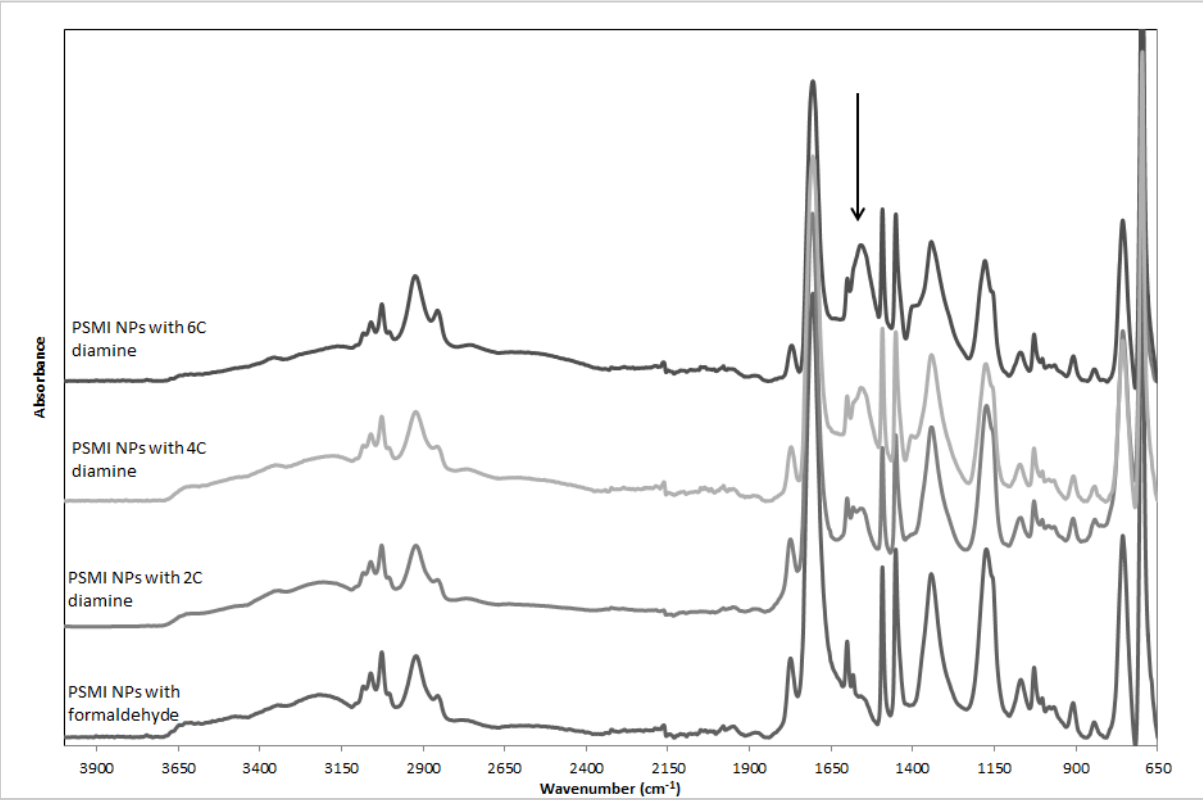

Figure 19: FTIR spectral comparison of PSMI NPs functionalised with three different diamine compounds.

To confirm this, the spectra were overlayed and the areas between 2000 cm^{-1} and 1350 cm^{-1} and between 4000 cm^{-1} and 2000 cm^{-1} were enlarged and shown in Figure 20 and Figure 21 respectively. On closer examination of the absorption region between 1600 cm^{-1} and 1500 cm^{-1}, the intensity of the peak at 1555 cm^{-1} was more pronounced for the 6C diamine functionalised PSMI NPs than for the NPs functionalised with the 2C and 4C diamine compounds, indicating increased amine-functionalisation. This could be explained by the increased flexibility of the longer aliphatic chain possessed by the 6C diamine compared to the 2C and the 4C compounds. This increased flexibility could theoretically facilitate better attachment between the diamine capped chain and the methylol moieties on the NP

surfaces during functionalisation compared to the possibly reduced access to the methylol groups provided by the more rigid aliphatic chains of the 2C and 4C diamine compounds.

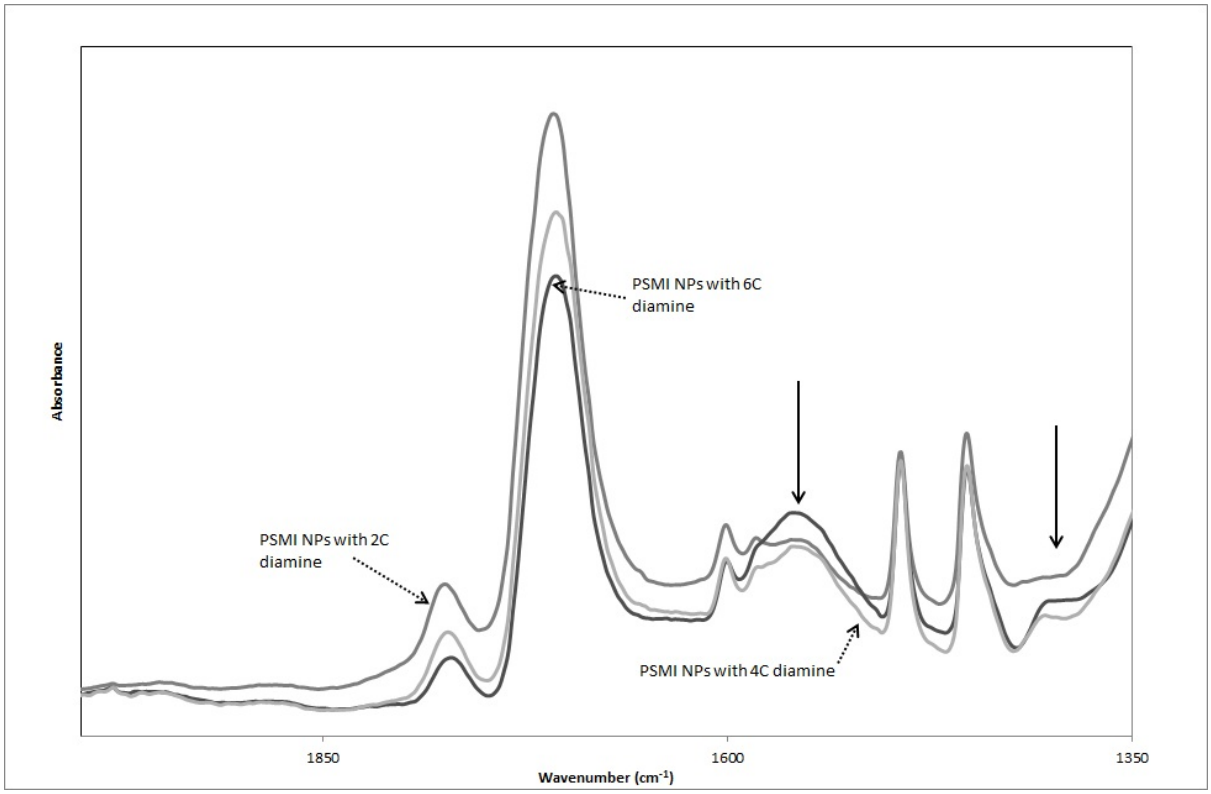

Figure 20: FTIR spectral comparison of PSMI NPs functionalised with 3 different diamine compounds with spectra overlapping and detail of the absorption region between 2000 cm^{-1} and 1350 cm^{-1}.

From Figure 20 it could also be seen that for the 2C and 4C modified NPs two resolved peaks appear in this region at 1584 cm^{-1} and 1560 cm^{-1} respectively, while for the 6C modified NPs, only the broad peak at 1555 cm^{-1} is clearly defined. The shoulder peak at 1584 cm^{-1} can be attributed to the styrene C=C stretch as stated in Table 1 for the PSMI NPs with no surface-functionalisation, while the peak at 1555 cm^{-1} is due to the primary amine attachment. The apparent increase in absorption intensity shown by the 6C functionalised NP spectrum in Figure 20 could thus possibly be partly as a result of the combined intensity of the peaks indicative of the amine and the styrene groups, and not necessarily be an indication of increased amine-functionalisation.

In Figure 21, a detailed study of the absorption region between 4000 cm^{-1} and 2000 cm^{-1} shows an increase in the intensity of the absorption peak at 2925 cm^{-1} (indicative of CH_2 stretching) as the length of the carbon chain of the diamine, and thus the amount of CH_2 linkages introduced, used for surface-functionalisation increased.

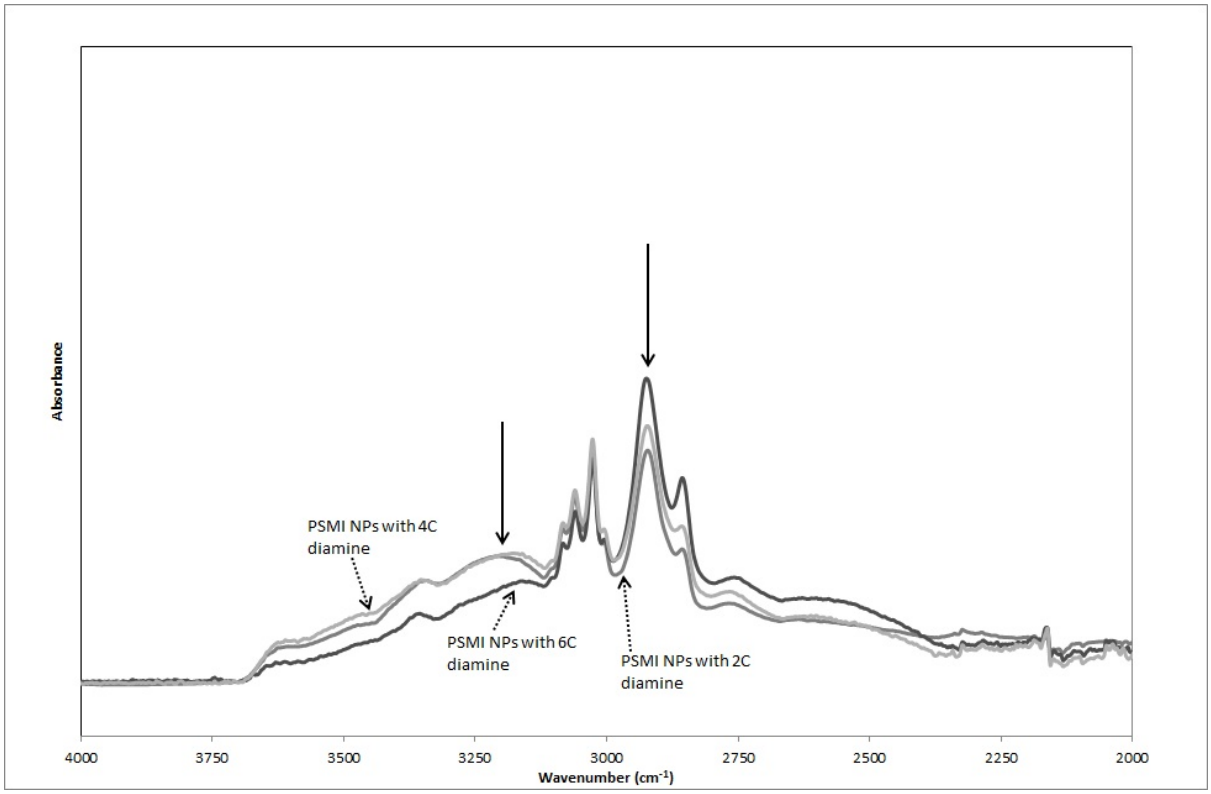

Figure 21: FTIR spectral comparison of PSMI NPs functionalised with 3 different diamine compounds with spectra overlapping and detail of the region between 4000 cm^{-1} and 2000 cm^{-1}.

The broad peak between 3600 cm^{-1} and 3100 cm^{-1} showed similar intensities for the 2C and the 4C functionalised PSMI samples, with reduced intensity upon functionalisation with the 6C diamine. As the characteristic peaks for both N-H stretching and O-H stretching fall within this broad peak it was difficult to conclude the exact reason for the decreased intensity. The reduced intensity could be attributed to more efficient surface-functionalisation achieved (and thus less unreacted O-H groups present), if one assumes that the O-H groups have a more pronounced affect than the N-H groups on the intensity of the broad peak between 3600 cm^{-1} and 3100 cm^{-1}.

Increases in the excess of 4C diamine and of 6C diamine used for surface-functionalisation were compared to determine whether larger excesses could increase the intensity of the amine peak seen in the FTIR spectra of the functionalised NPs. Figure 22 and Figure 23 show the comparisons between spectra of NPs functionalised with increasing molar excess of the 4C diamine and of the 6C diamine respectively.

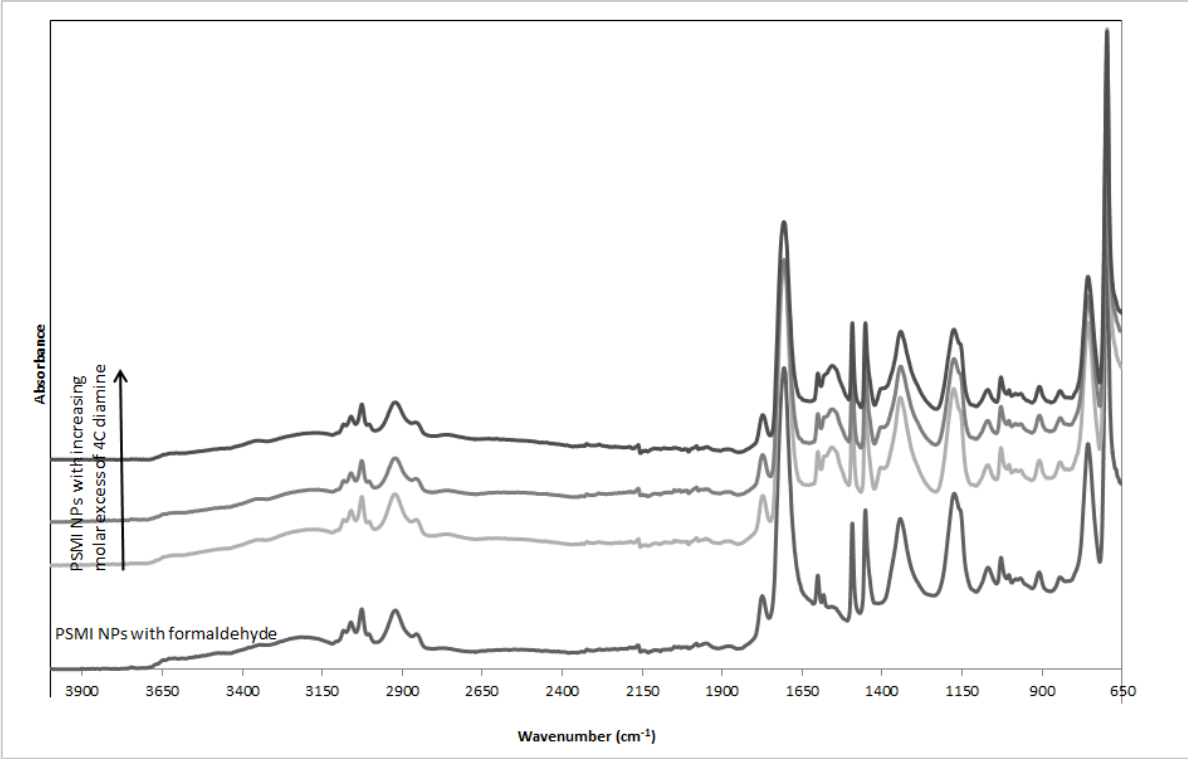

Figure 22: Comparison of FTIR spectra of samples functionalised with an increasing molar excess of 1,4-diaminobutane.

The surface-functionalisation had, as with the previous experiments, resulted in a new characteristic peak appearing at between 1558 cm^{-1} to 1555 cm^{-1} for all of the samples, along with the appearance of a small shoulder peak at about 1400 cm^{-1}. Increasing the molar excess of the 4C diamine used for surface-functionalisation did not result in a clear increase in intensity of the characteristic amine peak, but from Figure 23 it seemed that by increasing the 6C diamine molar excess a slight increase in the intensity of the amine-characteristic peak was achieved. Whether these increases in intensity relate to sufficiently

significant increases in amine groups on the NP surfaces to justify the use of extra reagent is however difficult to determine.

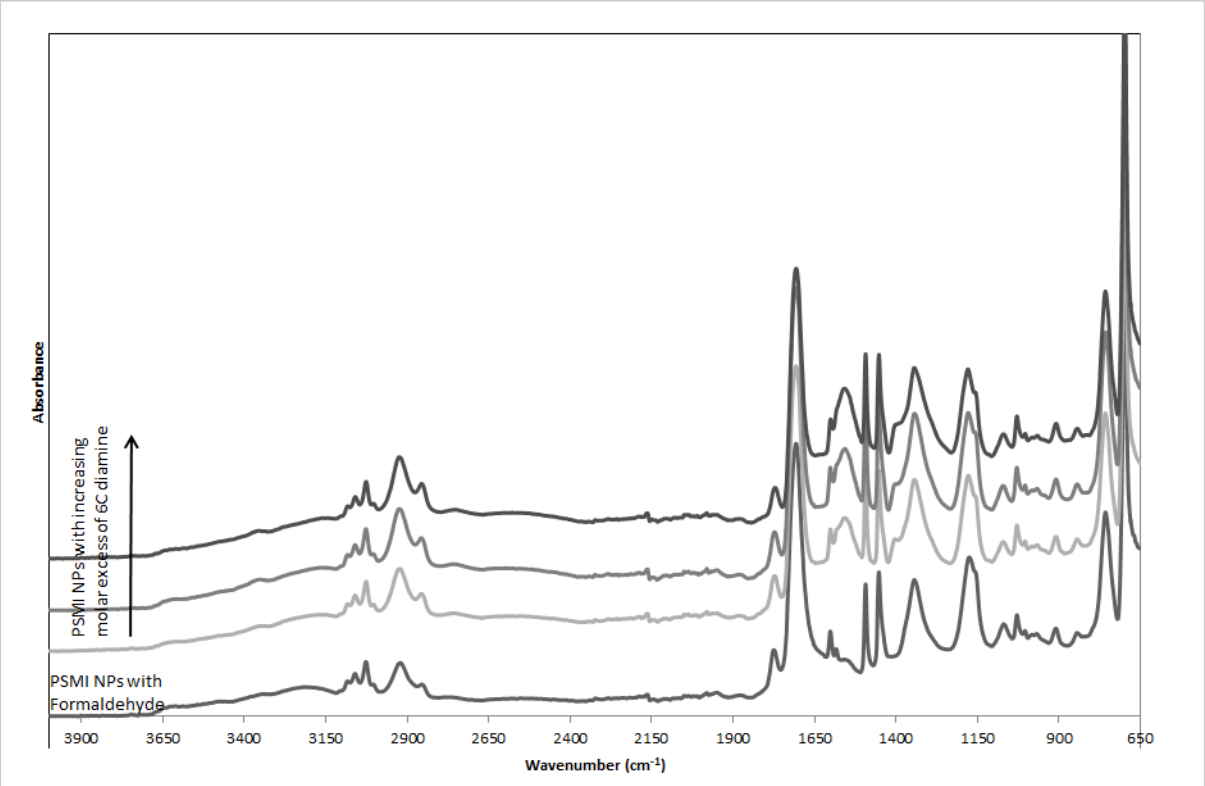

Figure 23: Comparison of FTIR spectra of samples functionalised with an increasing molar excess of 1,6-diaminohexane.

The amine surface-functionalised NPs retained suspension stability when stored, granted that the particle concentration was low enough. High particle concentrations resulted in agglomeration of stored NPs that could be reversed by agitation of the suspension. At comparable concentrations the 6C diamine-functionalised NP suspensions demonstrated a slightly higher viscosity compared to the completely fluid nature of the 2C and 4C functionalised samples.

The operating window as defined by the minimum excess of formaldehyde and of diamine required in order to avoid crosslinking varied from batch to batch of synthesised particles. This could be explained by variations in particle size distributions among batches, leading to

equivalent mass samples displaying either larger or smaller surface areas for surface-functionalisation. The minimum molar excess of formaldehyde and diamine needed for surface-functionalisation would thus have to be re-calculated for every new batch of NPs used.

Conservative estimates regarding the amounts of reagents required per volume of NP suspension to be functionalised were determined after reviewing and comparing the amounts of formaldehyde and diamine compounds used to successfully functionalise various batches of PSMI NPs. These estimates are recommended as a (maximum) starting point for surface-functionalization of new batches of PSMI NPs, to be followed by optimisation of reagent use per NP batch as determined by individual size range distributions.

The values are as follows:

- 1.7 mL of a 38% formaldehyde solution per mL of dialysed PSMI suspension
- 0.121 mL of EDA per mL of formaldehyde functionalised PSMI
- 0160 g of 4C diamine per mL of formaldehyde functionalised PSMI
- 0.211 g of 6C diamine per mL of formaldehyde functionalised PSMI

3.4.1.3 Dye-loading variation and varying degrees of imidisation

Increased dye loading

The standard particle formulation given in Section 3.2.2 *Synthesis of PSMI nanoparticles* was adjusted by increasing the amount of Exalite 613 added to the reaction mixture in the reactor during particle synthesis. The increased dye loading resulted in a NP suspension with increased colour intensities, as seen in Figure 24.

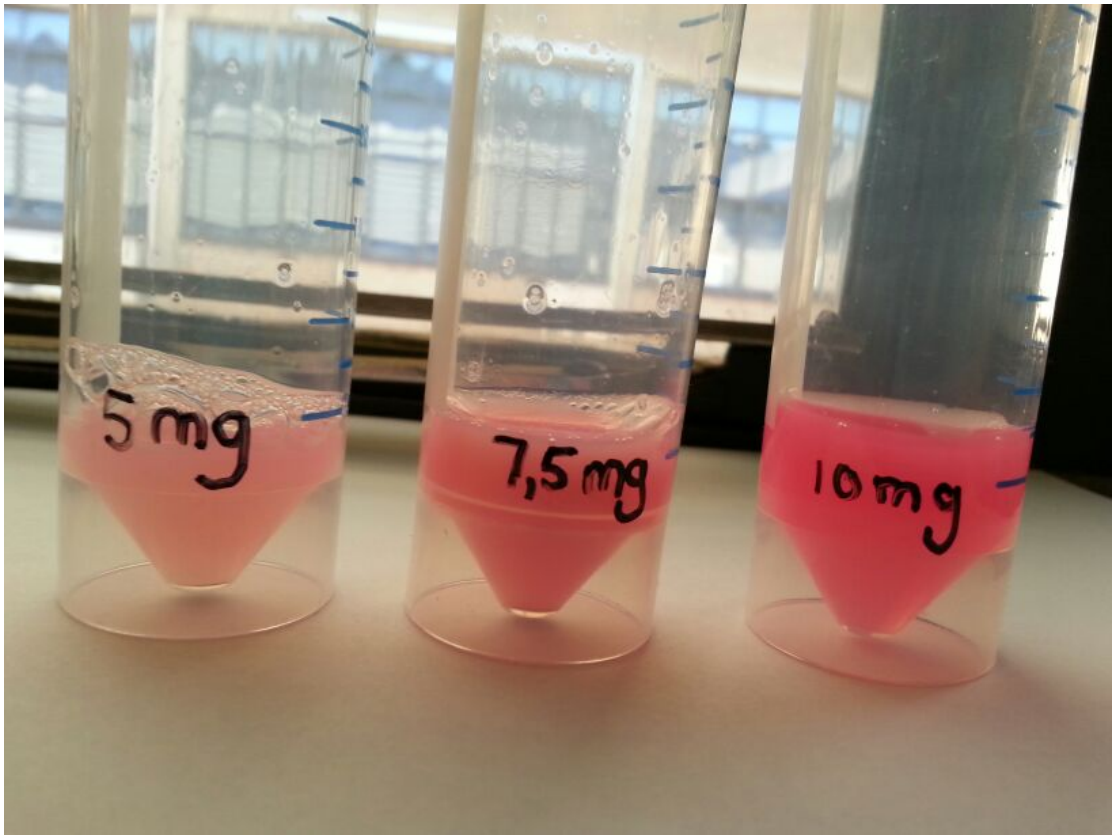

Figure 24: Differences in colour intensities of increased dye loaded NP suspensions from 5 mg per 20 g of PSMA (standard formulation) to 10 mg dye per 20 g PSMA inclusion.

It was observed that when dialysing the 5 mg dye-loaded PSMI suspension, the dialysis water remained colourless. The dialysis water for the 7.5 mg and the 10 mg dye loaded particle suspensions however appeared light pink, suggesting that non-encapsulated and possibly excess dye was washed from the NP suspensions during dialysis. It would also

suggest that the maximum dye loading for the standard particle formulation is between 5 mg and 7.5 mg of Exalite 613 per 20 g PSMA starting material.

PSMI particles were prepared in batches according to availability of the reactor required for particle synthesis. When comparing the FTIR spectra of the newly synthesised batches to that of previously synthesised batches with a standard dye loading of 5 mg, some changes were observed in the absorption region between 1560 cm^{-1} and 1510 cm^{-1} (Figure 25). The intensity of the peak in this region, when compared to that of the 1710 cm^{-1} imide peak, was especially high in the case of the 7.5 mg and 5 mg dye-loaded NPs.

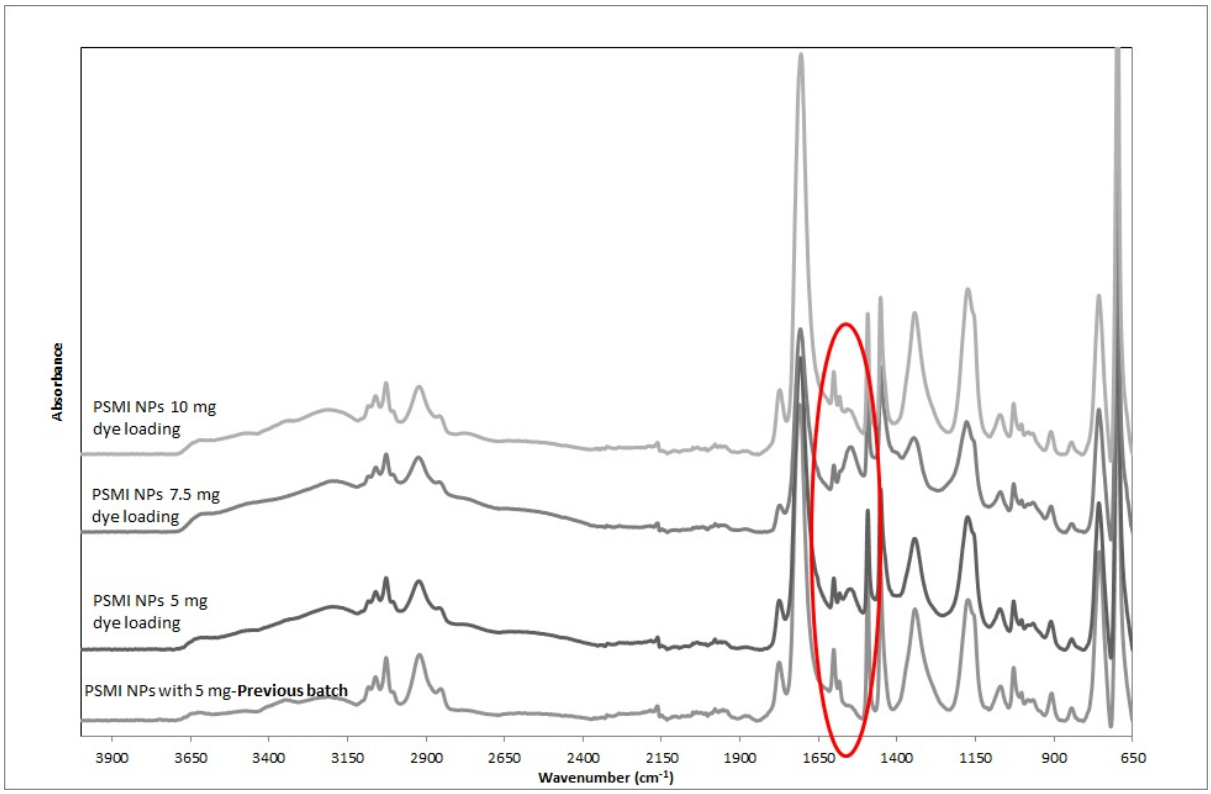

Figure 25: Comparison of the FTIR spectra of newly synthesised PSMI NPs with varied dye loadings (5 mg, 7.5 mg and 10 mg) with an FTIR spectrum of the standard formulation 5 mg dye loaded PSMI NPs of the initially synthesised batches.

Samyn and colleagues (2010) observed similar differences between the FTIR spectra of PSMI NPs dried from aqueous dispersion at pH>4 and that of PSMI NPs after precipitation

at pH<4. At the lower pH values, a definite absorption band in the region between 1580 cm^{-1} and 1520 cm^{-1} appeared, indicative of amide II, N-H bending (Samyn *et al*., 2010). The characteristic absorption peak at 1710 cm^{-1} had also split into multiple components, and a definite absorption band had appeared at 1412 cm^{-1}, explained as representative of amide stretching in polyamic acid (Samyn *et al*., 2010). The appearances of these peaks were, according to Samyn *et al*. (2010) indicative of the formation of amic acid moieties at lower latex pH. As previously shown in Figure 6, amic acid is the intermediate compound that forms when the maleic anhydride ring is opened (Structure I). The authors thus concluded that at a pH lower than 4, the conformation around the maleic anhydride groups as well as around the residual anhydride groups had changed. The authors also determined that the degree of imidisation of a NP suspension i.e. the success of conversion to imide moieties, could be correlated to the pH of the dispersion. They found that a pH approaching 7 led to a higher degree of imidisation as compared to a more acidic pH that resulted in a lower degree of imidisation (Samyn *et al*., 2010).

The pH values of the pristine and the dye-loaded PSMI NP suspensions, both initially and newly synthesised, were subsequently measured and are given in Table 2.

Table 2: Variation in pH for pristine and dye-loaded PSMI NP latexes initially and newly synthesised.

	Sample	pH
Initial batches	PSMI NPs-pristine	7.11
	PSMI NPs-5 mg dye-loaded	8.01
Newly synthesised batches	PSMI NPs-5 mg dye loaded	6.67
	PSMI NPs-7.5 mg dye loaded	6.54
	PSMI NPs-10 mg dye loaded	7.27

The initially synthesised PSMI suspension, with no dye added, had a pH of close to 7, while the dye-doped NP suspension showed an increased pH of about 8. The pH values

measured for the newly synthesised dye-loaded NP suspensions were all lower than that of the initially synthesised dye-loaded NPs, except for the 10 mg dye-loaded batch.

These pH results corroborated the increased absorption in the region characteristic to amic acid moieties shown by the 5 mg and the 7.5 mg dye-loaded NP FTIR spectra in Figure 25. It could thus be concluded that there existed definite variations between the NP batches shown in Figure 25 with regards to the degree of imidisation achieved.

The influence of dye-doping on pH was difficult to establish since pristine and dye-doped NP samples had to be prepared in different batches, possibly with varying degrees of imidisation. Any variations in pH between pristine and dye-doped PSMI NPs could thus be interpreted as either a result of dye-doping or due to different amounts of amic acid moieties present in the samples.

Varying degrees of imidisation were thus concluded to be the reason for the differences in peak intensities between the pristine and dye-doped NPs shown in Figure 12 in Section 3.4.1.1 *Pure PSMA, pure PSMI & dye-doped PSMI*, and not due to dye-doping. Comparison of the two spectra in Figure 12 in the absorption region between 1580 cm^{-1} and 1560 cm^{-1} showed higher intensity of absorption for the pristine than for the dye-loaded NPs, suggesting differences in the degree of imidisation achieved between the two samples.

A detailed comparison of the FTIR spectra of the NP batches shown in Figure 25 in the absorption region between 2000 cm^{-1} and 1000 cm^{-1} is shown in Figure 26. The 5 mg dye-loaded PSMI NPs synthesised initially (blue spectra) showed the lowest absorption intensity in the 1560 cm^{-1} to 1510 cm^{-1} region, with the newly synthesised 7.5 mg dye-loaded PSMI NPs (red spectra) showing the highest absorption in this region. The 7.5 mg dye-loaded NPs also showed the lowest absorption of all samples for the characteristic peaks at 1710 cm^{-1}, 1345 cm^{-1} and at 1177 cm^{-1}. As already mentioned, these three peaks are characteristic of stretching vibrations of the imide structure, and it could be reasoned that the lower intensity

of these peaks compared to the other samples showed a lower degree of imide content, suggesting a lower degree of imidisation achieved.

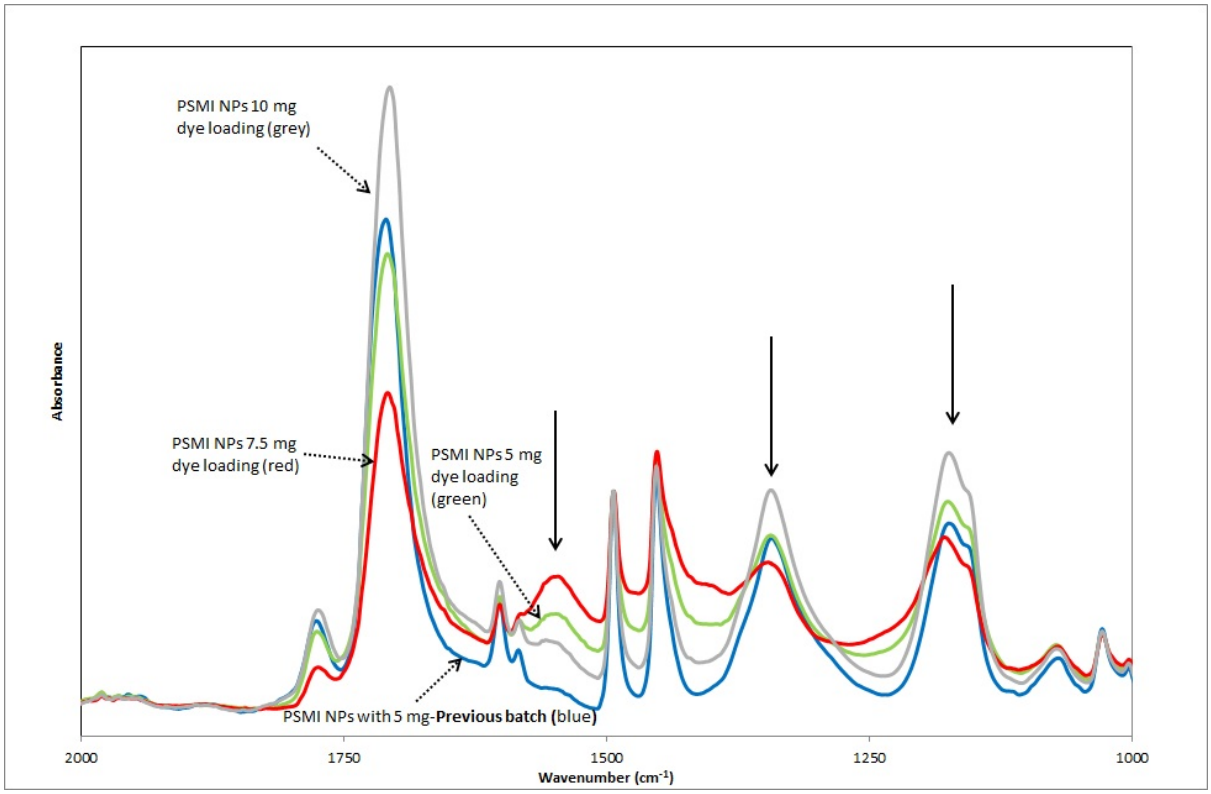

Figure 26: Comparison of the FTIR spectra of newly synthesised PSMI NPs with varied dye loadings (5 mg, 7.5 mg and 10 mg) with an FTIR spectrum of the standard formulation 5 mg dye loaded PSMI NPs of the initially synthesised batches, in the area between 2000 cm^{-1} and 1000 cm^{-1}.

The suggestion of a slight peak forming between 1400 cm^{-1} and 1415 cm^{-1} is also consistent with Samyn and colleagues' explanation of the presence of amide stretching of an acid compound, suggesting the presence of a higher degree of amic acid when compared with the other samples.

Comparison of the newly synthesised 5 mg dye-loaded NPs with the initially synthesised 5 mg loaded NPs showed good agreement between the intensities of the imide peaks at 1710 cm^{-1}, 1345 cm^{-1} and 1177 cm^{-1}. The newly synthesised 5 mg loaded NPs however showed higher intensity in the 1560 cm^{-1} to 1510 cm^{-1} region than the initial sample. Of the three

newly synthesised PSMI samples, the 10 mg dye-loaded sample showed the lowest intensity in the absorption region between 1560 cm^{-1} to 1510 cm^{-1}, combined with the highest intensity for the characteristic peaks at 1710 cm^{-1}, 1345 cm^{-1} and at 1177 cm^{-1} of all the samples.

When analysing the information given by the comparison of the FTIR spectra of the different NP suspensions with the pH values it could be concluded that the newly synthesised PSMI suspensions suffered from lower degrees of imidisation than the previously synthesised batches, except for the 10 mg dye-loaded sample. It could be concluded that the 7.5 mg dye-loaded sample most probably displayed the lowest degree of imidisation out of all the monitored samples, while the 10 mg dye-doped newly synthesised NPs showed higher degrees of imidisation more in-line with those of the initially synthesised batches. The differences in imidisation could be attributed to deviations in reaction conditions (such as temperature or pressure regulation in the reactor) during synthesis of the individual batches.

The FTIR spectra of the newly synthesised batches before and after surface-functionalisation were compared to determine if the varying degrees of imidisation of the various samples affected the surface-functionalisation process (Figure 27).

The spectra of the 5 mg dye-loaded NPs functionalised with the 2C, 4C and 6C diamines are shown in varying shades of green, and compared to the spectra of the 7.5 mg (spectra shown in shades of red) and the 10 mg (spectra shown in shades of grey) dye-loaded NPs functionalised with the different diamine compounds. It was observed that the difference in intensity between the amine characteristic peak introduced via surface-functionalisation and the intensity of the 1710 cm^{-1} imide characteristic peak were much smaller for the 5 mg and the 7.5 mg dye-loaded PSMI NPs than for the 10 mg dye-loaded NPs. When comparing the NPs of varied dye-loadings functionalised with the various diamine compounds in the region between 1595 cm^{-1} and 1550 cm^{-1}, it appeared that the intensity of the absorptions peaks of the 5 mg dye-loaded NPs were greater than those of the 7.5 mg dye-loaded NPs.

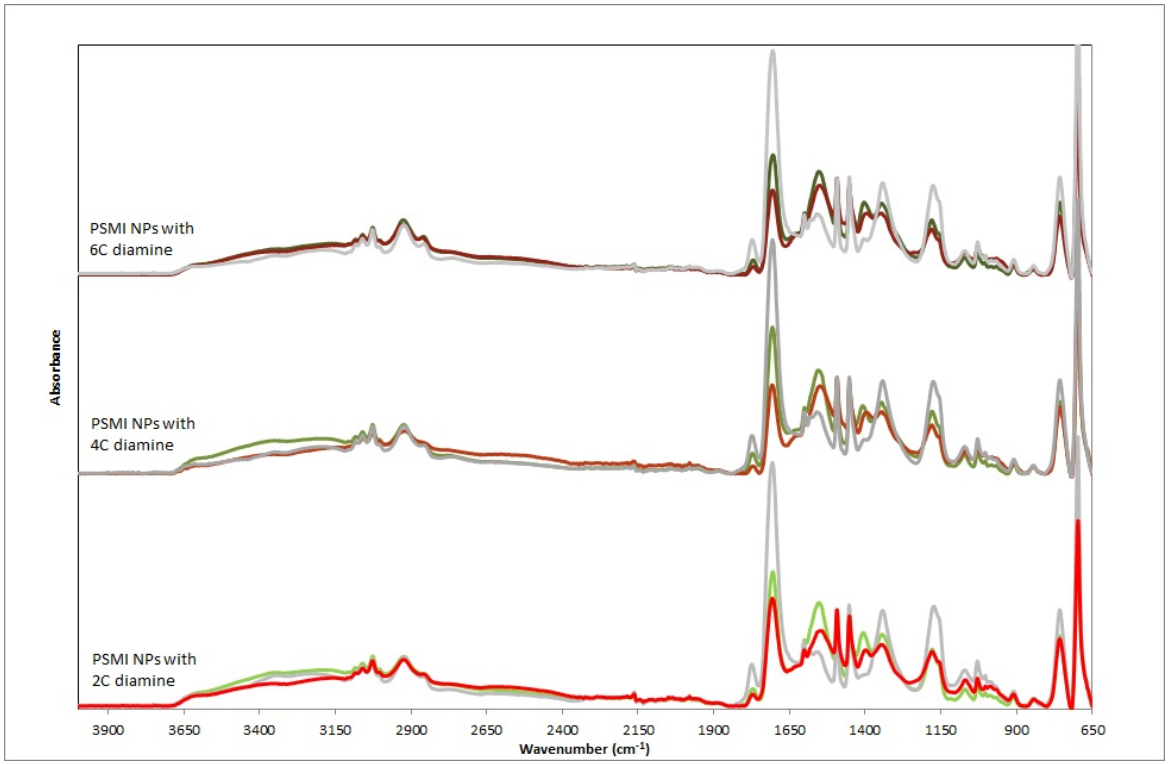

Figure 27: FTIR spectra of the newly synthesised PSMI NPs surface-functionalized with the 2C, 4C and 6C diamine compounds, comparing the surface-functionalisation for the 5 mg (shades of green), the 7.5 mg dye-loaded (shades of red) and the 10 mg dye-loaded NPs.

The 10 mg dye-loaded NPs showed the lowest intensity absorption in the stretching amine absorption region for functionalisation with all three of the diamine compounds. A more detailed inspection of the absorption area between 2000 cm^{-1} and 1000 cm^{-1} is shown in Figure 28.

As seen in Figure 26 with the non-functionalised PSMI NPs, the 10 mg dye-loaded functionalised sample in Figure 28 showed the lowest intensity in the absorption region between 1560 cm^{-1} to 1510 cm^{-1}, combined with the highest intensity for the characteristic peaks at 1710 cm^{-1}, 1345 cm^{-1} and at 1177 cm^{-1} of all the samples for all three of the diamine compounds used for functionalisation.

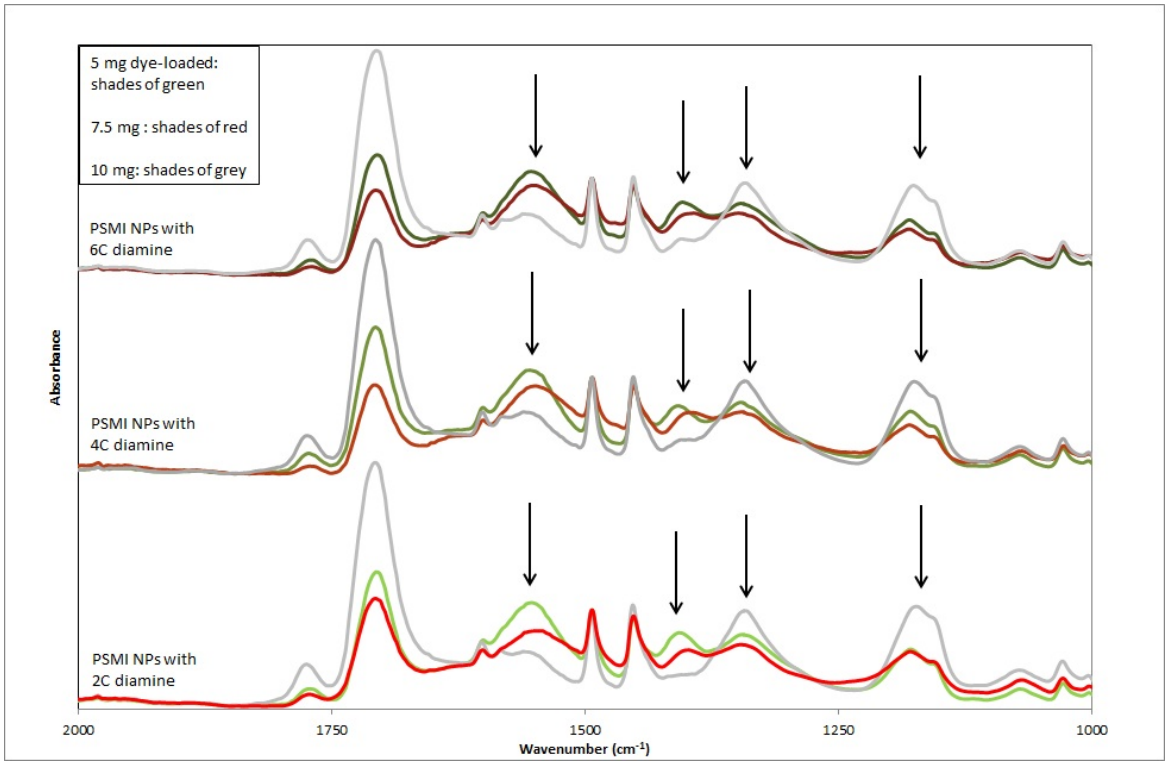

Figure 28: Detailed FTIR spectra of the samples shown in Figure 27 specific to the absorption region between 2000 cm^{-1} and 1000 cm^{-1}.

The 5 mg dye-loaded functionalised NPs showed the highest intensity of the three varied dye-loadings, in case of functionalisation with all three of the diamine compounds, in the absorption region between 1580 cm^{-1} to 1510 cm^{-1}. The absorption peak in this area for both the 5 mg and the 7.5 mg dye-loaded NPs displayed as a single peak, when compared to the same absorption region of the 10 mg dye-loaded NPs, where two peaks could be distinguished.

As discussed earlier, it is therefore difficult to determine to what extent the increased peak intensities seen for the 5 mg and the 7.5 mg dye-loaded NPs could be attributed to possibly more effective amine-functionalisation, or whether the increased intensities are simply as a result of overlapping peaks from the amine characteristic and the styrene characteristic absorption regions.

A closer inspection of the absorption area between 3800 cm^{-1} and 2800 cm^{-1} for the spectra compared in Figure 27 is given in Figure 29. For the 2C and the 4C diamine-functionalised NPs with varied dye loadings, the 5 mg dye-loaded NPs (green shaded spectra) showed the highest absorption intensity between 3600 cm^{-1} and 3400 cm^{-1} (in the amine absorption region). The 7.5 mg and the 10 mg dye-loaded NPs showed lower absorption intensities in this region for all three diamine compounds used for functionalisation, except for the 6C diamine functionalised NPs. Since the absorption peak at 2920 cm^{-1} is indicative of CH_2 groups in the backbone, successful functionalisation of aliphatic diamine compounds could also be indicated by an increase in absorption intensity of the 2920 cm^{-1} peak. The 2920 absorption peak for the 10 mg dye-loaded NPs showed comparable intensity to the 5 mg dye-loaded NPs when functionalised with 2C and 4C diamine compounds, despite showing lower absorption intensity between 3600 cm^{-1} and 3400 cm^{-1}.

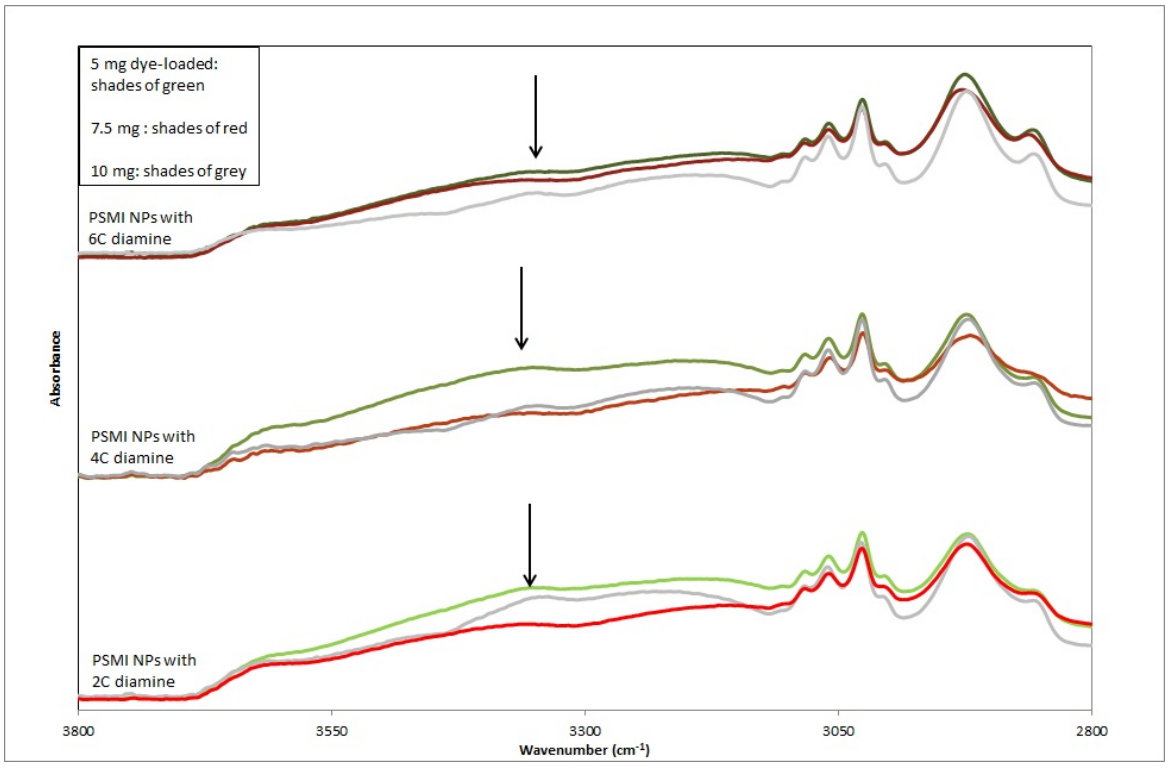

Figure 29: Detailed FTIR spectra of the samples shown in Figure 27 specific to the absorption region between 3800 cm^{-1} and 2800 cm^{-1}.

It is thus difficult to conclude to what extent the differences in degree of imidisation between the different dye-loaded PSMI NP batches influenced the surface-functionalisation of said PSMI NPs based on FTIR analysis alone. Increased degrees of bioconjugation of the amine surface-functionalised NPs with avidin and antibodies should serve as an indirect indication if any of the dye-loaded samples did indeed show significantly increased amine functionalisation. Preliminary conclusions based on the FTIR data shown do seem to indicate that the 5 mg dye-loaded NP suspension display more functionalised amine groups to be used as handles for bioconjugation compared to the 7.5 mg and the 10 mg dye-loaded samples.

3.4.2 TEM results

Samples of the PSMI NPs prepared (with and without dye) were studied with TEM. PSMI particles from the original batch as well as the newly synthesised particles were characterised. The sample preparation method that was followed is listed in Section 3.3.2 *Transmission Electron Microscopy (TEM)*.

3.4.2.1 TEM results: Originally synthesised nanoparticles

PSMI NPs (from the original batches) without dye, before surface-functionalisation are shown in Figure 30. The particles appeared to be spherical in shape, and ranged in size between 20 and 70 nm, although it could be observed that the particles were bimodal with smaller particles ranging between 20-30nm and larger particles of particle size between 50-60nm.

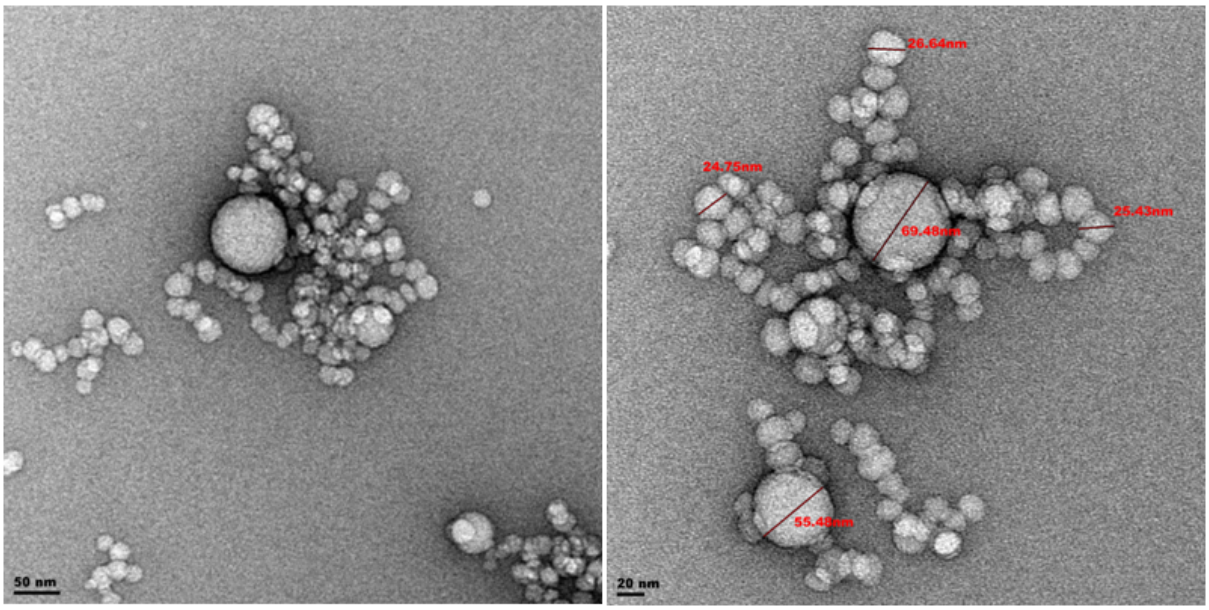

Figure 30: PSMI NPs without dye before surface-functionalisation.

The samples of NPs inspected after surface-functionalisation with formaldehyde and 2C diamine are shown in Figure 31. The particles were still spherical in shape, and the bulk of the particles viewed seemed to be about 20 nm in size.

When comparing Figure 30 and Figure 31 it would seem that as expected, the process of surface-functionalisation did not alter the size or shape of the particles. The particles in Figure 31 also seemed to be better dispersed than those of the non-functionalised sample. This could be explained by the fact that the surface functionalisation process diluted the particle suspension after every step as more liquid was introduced to the original NP suspension sample. High concentrations of particles in suspension should thus not be confused with irreversible (chemical) agglomeration.

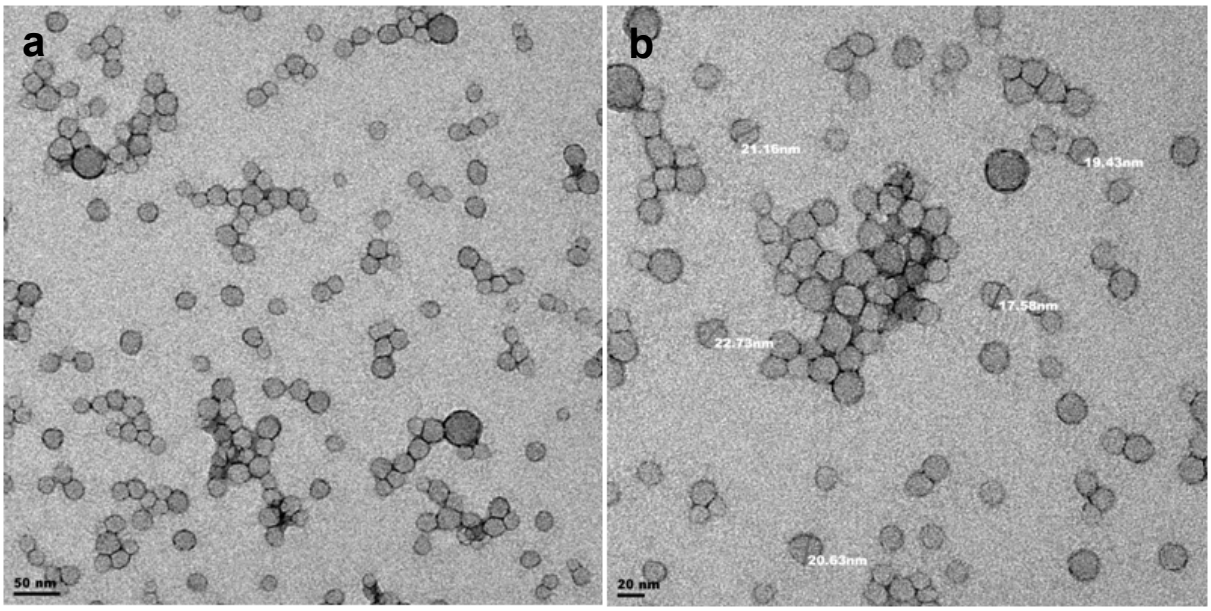

Figure 31: PSMI NPs without dye after surface-functionalisation with a) formaldehyde and b) 2C diamine.

In Figure 32, PSMI particles loaded with Exalite 613 dye are shown. The particles, as with those without dye added, were spherical in shape and seemed to be about 20 to 30 nm in size, with a few larger particles also present.

From these images it could be concluded that the addition of the dye to the reactor did not disrupt the process of particle formation or noticeably increased the size of the particles.

In Figure 33 the dye-encapsulated particles are shown after having been surface-functionalised with formaldehyde. Similar to the comparisons between Figure 30 and Figure

31, it would seem that when comparing Figure 32 and Figure 33 it could be concluded that the surface-functionalisation process (or at least the first step of the process) did not alter the size or the shape of the particles significantly, and that the average particle size of formaldehyde surface-functionalised NPs with dye encapsulated was around 20 to 30 nm with a few larger outliers present.

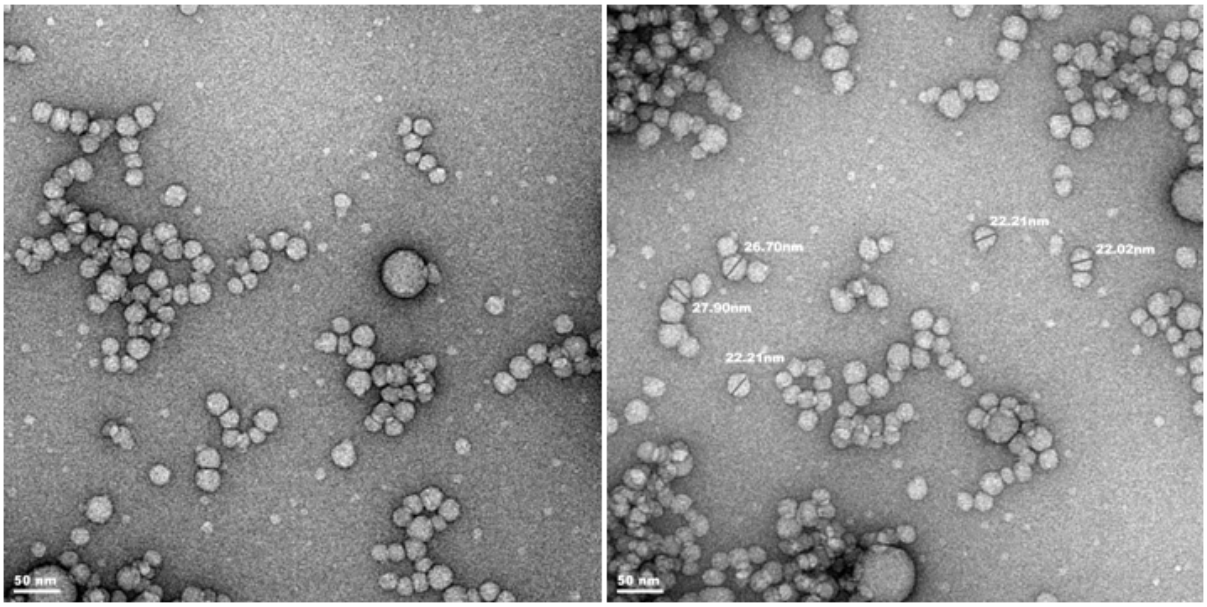

Figure 32: PSMI NPs with 5 mg of Exalite 613 dye encapsulated before surface-functionalisation.

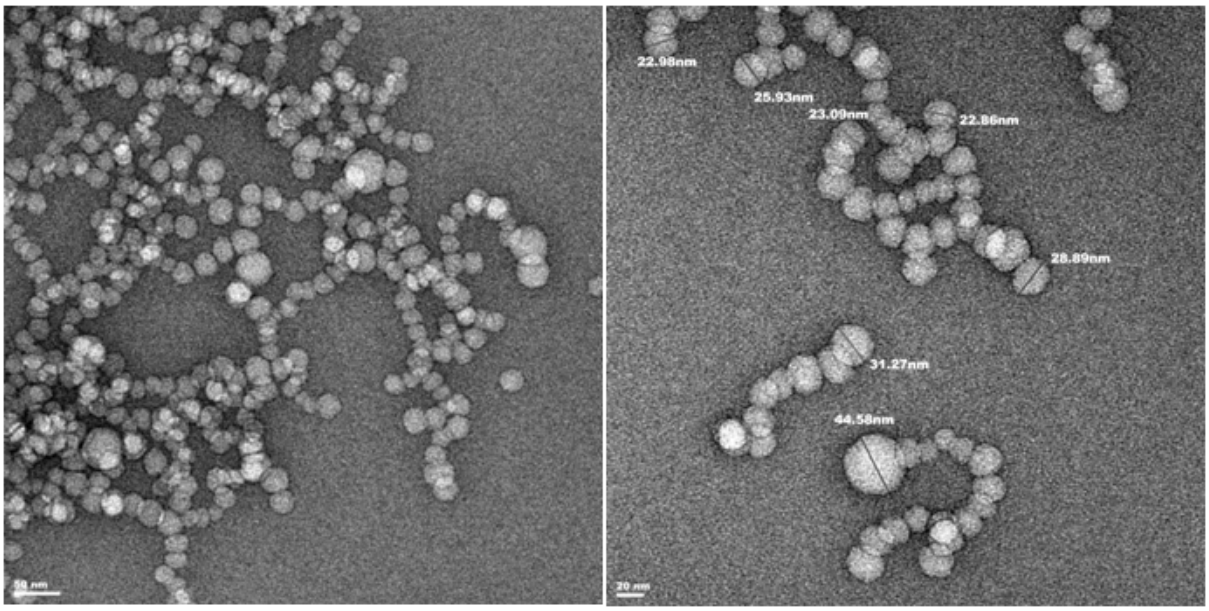

Figure 33: PSMI NPs with a loading of 5 mg of Exalite 613 encapsulated after surface-functionalisation with formaldehyde.

3.4.2.1 TEM results: Newly synthesised PSMI nanoparticles

The newly synthesised NP batches were also imaged. The increasing dye loadings of 5 mg, 7.5 mg and 10 mg are shown in Figure 34, Figure 35 and Figure 36, respectively.

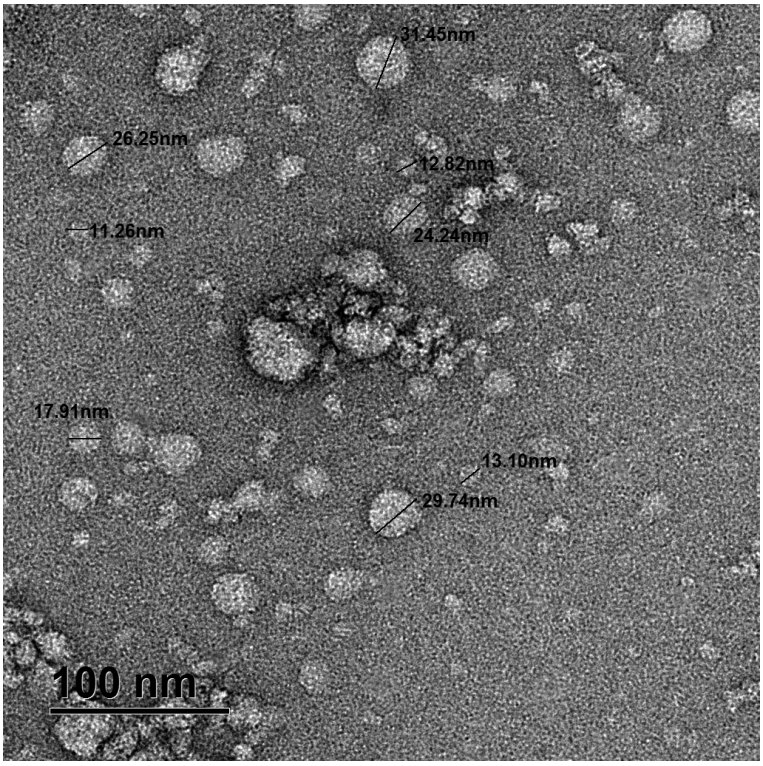

Figure 34: Newly synthesised pure PSMI NPs with a dye loading of 5 mg per 20 g of PSMA.

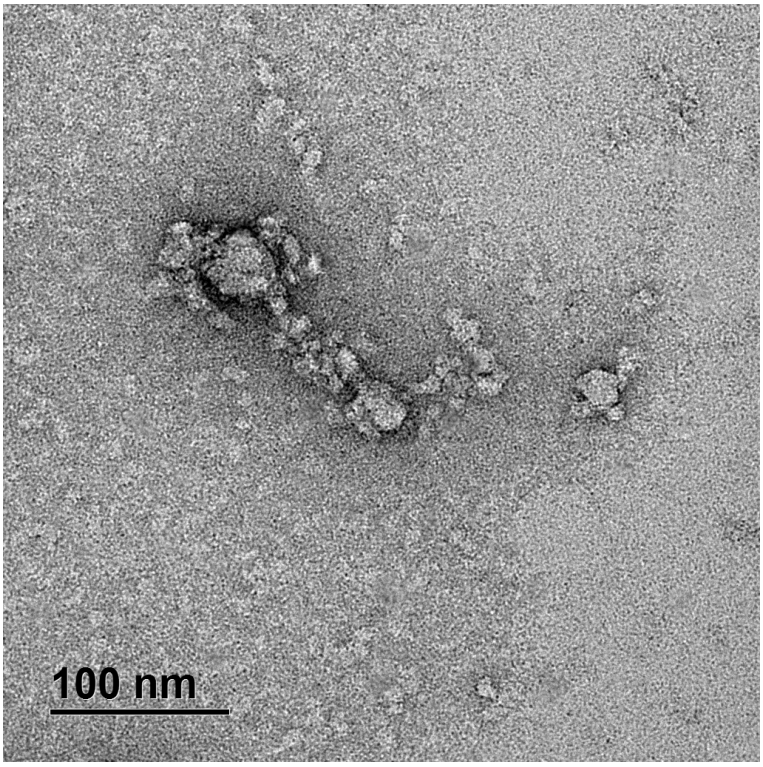

Figure 35: Newly synthesised pure PSMI NPs with a dye loading of 7.5 mg per 20 g of PSMA.

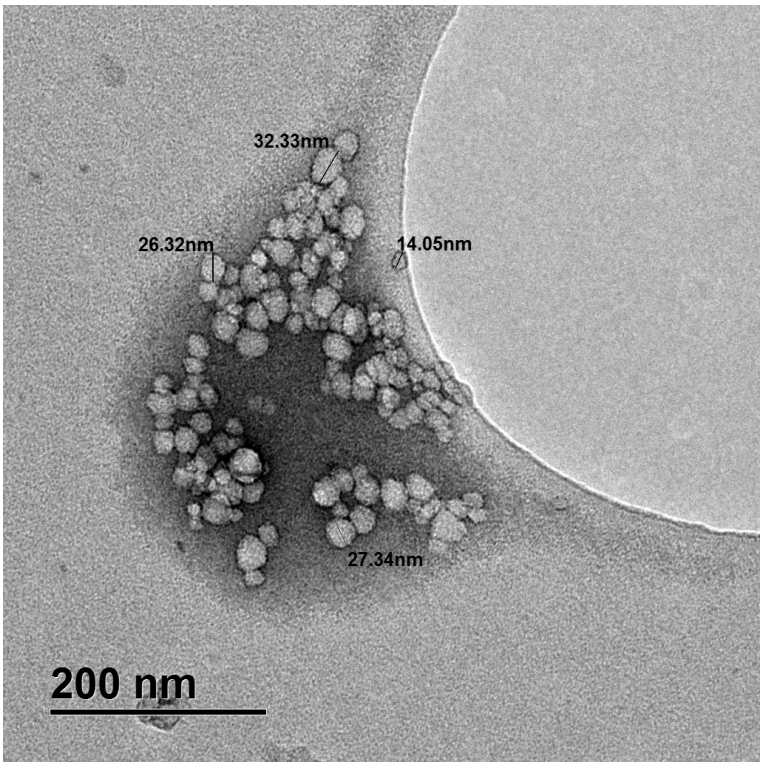

Figure 36: Newly synthesised pure PSMI NPs with a dye loading of 10 mg per 20 g of PSMA.

The TEM images show that NPs were successfully formed despite the lower degrees of imidisation experienced. Difficulties in obtaining clear images were experienced (at both the UCT and the CSIR characterisation facilities) due to the low contrast given by the PSMI material as well as to a lack of robustness in the sample preparation method. It was found to be extremely difficult to repeatedly prepare the TEM disk with an optimum coating of NPs in order to provide well dispersed NPs in a single layer for imaging.

It did however seem that the size distributions of the PSMI NPs with lower degrees of imidisation contained more NPs of smaller particle sizes (< 20 nm) when compared to the size distributions of the initial PSMI NPs with higher degrees of imidisation shown in Figure 30, Figure 31, Figure 32 and Figure 33. Samyn *et al.* (2010) however found that NP dispersions with higher degrees of imidisation contained smaller NPs on average than dispersions with lower degrees of imidisation. The supposed presence of smaller NPs for batches with lower degrees of imidisation is thus most likely more of an exception than a norm and due to sampling variability.

The PSMI NPs with a 7.5 mg dye loading shown in Figure 35 also appeared to include more irregularly shaped particles when compared with the other samples. These irregularities in NP morphology could also be attributed to agglomeration of NPs but that is not clearly visible due the low contrast achieved with the TEM imaging. The FTIR spectra comparison of the newly synthesised PSMI NPs with varied dye loadings in Figure 25 seemed to indicate a lower degree of imidisation for the 7.5 mg batch than reached by the 5 mg or the 10 mg dye loaded NPs. This lower degree of imidisation is a possible explanation for the more ‘irregularly shaped NPs’ seen in Figure 35 as it is known that higher degrees of imidisation lead to more inert and better dispersed NPs and vice versa for batches with lower degrees of imidisation.

3.4.4 Surface charge

The surface charge of the PSMI NPs was measured via photon correlation spectroscopy. The pure PSMI NPs possessed high negative surface charges that were consistently measured at approximately -68 mV, similar to the range of -60 to -55 mV as reported by Samyn and colleagues (2010). These high negative surface charges were not affected by the dye loading (a charge of -67.8 ± 1.3 was recorded), providing further evidence that the Exalite dye was successfully encapsulated into the NPs and not simply passively adsorbed on the NP surfaces.

Surface-functionalisation of the PSMI NPs with the 3 different diamine compounds resulted in decreases in the high negative surface charge of the pure PSMI NPs. The results are shown in Table 3. The reduction in high negative surface charge was as expected, as the NPs were functionalised with positively charged amine groups.

Table 3: Comparison of surface charge of NPs functionalised with increasing chain length diamine compounds.

Sample	Zetapotential (mV)
PSMI NPs	-59.1 ± 0.907
PSMI NPs with 2C diamine	-44.5 ± 0.866
PSMI NPS with 4C diamine	-31 ± 0.757
PSMI NPs with 6C diamine	-25.1 ± 0.404

From the results given in Table 3 it was also clear that the high negative surface charge of the pure PSMI NPs was increasingly reduced as the chain length of the diamine used for surface-functionalisation was increased.

As mentioned in the experimental section, the surface charge of the particles was measured by diluting the samples in deionised water to a 1% v/v solution, with the surface charge measured at the in situ pH of the dilution. The pKa values of the three diamine compounds are given in Table 4.

Table 4: pKa values for the three different aliphatic diamines used for surface-functionalisation.

Compound	pKa1	pKa2
2C diamine	9.9	6.9
4C diamine	10.8	9.6
6C diamine	11.02	10.7

The pKa values for the three compounds increase as the diamine carbon chain length of the compounds increase, indicating an increase in basicity of the amine compound, and the higher the required solution pH for the conjugate acid (i.e. R-NH3^{+}) to become fully deprotonated. It must be noted that in order to simplify this explanation, the dissociation behaviour of the diamine compounds will be discussed with reference to the individual compounds, assuming that any dissociation effects resulting from interaction between the compound and the hydrolysed PSMI matrix are similar for all three compounds.

Based on the increasing pKa values associated with the increasing carbon chain lengths of the three diamine compounds, it could be concluded that at a given pH value of e.g. 7, there will be a larger fraction of protonated positively charged amine groups on the 6C diamine compared to the 4C and 2C diamines respectively and similarly the 4C diamines will be more protonated than the 2C functionalised compound. The higher the degree of protonation, the more R-NH_3^+ groups are present, thereby increasing the positive charge. In the case of PSMI surface-functionalised with these compounds, this would translate into more positively charged ions present (increasing in number with the increase in carbon chain length of the compound used for functionalisation) that would interact with and reduce the inherently high negative surface charge of the non-functionalised NPs. This explains the decrease in negative surface charge of the NPs when functionalised with diamine compounds of increasing pKa values.

Since the NPs were synthesised and functionalised for the purpose of use with bacteria it was decided to test the surface-functionalised (newly synthesised, with a 5 mg dye-loading)

PSMI NPs for surface charge in PBS at an adjusted pH value of 7.4. The results are given in Table 5.

Table 5: Zetapotential values for surface-functionalised NPs at pH 7.4.

Sample	Zetapotential (mV)
	pH = 7.4
PSMI NPs with 2C diamine	-28.8 ± 0.208
PSMI NPS with 4C diamine	-32.3 ± 0.814
PSMI NPs with 6C diamine	-33.5 ± 1.16

The results indicated that the surface charge of the diamine-functionalised NPs could be expected to be around -28 to -33 mV when used in a PBS buffer, as would be the case when bioconjugating the NPs for antibody attachment. The NPs should thus still be stable as a suspension for the bioconjugation process as NP stability is widely accepted to be associated with surface charges of greater than 30 mV or less than -30 mV.

3.4.5 Thermal analyses

The effects of the surface-functionalisation in terms of the thermal properties of the PSMI NPs were monitored via differential scanning calorimetry (DSC). The effect of surface-functionalisation on the glass transition temperature (T_g) of the initially synthesised NPs is shown in Table 6.

Table 6: Effect of surface-functionalisation on the glass transition temperature (n=3) of initially synthesised PSMI NPs.

Sample	T_g (^{0}C)	
	Pristine	Dye Loaded
PSMI NPs	179 ± 1.7	183 ± 0.5
PSMI NPs after formaldehyde modification	191 ± 0.9	192 ± 1.1
PSMI NPS after 2C diamine modification	191 ± 2.1	190 ± 0.8
PSMI NPS after 4C diamine modification	190 ± 0.2	Not measured
PSMI NPS after 6C diamine modification	183 ± 1.0	Not measured

A T_g of 181 °C for PSMI NPs dried from aqueous suspension was reported by Samyn *et al*. The T_g of the pristine PSMI NPs was found to be 179 ± 1.7, as shown in Table 6, which agreed well with the published value. Upon surface-functionalisation with formaldehyde, the T_g increased to 191 ± 0.9, and with subsequent 2C diamine-functionalisation a T_g value of 191 ± 2.1 was recorded.

When comparing the different surface-functionalisation steps for the pristine NPs, it was found that the increase in T_g caused by the surface-functionalisation was statistically significant according to a student's t-test with p-values of 0.009 and 0.021 when comparing the PSMI NPs with the formaldehyde-functionalised and the 2C diamine-functionalised PSMI NPs respectively to the pure PSMI NPs (not functionalised). The same trends could be observed for the dye-loaded NPs with p-values of 0.0019 and 0.0009 reported when comparing dye-doped PSMI NPs with their formaldehyde-functionalised and diamine-functionalised counterparts.

Statistical comparisons between the pristine and dye-loaded NPs samples showed no significant differences between the pristine and dye-loaded NPs, between the pristine and dye-loaded PSMI NPs with formaldehyde and between the pristine and dye-loaded PSMI NPs functionalised with the 2C diamine (p-values of 0.065, 0.273 and 0.282 respectively). It can thus be concluded that the inclusion of dye into the NPs did not alter the thermal properties of the NPs.

Thermal analyses of the 4C and 6C functionalised NPs (pristine) showed average glass transition temperatures of 190 ± 0.2 and 183 ± 1.0 ºC respectively. The change in T_g upon functionalisation with the 4C diamine was found to be a statistically significant (p=0.006) increase when compared to the pure NPs, similarly to functionalisation with the 2C diamine. A statistical comparison showed a significant difference in T_g between the 2C and 4C diamine-functionalised NPs versus the 6C diamine-functionalised NPs with p-values of 0.028 and 0.009 recorded respectively. The reduced T_g measured for the 6C diamine-functionalised samples could theoretically lead to the NPs becoming 'softer' (as higher T_g values indicate higher resistance to thermal softening) and thus increasing the risk of NP agglomeration. The T_g of the 6C diamine-functionalised NPs however was still comparable with the pure NPs (before surface-functionalisation).

The increase in T_g after NP functionalisation with formaldehyde from 179 ºC to 191 ºC could be attributed to the effective replacement of the H atom of the maleimide ring with a hydroxyl group terminated structure. Fernandez-Garcia and colleagues (2000) found that when converting poly(ethyl methacrylate) to poly(ethyl α-hydroxymethacrylate), an increase in T_g of 18 K was observed. This was ascribed to the inter- and intramolecular interactions between the newly introduced hydroxyl groups (Fernandez-Garcia *et al.*, 2000). The increase in T_g caused by the functionalisation of the PSMI NPS with formaldehyde could thus be due to inter- and intramolecular hydrogen bonding of the hydroxyl groups introduced during surface-functionalisation (Lange & Meijer, 1995), although the strong hydrogen-bonding N-H of the original maleimide disappears in this process.

The lack of statistical difference between the formaldehyde-functionalised and the 2C and 4C diamine-functionalised NPs showed that the addition of the diamine and the subsequent loss of the hydroxyl group did not negate the increase in T_g caused by the formaldehyde-functionalisation. In 2005 Allen & Ishida prepared polybenzoxazines using diamines of varying aliphatic chain length, and subsequently observed a dependence of the measured T_g on aliphatic chain length (Allen & Ishida, 2005). They found that as the length of the flexible aliphatic chain increased, the T_g of the material decreased. This phenomenon was also shown in methlacrylates (Godard & Saiter, 1998) and copolymers of *N*-substituted maleimides (Dörr et al., 1998).

The statistical decrease observed in the T_g when functionalising the PSMI NPs with the 6C diamine compared to the 4C and the 2C diamines could thus be explained as a function of the influence the flexible aliphatic chain had on the T_g. Functionalisation with the 6C diamine introduced a critical aliphatic chain length with sufficient flexibility to cause a significant decrease in the T_g when compared to the 2C and the 4C diamine functionalised NPs.

Unfortunately the T_g values for the initially synthesised dye-doped NPs functionalized with the 4C and the 6C diamine compounds were not recorded. Possible confirmation of the trend seen with the pristine NPs initially synthesised and functionalised with the 4C and 6C diamine compounds were determined by T_g measurements of the newly synthesised dye-doped NPs. The glass transition temperatures recorded for the initially synthesised dye-doped NPs were firstly compared to those of the newly synthesised NPs (not surface-functionalised) with varying dye-loadings. The results are shown in Table 7.

The T_g of the initially synthesised NPs corresponded well with that of the newly synthesised 10 mg dye-loaded NPs, while the T_g values determined for the newly synthesised 5 mg and 7.5 mg dye-loaded NPs were 8 to 9 degrees lower. As mentioned in the literature review, PSMA is imidised in order to provide improved heat resistance via the replacement of maleic anhydride groups with a maleimide groups.

Table 7: Comparison of the T_g of initial and newly synthesised dye-doped PSMI NPs.

Sample	T_g (^{0}C)
Initially synthesised PSMI NPs, 5 mg dye-loaded	183 ± 0.5
Newly synthesised NPs, 5 mg dye-loaded	175 ± 0.4
Newly synthesised NPs, 7.5 mg dye-loaded	174 ± 0.4
Newly synthesised NPs, 10 mg dye-loaded	183 ± 0.1

It could thus be concluded that a lower T_g value would indicate a lower degree of conversion from maleic anhydride groups to maleimide groups, thus a lower degree of imidisation achieved. The lower T_g values recorded for the newly synthesised 5 mg and 7.5 mg dye-loaded NPs thus supports the FTIR and pH measurement results given in Section 3.4.1.3 *Dye-loading variation and varying degrees of imidisation* whereby it was concluded that the newly synthesised 5 mg and 7.5 mg dye-loaded batches had lower degrees of imidisation than the initially synthesised NPs as well as the newly synthesised 10 mg dye-loaded NPs.

The T_g values of surface-functionalised newly synthesised NPs loaded with 5 mg and 10 mg were measured. In both cases functionalisation with formaldehyde led to significant increases in T_g when compared to the non-functionalised PSMI NPs, as shown in Table 8.

Table 8: T_g values recorded for newly synthesised dye-doped PSMI NPs functionalised with formaldehyde and 6C diamine compound.

Sample	T_g (^{0}C)	
	5 mg dye-loaded	**10 mg dye-loaded**
PSMI NPs	175 ± 0.4	183 ± 0.1
PSMI NPs with formaldehyde	186 ± 0.3	190 ± 0.1
PSMI NPS with 6C diamine	187 ± 0.5	190 ± 0.8

The T_g values recorded for the 2C and 4C functionalised PSMI NPs were similar to that of the formaldehyde-functionalised NPs, similar to the results shown in Table 6.

Functionalisation with the 6C diamine compound however did lead to a significantly reduced T_g when compared to the formaldehyde-functionalised equivalent NPs, as was seen with the initially synthesised functionalised pristine NPs. As the initial decrease in T_g upon 6C diamine surface-functionalisation could be explained by the addition of flexible aliphatic carbon chains of a certain length, the absence of such decreases in T_g for different batches of 6C diamine-functionalised NPs could be reasoned to be an indication of less 6C aliphatic diamine chains functionalised onto the NP surfaces than before. These variances between the T_g values for different batches of 6C functionalised NPs thus seemed to indicate that the T_g of samples could be used to give an indication of the degree of successful amine surface-functionalisation achieved for functionalisation with the 6C diamine compound.

3.4.6 Fluorescence of dye-loaded nanoparticles

The normalised absorption and emission spectra for free Exalite 613 dye are shown in Figure 37. The maximum absorption was observed at 569 nm while the maximum emission occurred at 599 nm (dissolved in acetone). These values correspond well with what was given by the manufacturer of the dye, namely maximum absorption (when dissolved in methylene chloride) at 575 ± 1 nm and a maximum emission at 609 ± 3 nm. The wavelength at which maximum emission occurred did not change whether excitation was performed at 569 nm or at 400 nm.

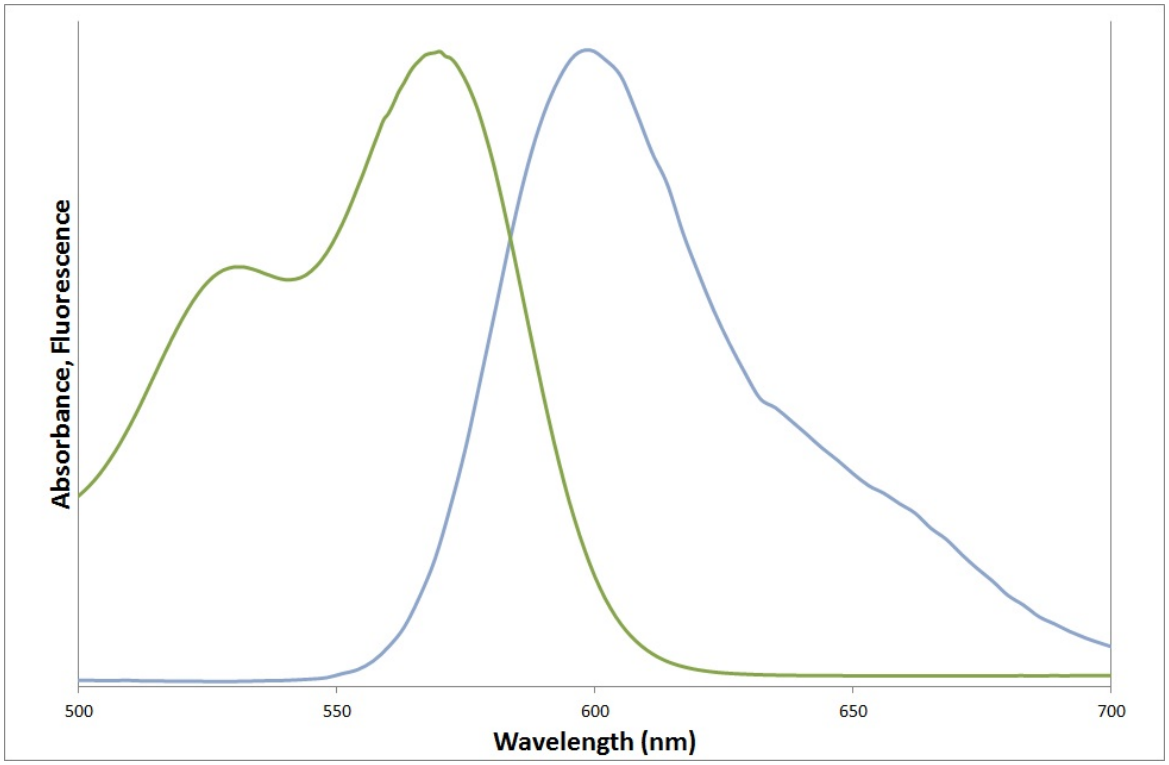

Figure 37: The absorption and emission profiles of Exalite 613 dye when dissolved in acetone.

Fluorescence emission intensity was measured for serial dilutions of the free Exalite 613 dye as well as for the three different dye-loaded NPs. A linear relationship between free dye concentration and emission intensity was established at free dye concentrations of 0.0001 mg/mL or lower, as seen in Figure 38. The three different concentrations of dye-loaded NPs showed linear relationships between NP concentration and emission intensity at less than 0.4 to 1 mg/mL, as shown in Figure 39. The data were fitted with linear regression curves.

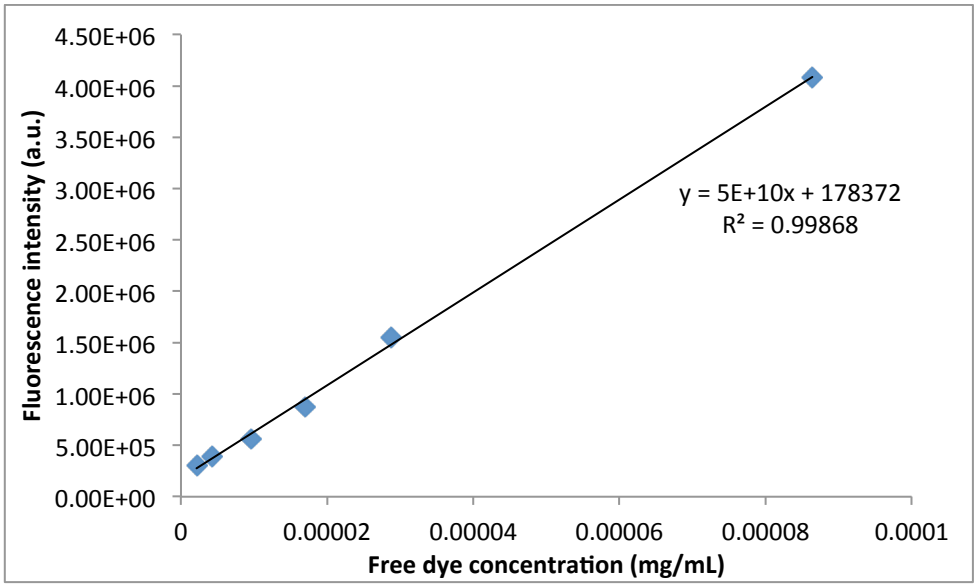

Figure 38: Relationship between free Exalite 613 dye concentration and emission intensity.

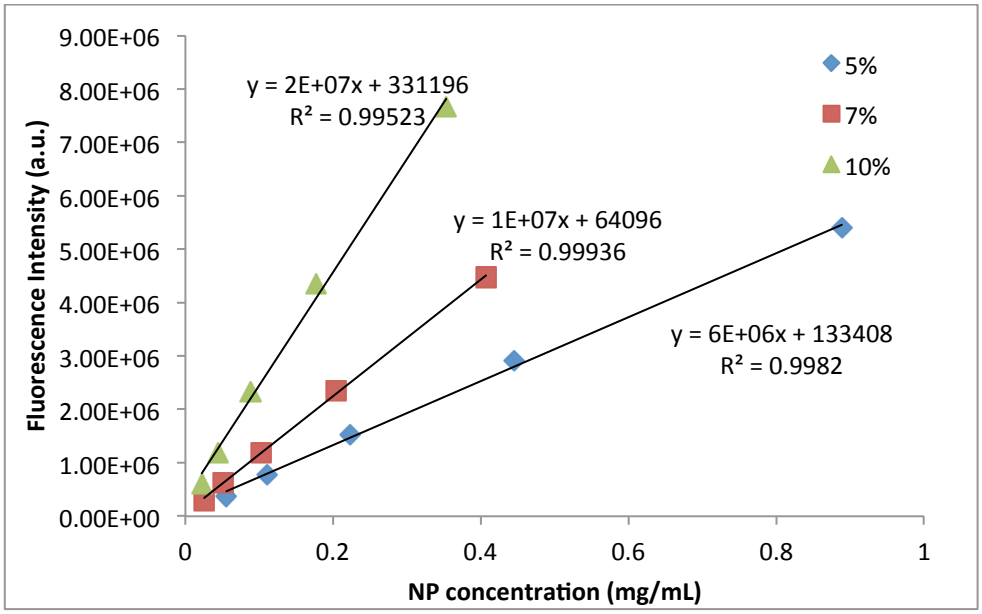

Figure 39: Relationships between NP concentration and emission intensity for PSMI NPs with 3 different dye-loadings of 5 mg, 7.5 mg and 10 mg.

The free dye molecules showed very high fluorescence intensity at very low concentrations. The data shown in Figure 39 suggested that for a similar NP concentration the 10 mg dye loaded NPs would give the highest fluorescent intensity while the 5 mg dye-loaded NPs would give the lowest fluorescent signal. This was confirmed when directly comparing the

emission profiles of the three different dye-loaded NPs at a similar concentration of 0.3 mg/mL, as shown in Figure 40.

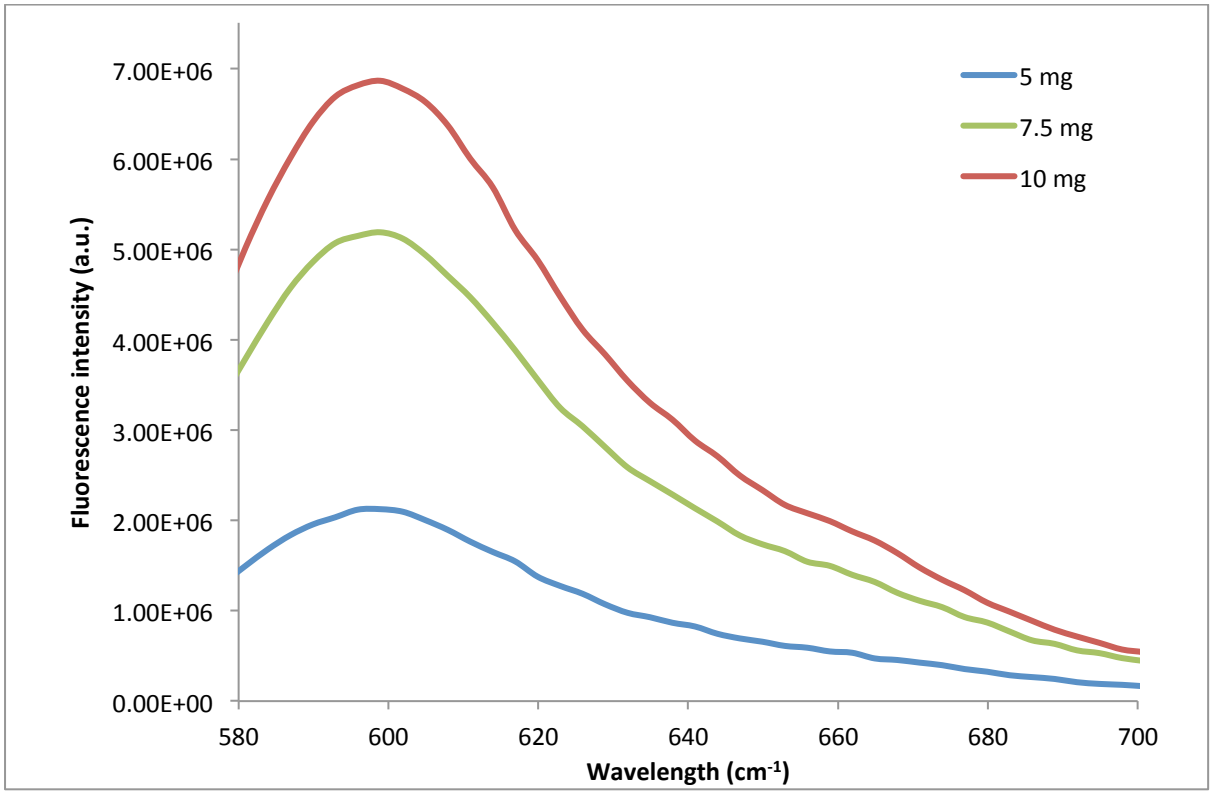

Figure 40: Emission spectra for 0.3 mg/mL of the three different dye-loaded NPs.

The emission intensity of the free dye was compared to that of the dye-doped NPs at an arbitrary concentration of 0.00008 mg/mL (of free dye) using the regression curves fitted to the data. The free dye emission was compared to the emission of the amount of dye-loaded NPs determined to contain a similar amount of dye as the arbitrary concentration chosen, as calculated based on the weight% of dye loaded to PSMA polymer during synthesis. The calculations are shown in Table 9. According to the calculations the 5 mg and 10 mg dye-loaded NPs did not show any signal enhancement above the signal generated by the corresponding free dye concentration, with enhancement factors (calculated as emission intensity of the NPs divided by the emission intensity of the free dye, as performed by Herz *et al*., 2009) below 1. The 7.5 mg dye-loaded NPs displayed a slight enhancement in signal above that of the free dye molecules at 1.1.

Table 9: Calculations to determine fluorescent emission enhancement factors for three different dye-loaded PSMI NPs.

Parameter	Free Dye	Dye-Loading		
		5 mg	7.5 mg	10 mg
Slope of regression curve	5.E+10	7.E+06	2.E+07	8.E+06
Regression curve constant	176 800	156 643	279 925	303 125
Free dye concentration (mg/mL)	0.00008			
Free dye emission (a.u.)	4.E+06			
Dye loading (w/w)		0.00025	0.00038	0.00050
Corresponding particle concentration (mg/mL)		0.32	0.21	0.16
NP Emission (a.u.)		2.E+06	5.E+06	2.E+06
Enhancement Factor (NP emission/Free dye concentration)		0.6	1.1	0.4

As mentioned in the Section 3.4.1.3 *Dye-loading variation and varying degrees of imidisation*, the dialyses water of the PSMI NPs directly after synthesis appeared clear when the PSMI NPs were loaded with 5 mg of dye, while the dialysis water of the 7.5 mg and the 10 mg loaded NPs appeared light pink. The drop in enhancement factor between that calculated for the 7.5 mg and the 10 mg dye-loaded NPs could thus be explained by an overestimation of the actual dye-content of the 10 mg dye-loaded NPs influencing the calculations. If one were to assume that approximately 90% (8 mg) of the 10 mg was successfully encapsulated, the dye-loading of the NPs would actually be only 0.04%, and the adjustments in the calculations would then result in a calculated enhancement factor of 0.5. If the same argument were to be applied to the 7.5 mg dye-loaded NPs, an actual encapsulation efficiency of 90% (6.75 mg actually encapsulated) would lead to a calculated enhancement factor of 1.2 instead of 1.1. Based on these calculations it could be concluded that for the synthesis of dye-loaded PSMI NPs a dye-loading at a point between 0.025% and

0.038% (w/w) represented the optimum dye-loading level, and that the encapsulation of the Exalite 613 dye into the PSMI NPs did result in a slight enhancement in fluorescence emission intensity (when compared to free dye emission) when loaded at a maximum weight% of 0.038%.

Chapter 4: Bioconjugation of dye-doped poly(styrene-*co*-maleimide) nanoparticles

4.1 Introduction: Bioconjugation to PSMI nanoparticle surfaces

Literature contains many examples of the attachment of antibodies and other protein-like structures to polymers and polymer scaffolds, including polymer particles (Napp *et al.,* 2011; Matsuya *et al.,* 2003; Qiu *et al.,* 2005) and electrospun scaffolds (Ignatova *et al.,* 2009; Stoilova *et al.,* 2010; Cloete *et al.,* 2011). According to Skottrup *et al.*, polymer-protein conjugation can be achieved either via passive adsorption, or through covalent attachment (Skottrup *et al.,* 2008).

Passive adsorption (simple incubation) is a simple and flexible technique with the adsorption primarily based on hydrophobic interactions, while covalent attachment is used when a stable and active product is required. This technique is more complicated than passive adsorption with the use of crosslinking agents and spacers to ensure active binding and minimised steric hindrance. Simple conjugation techniques however lead to heterogeneous products due to non-specific binding of the reactive groups to random amine residues, which can cause a significant reduction in bioavailability (Heredia & Maynard, 2007).

Antibodies have long been the staple of accurate biological detection, offering high levels of sensitivity and selectivity (Van Dorst *et al.,* 2010). The most commonly found type of antibody is the immunoglobulin G (IgG) y-shaped antibody oligomer. A schematic of an antibody and its different parts or fragments are given in Figure 41. Antibodies consist of two identical light chains and two identical heavy chains, joined by disulfide bonds in the hinge region (labelled 'H' in the figure). The antibody can be subdivided into 2 parts, namely the Fc fragment and the $F(ab')_2$ fragment, which in turn consists of 2 identical Fab′ fragments. The Fab′ fragments contain the antigen binding sites, shown in Figure 41 as Fv (variable fragment). The Fd fragment consists of the variable and constant chains of the heavy chain.

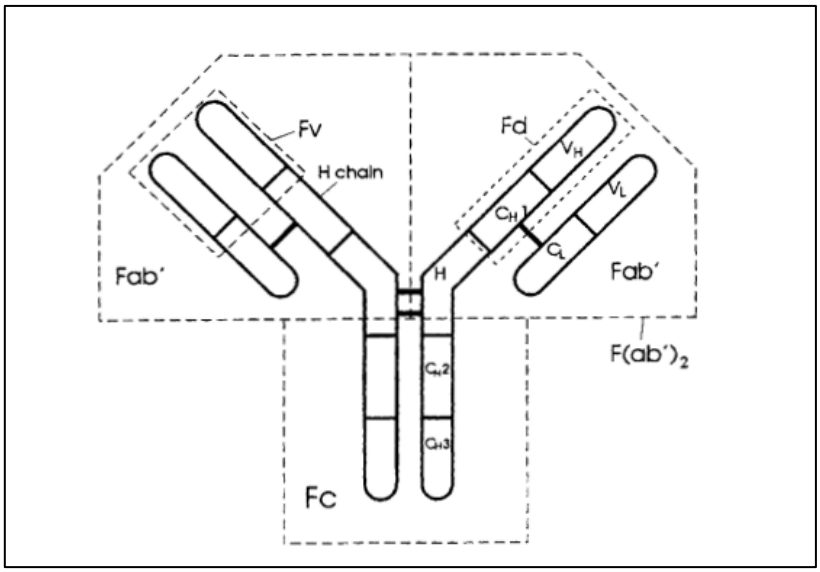

Figure 41: Schematic representation of antibody structure. Reproduced from (LU, B., SMYTH, M.R. and O'KENNEDY, R., 1996. Tutorial review. Oriented immobilisation of antibodies and its applications in immunoassays and immunosensors. *Analyst*, 121(3), pp. 29R-32R.) with permission of The Royal Society of Chemistry.

The attachment of antibodies to NPs (and any other substrate for that matter) must be conducted in such a way that the binding efficiency of the antibody is not compromised (or completely destroyed) through the attachment process. The Fv regions shown above must thus be exposed to the environment in order for antigen attachment to be possible, as shown in Figure 42.

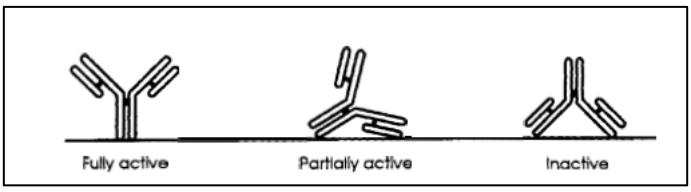

Figure 42: Schematic representation of ideal and non-ideal immobilisation of IgG antibody. Reproduced from (LU, B., SMYTH, M.R. and O'KENNEDY, R., 1996. Tutorial review. Oriented immobilisation of antibodies and its applications in immunoassays and immunosensors. *Analyst,* 121(3), pp. 29R-32R.) with permission of The Royal Society of Chemistry.

Cheng *et al.* (2009) covalently attached antibodies to the surface of amine-functionalised NPs using a combination of *N*-hydroxysuccinimide (NHS) and 1-ethyl-3-(3-dimethlyaminopropyl) carbodiimide (EDC). EDC is commonly used to couple or crosslink to carboxylic acids, while the inclusion of NHS creates a stable active ester intermediate that can conjugate to primary amines at neutral pH. In another study an *L*-Aspartic acid solution was used to impart amino and carboxyl groups on magnetic nanoparticle surfaces (Ravindranath *et al.,* 2009). The functionalised particles were then activated using an EDC/NHS solution, after which incubation with antibodies was performed. Carbodiimide chemistry was also utilised to attach proteins to the surfaces of commercially available latex NPs, prepared with COOH surface functional groups, in order to study specific sequences on single DNA molecules (Taylor *et al.,* 2000).

Cheng and colleagues also attached biotinylated antibodies to the amine-functionalised NP surfaces via the streptavidin-biotin binding mechanism (Cheng *et al.,* 2009). This well-known biotin-streptavidin or biotin-avidin conjugation technique is often used to immobilise antibodies onto substrates such as NPs while ensuring retention of the antibody activity. Avidin (and streptavidin, the non-glycosylated bacterial form of avidin) is an egg-white glycoprotein that binds to the vitamin biotin with very high affinity ($K_d = 10^{-15}\ M^{-1}$), forming a bond that is unaffected by pH and organic solvents (De Dios & Díaz-García, 2010). A schematic of the reactions that occur during EDC/NHS mediated binding of avidin to amine-functionalised NP surfaces is shown in Figure 43.

The efficiency of the avidin-biotin technique was shown when Cheng and colleagues (2009) found that the random attachment of antibodies achieved via the NHS/EDC activation was less effective at capturing *E. coli* than the antibody-nanoparticle conjugates prepared via the streptavidin-biotin route (Cheng *et al.,* 2009). The authors attributed this increased capturing efficiency to the streptavidin-biotin linkage that ensured the immobilisation of antibodies orientated with binding sites away from the NPs, thus enabling improved antibody activity (when compared to random attachment).

In 2012, Chen and colleagues utilised carboxyl-modified dye-doped SiO_2 NPs for the imaging of cancer cells (Chen *et al.,* 2012). The SiO_2 probes were bioconjugated with avidin via carbodiimide chemistry and incubated with biotinylated antibodies. Successful imaging of human lung carcinoma cells was achieved with the antibody-NP conjugates, compared to a control of NP-avidin conjugates.

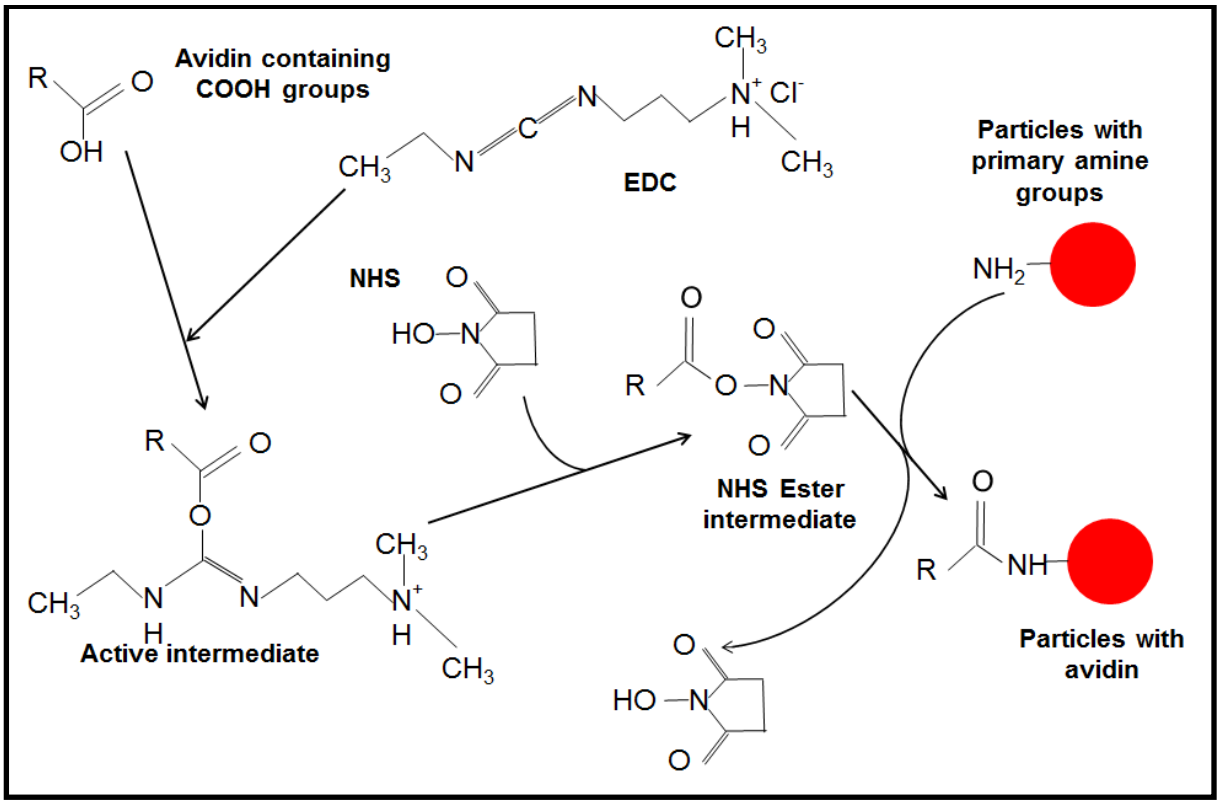

Figure 43: Chemical reactions occurring during carbodiimide chemistry for the attachment of avidin to amine-functionalised NPs.

There thus exist well-known protocols for the attachment of avidin or streptavidin to biotinylated antibodies onto NP surfaces by targeting either amine or carboxyl surface groups. However due to the high cost of streptavidin as compared to avidin, in many cases avidin-biotin binding is preferred. Streptavidin is obtained from the bacterium, *Streptomyces avidinii*, while avidin is (relatively easily) obtained via purification of chicken egg whites, hence the higher costs associated with streptavidin. Amide linkages between the amine groups functionalised onto the PSMI NP surfaces and carboxyl groups on the avidin

molecule can thus be introduced via the use of carbodiimide chemistry. Once avidin is successfully attached, simple incubation of the avidin-coated NPs and biotinylated antibodies should result in antibody conjugated NPs with a high degree of retained antibody activity due to orientated immobilisation of the antibodies onto the NPs.

Avidin quantification

Due to the widespread use of avidin in many fields of study, various methods exist for quantification of avidin. Of these methods, photometric or fluorometric methods are cheap to perform and relatively simple to use (Kada *et al.,* 1999a). These methods rely on compounds such as biotin-fluorescein conjugates with inherent fluorescence. When these compounds are contacted with avidin-containing solutions, the inherent fluorescence of the biotin-fluorescein conjugate is quenched due to the preferential binding between avidin and the biotin part of the conjugate.

In 2012, Chen and colleagues indirectly quantified the amount of avidin immobilised onto dye-doped SiO_2 NPs using a commercial biotin-fluorescein conjugate (Chen *et al.,* 2012). The supernatant separated from the conjugated NPs after avidin attachment was analysed, and with the use of an avidin standard curve, the concentration of avidin in the supernatant was determined (Chen *et al.,* 2012). By assuming that the fraction of avidin not present in the supernatant was immobilised onto the NPs, the percentage of total avidin added that was successfully immobilised onto the NP surfaces could be determined.

In this study a combination of the methods proposed by Kada *et al.,* (1999b) and Chen *et al.,* (2012) will be used in conjunction with a commercially available biotin(5-fluorescein) (B5F) conjugate in order to quantitatively describe the amount of avidin functionalised onto PSMI NP surfaces. Successful conjugation of antibodies onto the avidin-functionalised NPs can be confirmed via sandwich assays or imaging of NP-bound bacteria via fluorescence microscopy.

4.2 Experimental: PSMI nanoparticle bioconjugation

4.2.1 Materials and equipment

Bioconjugation and avidin quantification of the PSMI NPs was performed with the use of *N*-hydroxysuccinimide (NHS) (Aldrich), 1-ethyl-3-(3-dimethlyaminopropyl) carbodiimide (EDC) (Aldrich), bovine serum albumin (BSA) (Fluka), Tween 20 (Aldrich), trisma hydrochloride (Tris-HCl) (Aldrich), biotin(5-fluorescien) (Sigma), Rabbit anti *E. coli*:Biotin antibodies (AdB Serotec, distributed by Celtic Diagnostics in RSA) and avidin (from egg white, distributed by Life Technologies). A 10x phosphate buffered saline (PBS) stock solution at a concentration of 0.1 M was prepared by combining 1.71 M NaCl (Sigma), 0.03 M KCl (Fluka), 0.13 M Na_2HPO_4 (Fluka) and 0.02 M KH_2PO_4 (Fluka). The pH of the stock solution was adjusted to 7.4. This stock solution was diluted to a working concentration of 0.01 M or 1x PBS.

4.2.2 Bioconjugation of PSMI nanoparticles with avidin and biotinylated antibodies

Avidin attachment was performed as described by Cheng and colleagues (Cheng *et al*., 2009).

For every 3 mg equivalent NP mass the following was added:

- 2.3 mg EDC
- 5.2 mg NHS
- 6 mL PBS
- 37.5 µL of a 4 mg/ml avidin solution (avidin obtained from egg white)
- 40 µL of a 4 mg/ml Rabbit Anti-*E. coli* biotinylated antibody suspension

The EDC and NHS were dissolved in the 1x PBS, and the NPs and avidin added. The mixture was left to incubate for 24 hours at 37 ºC while being gently agitated. The particles were centrifuged at 24 276 x g for 10 minutes at 20 ºC to obtain a pellet of bioconjugated

NPs. The supernatant from this first centrifuging step was kept for analysis via a B5F assay. The particles were then washed once with a 0.05% Tween 20-PBS solution, and resuspended in a Tris-HCl BSA-Tween solution. The NPs were incubated for 1 hour at 25 ºC under gentle agitation. After incubation the NPs were washed and resuspended in PBS-Tween.

The specified amounts of biotinylated antibodies were added and incubated for 1 hour at 37 ºC under gentle agitation. The bioconjugated NPs were again separated via centrifuging, and washed once with 1x PBS-Tween and resuspended in 4.5 mL of 1x PBS-Tween with 10 mg/ml BSA.

4.2.3 Avidin quantification

Quantification of the immobilised avidin was performed according to the method given by (Chen *et al*., 2012) using the commercially available B5F assay. All data points in the assay were prepared in 1.5 ml volumes. For every assay an avidin standard was constructed with data points containing avidin concentrations ranging from 0 µg/mL to 2.2 µg/mL. A volume of 52.5 µL of a 1 µg/mL B5F solution was added to each data point. The composition of each data point is given in Table 10.

In order to determine the concentration of avidin in the sample supernatant, data points of increasing sample volume were constructed. To each of these data points, the same amount of B5F used for the avidin standard (52.5 µL of a 1 µg/mL solution) was added, and the volume of the data points were adjusted to a total of 1.5 mL by adding 1x PBS. Table 11 contains the composition for each individual data point in the supernatant titration assay.

A volume of 300 µL of each data point was placed into a 96-well black plate and analysed with a fluorescent plate reader (FL_x800, Bio-Tek Instruments Inc). The appropriate filters

were used to ensure excitation of the B5F at 490 nm and to detect the associated emission at 524 nm.

Table 10: Composition of data points for the avidin-biotin(5-fluorescein) standard curve.

Data Point ID: Avidin concentration (µg/mL)	Avidin [4 mg/mL] solution (µL)	B5F (µL)	1xPBS (µL)
0	0	52.5	1447.5
0.2	30	52.5	1417.5
0.4	60	52.5	1387.5
0.6	90	52.5	1357.5
0.8	120	52.5	1327.5
1	150	52.5	1297.5
1.2	180	52.5	1267.5
1.4	210	52.5	1237.5
1.6	240	52.5	1207.5
1.8	270	52.5	1177.5
2	300	52.5	1147.5
2.2	330	52.5	1117.5

Table 11: Composition of data points to determine the avidin concentration in a NP supernatant sample.

Data Point ID: Supernatant concentration (%)	Supernatant volume (µL)	B5F (µL)	1x PBS (µL)
0.25	3.75	52.5	1443.75
0.5	7.5	52.5	1440
1	15	52.5	1432.5
1.67	24.98	52.5	1422.53
5	75	52.5	1372.5
7.5	112.5	52.5	1335
10	150	52.5	1297.5
12.5	187.5	52.5	1260
15	225	52.5	1222.5
17.5	262.5	52.5	1185
20	300	52.5	1147.5
22.5	337.5	52.5	1110

The avidin standard curve generated using the sample compositions given in Table 10 was normalised according to the first data point that contained no avidin. This normalised standard curve would thus indicate the change in or quenching of fluorescence associated

with a specific avidin concentration. A linear regression line with descriptive equation was fitted to the linear part of the standard curve. The generated curve was used to correlate the amount of fluorescent quenching inflicted on a volume of B5F by a supernatant sample to an avidin concentration in that supernatant sample.

4.2.4 Bacteria detection via sandwich assays

Sandwich assays were performed to test the ability of the bioconjugated NPs to attach to their target bacteria, *E. coli*. The particle concentration used for a specific concentration of *E. coli* was also varied in order to determine the detection limit of the particles.

A 96-well black plate was coated overnight with a solution of *E. coli* K-12 bacteria at a concentration of $1x10^8$ cells/mL. The plate was washed three times with PBS, blocked with a 3% BSA-PBS solution, washed again with PBS three times and contacted with bioconjugated NPs. The NPs and bacteria were incubated for 1 hour, washed three times with PBS and the fluorescent intensity of the wells read with a fluorospectrometer reader.

A simplified schematic of the process is shown in Figure 44

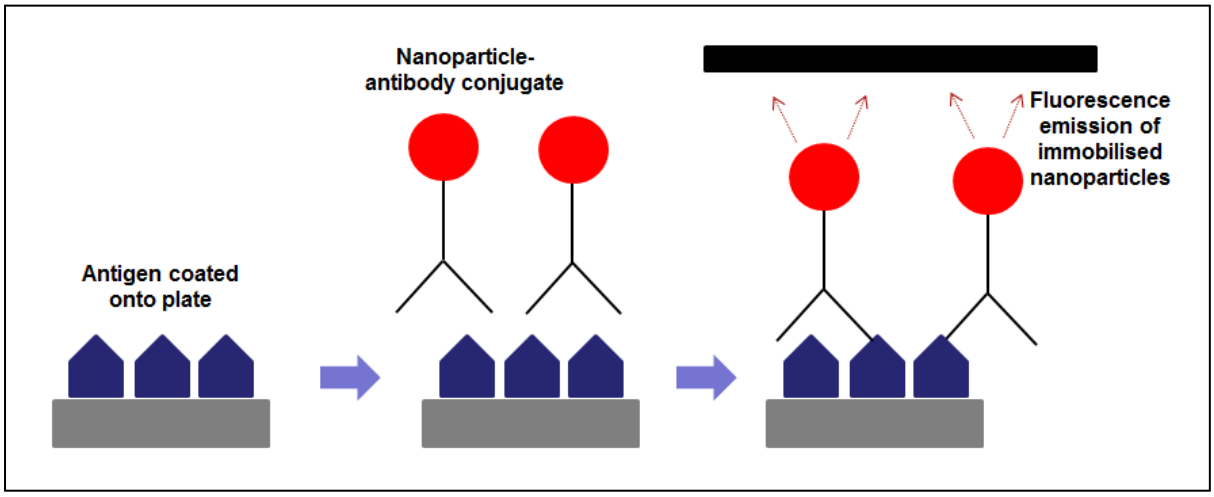

Figure 44: Schematic representation of the sandwich assay procedure.

4.2.5 Bacteria detection via centrifuge-based assays

Detection of bacteria via bioconjugated NPs was also tested via a centrifuge-based method as performed in (Zhao *et al*., 2004). Varying amounts of NPs were contacted with 500 µL of *E. coli* K-12 (in 1x PBS) solutions of various concentrations for 1 hour at 25 ºC under gentle agitation (400 rpm). The NP-bacteria suspensions were centrifuged with the intention of separating the NP-bound bacteria from free NPs. The NP-bound bacteria were washed once with PBS-Tween and resuspended in PBS-Tween for transfer in triplicate to a 96-well plate for analyses via the fluorospectrometer also used for the sandwich assays. Solutions of bacteria only were also added to the plate (at least three wells per bacteria concentration) to test whether bacteria by itself contributed to any signal generated. Initially positive NP controls were added, whereby the amount of NPs used for detection (or the minimum amount of NPs used when NP amounts were varied for detection of a single bacterial concentration) used was spun down at 21 500 x g for 10 minutes in order to collect all NPs, and resuspended in PBS-Tween for transfer to a 96-well plate, also in triplicate. Negative controls were also later included. These controls comprised of incubating NPs of similar amounts as used with bacteria (or the minimum amount of NPs used when NP amounts were varied for detection of a single bacterial concentration) incubated for an hour with 500 µL of PBS (similar to the volume of bacteria suspension used for the bacteria detection). The negative controls were then centrifuged, washed and resuspended in the same manner as with the NP-bound bacteria.

The supernatants obtained after the initial separation of NP-bound bacteria and free bacteria were also centrifuged at 21 500 x g for 10 minutes to recover any unbound NPs, and resuspended in 1x PBS for transfer to a 96-well black plate. Supernatant recovery was also performed for the negative control points.

Initially the NP-bound bacteria were centrifuged for 2100 x g at 10 minutes, as it was postulated that at such a low speed unbound NPs would not pellet, while bacteria are known to pellet at such relatively low speeds. Pelletisation of unbound NPs and loss of bacteria

required these initial centrifuging parameters to be altered to a speed of 24 276 x g for a period of 30 s for both the separation and wash steps. The fluorescent signals of the tests and controls were measured via a fluorospectrometer.

4.2.6 Fluorescence microscopy

Fluorescence microscopy was used to view the NPs bound to bacteria. Samples were prepared similarly to the method described in Section 4.2.5 *Bacteria detection via centrifuge-based assays*, *i.e*. incubation followed by separation and washing via centrifuging at 24 276 x g for 30 seconds. The samples were resuspended in 20 µL of 1x PBS for transfer to a microscope slide. The volumes of bacteria and NPs used were scaled down in order to present the entire sample on a single microscope slide. Bacteria solution volumes of 50 µL were incubated with a varying range of NP amounts of 0.67 mg/mL NP suspension. Controls of bacteria only and NPs contacted with PBS only were also included. A control of NPs plus PBS that was not centrifuged but vortexed and sonicated extensively was also included.

The slides were viewed via a fluorescence microscope (Olympus BX41, Olympus Microscopy, Essex, UK.) equipped with a 490 nm bandpass filter with a 510 nm cut-off filter for fluorescence emission.

4.3 Results and discussion

4.3.1 Bioconjugation and avidin quantification

Surface-functionalised PSMI NPs with lower degrees of imidisation, and with a dye loading of 5 mg, were bioconjugated to avidin according to the protocol described in Section 4.2.2 *Bioconjugation of PSMI nanoparticles with avidin and biotinylated antibodies.* The data points given in Table 10 and Table 11 were prepared and analysed with a plate reader.

The normalised avidin standard curve was calculated from the fluorescence intensity data and fitted with a linear regression equation, shown in Figure 45. The data points of the normalised standard curve were calculated by subtracting each data point from the point of maximum fluorescence *i.e.* the point at which only B5F is present. Each point thus represents the change/reduction in fluorescent intensity of this maximum point as caused by the corresponding concentration of avidin. The more avidin that is present, the more the inherent fluorescence of the B5F is quenched, hence the upwards trend present in Figure 45.

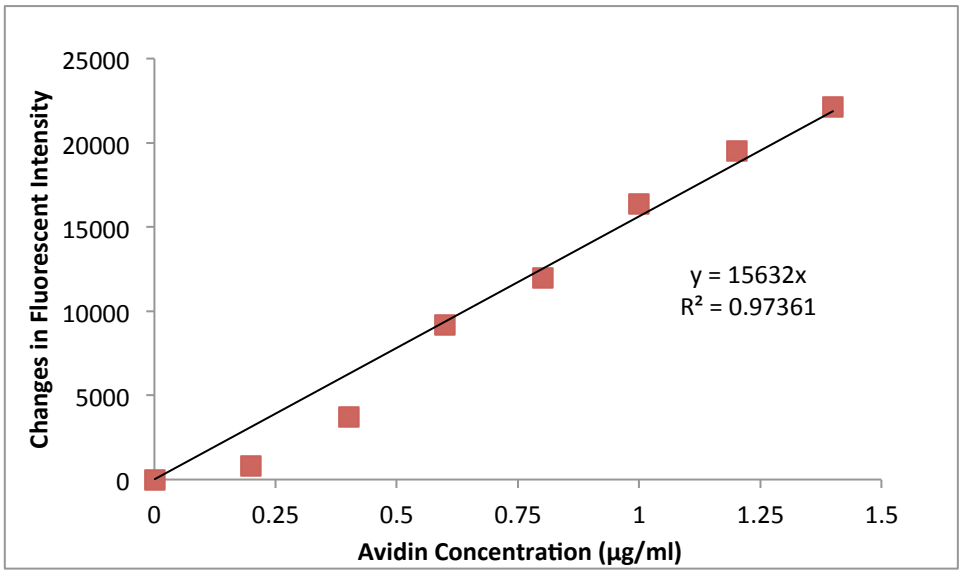

Figure 45: Normalised avidin standard curve reflecting the changes in fluorescent intensity of B5F as a result of varying avidin concentration.

The changes in fluorescent intensity with an increase in the supernatant sample concentration for supernatant samples of the 2C, 4C and 6C diamine-functionalised NPs are shown in Figure 46. PSMI NPs functionalized with formaldehyde only were also conjugated to avidin to act as control or baseline.

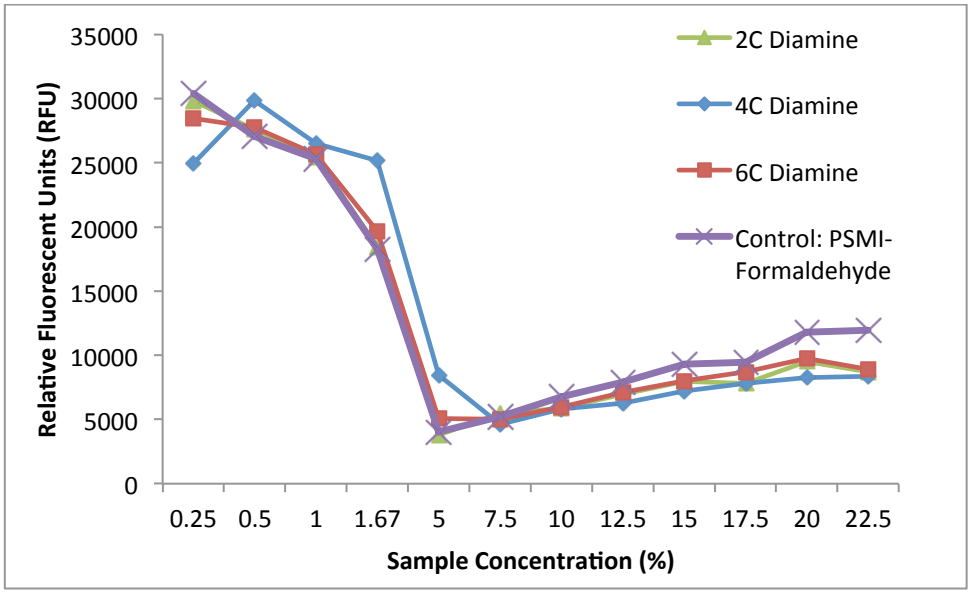

Figure 46: Effects of increasing supernatant sample concentration on the fluorescence intensity of B5F for avidin supernatant samples of 2C, 4C and 6C diamine-functionalised NPs compared to formaldehyde-functionalised NPs as control.

The fluorescence intensity decreases as the concentration of the supernatant sample is increased, until a minimum point is reached. A similar effect is seen with the control sample. These trends are similar to the published results shown in Figure 47, including slight increases in fluorescence intensity with increased sample concentration after the minima had been reached. In 1999, Kada and colleagues experimented with a biotin-fluorescein assay in order to quantify avidin in solution (Kada *et al.,* 1999b). Samples with variable (strept)avidin content were mixed with a set amount of biotin-fluorescein conjugate, and the fluorescence intensity monitored. A distinct 'breakthrough' or minimum point could be identified when plotting fluorescence intensity against (strept)avidin concentration, indicating

the point at which the set amount of biotin-fluorescein compound was effectively quenched, as shown in Figure 47 (Kada *et al.,* 1999b).

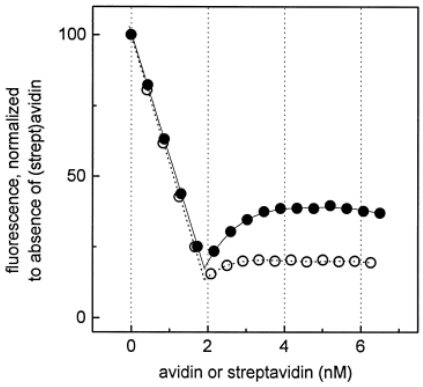

Fig. 1. Fluorescence quenching of biotin-4-fluorescein in the presence of avidin or streptavidin. Samples (1 ml) containing 8 nM biotin-4-fluorescein, 0.1 mg/ml of BSA, and the indicated concentrations of avidin (●) or streptavidin (○) were incubated for 30 min, and fluorescence was measured at 485 nm excitation (5 nm slit) and 525 nm emission wavelength (5 nm slit). The error bars were consistently smaller than symbol height and are omitted for clarity. Identical results were also obtained when using BSA precoating rather than inclusion of BSA in the assay buffer (data not shown).

Figure 47: Fluorescence quenching of biotin-4-fluorescein by (strept)avidin samples. Reprinted from Biochimica et Biophysica Acta (BBA)-General Subjects, 1427, KADA, G., KAISER, K., FALK, H. and GRUBER, H.J., Rapid estimation of avidin and streptavidin by fluorescence quenching or fluorescence polarization, pp. 44-48., , Copyright (1999), with permission from Elsevier.

The minima observed in Figure 46 were thus taken as the saturation points for the specific samples, *i.e*. at the respective minima the concentrations of avidin in the samples were sufficient to quench the specific amount of B5F conjugate added to the samples. The differences in fluorescence intensity between these minima and the fluorescence intensity of the specific amount of B5F conjugate with no sample added were then taken as the amounts of fluorescence quenching caused by avidin in the samples. The regression equation fitted to the normalised avidin standard was used to equate the amount of fluorescent quenching at the minima points to a concentration of avidin in the supernatants. The percentages of avidin that were retained in the supernatant after avidin conjugation to the NPs are given in Table 12. Sample calculations demonstrating how these values were obtained can be found in the appendix in Table 16.

From Table 12 it could be surmised that avidin conjugation was successful for the three variants of diamine-functionalised NPs, with all three types determined to have at least 93% of the initial avidin content successfully immobilised onto the NP surfaces.

The assay indicated that a similar level of avidin immobilisation was experienced by the control NPs functionalised only with formaldehyde. The assay was expanded to include another control sample consisting of pure PSMI NPs. The pure PSMI NPs were conjugated with avidin via the same protocol used for the diamine and formaldehyde-functionalised NPs and the supernatant analysed via a B5F assay.

Table 12: Avidin retained in the supernatant after bioconjugation to pure PSMI NPs (Control 1), formaldehdye-functionalised NPs (Control 2), and 2C, 4C and 6C diamine-functionalised NPs.

% Avidin in Supernatant				
Pure PSMI Control 1	**PSMI-Formaldehyde Control 2**	**PSMI-2C Diamine**	**PSMI-4C Diamine**	**PSMI-6C Diamine**
6.4	6.7	6.8	6.6	6.5

The added control of the supernatant of pure PSMI NPs also retained approximately 7% of the avidin added during bioconjugation, indicating that almost 93% of the avidin added to the pure PSMI NPs during bioconjugation was retained onto the NP surfaces.

These results at first thus seemed to indicate that there existed no need for surface functionalisation of the NPs for facilitation of bioconjugation. However upon further consideration, the possibility of passive adsorption of avidin onto the control NP surfaces was identified as a plausible explanation for the high degrees of avidin immobilisation onto the NP surfaces of the control samples. Passive adsorption is, as mentioned in the literature review in Section 4.1 *Introduction: Bioconjugation to PSMI nanoparticle surfaces*, a recognised and simple method for bioconjugation. This method however is characterised by low efficiency when compared to covalent bonding between functional groups.

Passive adsorption would also explain why the B5F assay showed comparable retention of avidin onto the pure PSMI NP surfaces compared to the formaldehyde-functionalised and diamine-functionalised surfaces. The increasing length of ligands introduced onto the NP

surfaces by the two steps of the surface-functionalisation method increased the steric hindrance experienced by molecules coming into contact with the NPs. In comparison, the unaltered surface area offered to the avidin molecules by the pure PSMI control NPs resulted in conditions more favourable to passive adsorption than what existed when bioconjugating to the altered surface areas of the functionalised NPs. When considering the number of wash steps involved in antibody conjugation and in any bacteria detection assay, it can be expected that the NPs bioconjugated via directed surface-functionalisation will better retain avidin and subsequently also biotinylated antibodies when compared to NPs where avidin was only passively adsorbed onto the NP surfaces.

In Section 3.4.1.3 *Dye-loading variation and varying degrees of imidisation*, FTIR analyses showed possible differences in the effectiveness of amine surface-functionalisation between PSMI NP suspensions of different dye-loadings, due to varying degrees of imidisation. It was postulated that increased amine-functionalisation would lead to more effective bioconjugation. In order to test the theory, PSMI NPs loaded with 5 mg, 7.5 mg and 10 mg, and functionalised with the 2C diamine, 4C diamine and the 6C diamine compounds, were bioconjugated with avidin and the residual avidin not retained on the NP surfaces determined via the B5F assay. The results are given in Table 13.

Table 13: Avidin retained in the supernatant after bioconjugation to 2C, 4C and 6C diamine-functionalised NPs with dye-loadings of 5 mg, 7.5 mg and 10 mg.

Diamine compound used for surface-functionalisation	% Avidin in Supernatant		
	5 mg	7.5 mg	10 mg
2C diamine	1.9	2.6	1.8
4C diamine	2.5	1.8	2.7
6C diamine	1.7	2.3	1.6

The results indicated no apparent differences in the effectiveness of avidin bioconjugation between the PSMI NPs of varied dye-loadings, as indicated by the similar amounts of avidin retained in the respective supernatants. The results shown in Table 13 were consistent with

those shown previously in Table 12 with regards to similar levels of avidin retention between PSMI NPs with similar dye-loadings but functionalised with different diamine compounds. Overall the results in Table 13 show more effective avidin bioconjugation to PSMI NPs, with between 1.5% and 2.8% of the total amount of avidin added to the NPs not retained on the NP surfaces, as opposed to the 6% to 7% of total avidin added not retained on the PSMI NPs analysed in Table 12. In order to provide a consistent baseline for comparison between the different dye-loaded NPs, NPs loaded with 5 mg of dye and surface-functionalised, similar to those analysed previously, were analysed again when analysing the 7.5 mg and the 10 mg dye-loaded NPs. The repeat analyses of the 5 mg dye-loaded NPs showed similar amounts of avidin retention to the amounts retained by the 7.5 mg and the 10 mg dye-loaded NPs. Due to the relative nature of the assay (measuring relative fluorescent units), and the possible variations that might exist with regards to NP size distribution (and thus surface area) and degree of surface-functionalisation achieved between samples of similar dye-loading and functionalised with the same diamine compound, some variation in the measured avidin retention between bioconjugated NP batches was to be expected.

It could however be concluded that the supposed variations in degree of imidisation between the NPs loaded with different amounts of dye did not affect the surface chemistry of the respective NPs to an extent that would influence bioconjugation of said NPs.

It could also be concluded that the PSMI NPs, irrespective of the diamine compound used for surface-functionalisation or the degree of imidisation achieved for the respective NP suspensions, could be expected to retain at least 94% to 98% of the avidin introduced during the bioconjugation process.

4.3.3 Bacteria detection and sensitivity limits

4.3.3.1 Sandwich assay

The efficiency of antibody attachment to the NPs, and the ability of the NPs to bind *E. coli*, was tested via a sandwich assay. The fluorescence intensity of an increasing concentration of NPs that were bound to a known concentration of *E. coli* ($1x10^8$ cells/mL) that was adsorbed onto the 96-well black plates, was measured and the results of an initial study are shown in Figure 48.

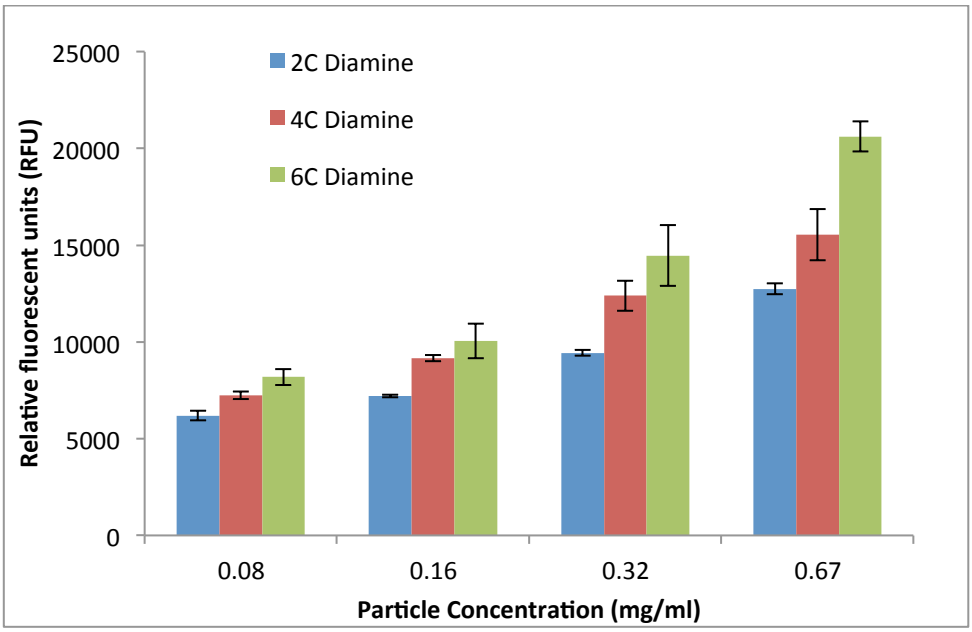

Figure 48: Changes in fluorescence intensity for increasing concentrations of dye-doped bioconjugated PSMI NPs contacted with $1x10^8$ cells/ml of *E. coli* K-12 as determined by sandwich assay.

A clear trend could be observed in Figure 48, showing increasing fluorescent intensity with increased particle concentration. This was taken as an indication that antibodies had been successfully immobilised onto the fluorescently doped NPs, and that these antibody-functionalised fluorescently doped NPs were effective in binding to the target *E. coli* coated onto the 96-well black plate.

Statistical analysis of the triplicate samples showed significant differences between the fluorescence intensities emitted by increasing particle concentrations for all 3 diamine

functionalised samples, except between the 0.32 mg/mL and the 0.67 mg/mL particle concentrations for the 4C diamine-functionalised sample (see Table 14).

Table 14: P-values as obtained by student's t-test comparing data points for each sample in the sandwich assay shown in Figure 48.

Comparison between data points	Different diamine-functionalised samples		
	2C	4C	6C
0.08 mg/mL vs. 0.16 mg/mL	0.015	0.006	0.033
0.16 mg/mL vs. 0.32 mg/mL	0.003	0.018	0.008
0.32 mg/mL vs. 0.67 mg/mL	0.003	0.112	0.006

When comparing the fluorescence intensities of the 3 different samples at the same particle concentration, it was found that the 4C and 6C diamine-functionalised NPs showed significantly higher fluorescent signals than the 2C diamine-functionalised NPs. The statistics also showed that no significant differences could be found between the 4C and 6C diamine-functionalised NPs, except at the highest particle concentration tested. The *P*-values supporting these observations are given in Table 15.

Table 15: P-values as obtained by student's t-test comparing different samples for each data point in the sandwich assay shown in Figure 48.

Comparison between different samples	Data points (mg/mL)			
	0.08	0.16	0.32	0.67
2C 4C	0.042	0.003	0.025	0.054
2C 6C	0.002	0.032	0.026	0.005
4C 6C	0.092	0.172	0.140	0.020

It could thus be concluded that although the avidin assay did not show large differences between the amount of avidin retained onto the three different functionalised NP types, the sandwich assay did show significant differences in bacterial attachment between the samples, most likely indicating an increased level/efficiency of antibody immobilisation onto the 4C and the 6C diaime-functionalised NPs compared to the 2C diamine-functionalised NPs.

The increasing trend in fluorescence intensity seen for all the samples also seemed to indicate that for the concentration of bacteria used for the experiment, namely $1x10^8$ cells/mL, the required amount of NPs for 100% detection and hence the saturation point had not yet been reached.

It was decided to repeat the assay with increasing particle concentrations (keeping the concentration of bacteria constant) of the three different functionalised NP types in order to determine the amount of NPs needed for maximum bacterial detection. It was also decided to include the controls of the avidin assays (the pure PSMI and the formaldehyde functionalised NPs) in the sandwich assay by conjugating these NPs with antibodies. If the comparatively high levels of avidin retention on these control NPs indicated by the avidin assays were due to passive adsorption, it would be expected that the antibody attachment to these NPs would be less efficient compared to that of the diamine-functionalised NPs. Subsequently bacteria capture would be less effective and lower fluorescence intensity would be detected compared to the signals generated by similar amounts of the diamine-functionalised NPs.

The initial sandwich method however proved not to be repeatable, as several following tests failed to deliver any type of fluorescence signal. This could possibly be attributed to the small surface area available per well in a 96-well plate that could possibly have complicated sufficient binding of bacteria onto the plates. The black plates required for the fluorescent assays also do not possess the high binding capacities found with transparent plates specifically used in ELISA type assays to ensure binding of reagents to the plate surface. Washing was performed manually, and thus the possibility of human error was introduced that is not found in automated washing systems used in dedicated molecular labs that subject plates and reagents to similar forces with every wash step. Eventually it was decided to replace the sandwich assay with a fluorescence assay based on centrifugation.

As mentioned previously, the initial sandwich assay suggested better bacteria detection with the 4C and the 6C diamine-functionalised NPs than with the 2C diamine-functionalised NPs. It was also noted that the 6C diamine NPs were more difficult to handle during bioconjugation, showing a higher prevalence for agglomeration than the 2C and 4C diamine-functionalised NPs. It was thus decided to focus on bioconjugation of the 4C diamine-functionalised NPs only, to focus the scope of the project as well as reduce the number of experiments that would require the use of expensive antibodies. Initial fluorescence microscopy images showed intense signals generated by the 5 mg dye-loaded NPs. It was thus decided to continue the initial bioconjugation with the 5 mg dye-loaded NPs instead of the 7.5 mg dye-loaded NPs in an effort to minimise possible background fluorescence.

4.3.3.2 Bacteria detection via centrifuge-based method

Bacteria detection was performed via a centrifuge based method. Initially a bacteria solution of a concentration of $1x10^6$ cells/mL was prepared and tested against the volume equivalents of 0.45 mg, 0.6 mg and 0.75 mg of bioconjugated NPs. The unbound NPs of each data point was also collected and analysed. This was achieved by collecting the supernatant decanted after the first centrifuge cycle into a separate Eppendorf tube, and centrifuging the supernatant at a speed and time (21 500 x g for 10 minutes) sufficient to concentrate any unbound NPs present. The concentrated NPs were then resuspended in 1x PBS and placed into a 96-well black plate for analyses. The experiment was also repeated for a bacteria concentration of $1x10^5$ cells/mL, with an extra data point for 0.3 mg of NPs included. The results are given in Figure 49.

As expected, the fluorescent signal increased with increased NP mass added as seen in Figure 49. The NP-bacteria signals were much higher than the signal of the bacteria only control point. The signals for the unbound NPs recovered from the supernatants in Figure 49a showed no definite trend, and very large spreads in the data. The unbound NPs recovered and shown in Figure 49b exhibited less spread between the three data points

Student's t-tests performed for the data in Figure 49a and Figure 49b indicated significant differences between the signal of the bacteria only control point and the signals generated when contacting the bacteria with 0.6 mg and 0.75 mg of NPs. Comparisons between the bacteria-only control and the 0.6 mg and the 0.75 mg data points contacted with $1x10^5$ cells/mL gave p-values of 0 and 0.033 respectively, while similar comparisons between the bacteria only control and the 0.6 mg and 0.75 mg data points contacted with $1x10^6$ cells/mL of bacteria gave p-values of 0.005 and 0.008 respectively. It was thus concluded that the NP detection limit for a 10^5 and 10^6 cells/mL bacteria solutions were 0.6 mg of NPs. It was decided to test 0.6 mg of NPs against solutions of different bacteria concentrations.

The results for 0.6 mg of NPs with volumes of $1x10^2$, $1x10^3$, $1x10^4$ and $1x10^5$ cells/mL bacteria solutions with corresponding bacteria-only controls as well as a positive NP control are given in Figure 50a.

Significant differences were found when comparing the 10^2, 10^3 and 10^5 bacteria-only control points with the data points representing 0.6 mg NPs contacted with the corresponding bacteria concentrations (*P*-values of 0.012, 0.009, 0.002 and 0.001 respectively). The supernatant signals for all of the data points were also quite high. It was decided to repeat the experiment, including a NP control consisting of 0.6 mg of NPs contacted with PBS only, incubated and centrifuged under similar conditions to those of the NPs contacted with bacteria. These results are shown in Figure 50b. Students *t*-tests indicated no significant differences between this new control and the data points consisting of NPs contacted with bacteria. The unbound NPs in the supernatants again indicated high signals, comparable or greater than those given when contacting NPs with bacteria. The spread of data of the triplicates used for each data point was quite big for the data presented in Figure 49 and Figure 50. These large spreads complicated the statistical analyses and most probably contributed to the failure to establish significant differences between NP controls and data points, especially in Figure 50.

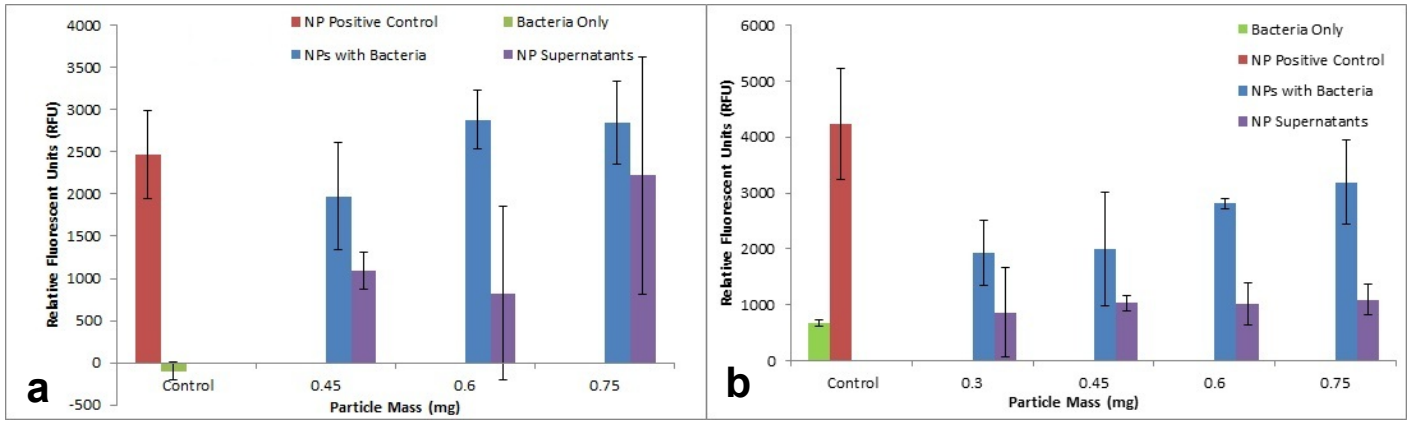

Figure 49: Detection limits of 5 mg dye-loaded 4C diamine-functionalised PSMI NPs of varying amounts against a bacterial concentration of a) $1x10^6$ cells/mL, b) $1x10^5$ cells/mL.

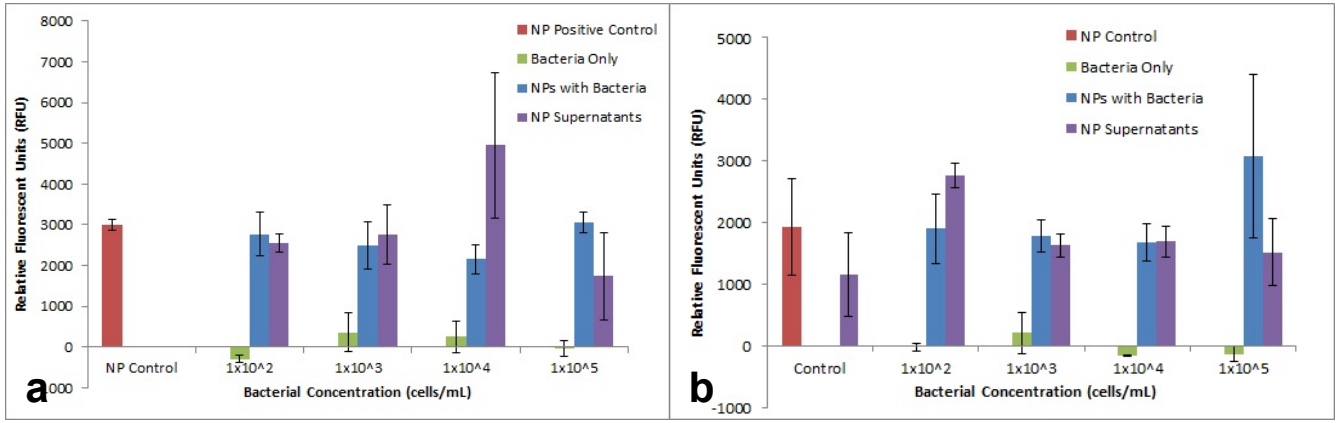

Figure 50: Detection limits of 0.6 mg of 5 mg dye-loaded 4C diamine-functionalised PSMI NPs against varying bacterial concentrations with a) a positive control and b) a negative control included.

It was decided to determine whether lower background signals could be achieved by altering the time and speed at which the NP bound bacteria were separated from unbound NPs. A published method was followed whereby the authors stated using a centrifuge time and a speed of 30 seconds at 24 276 x g to separate SiO_2 NPs of similar size as the PSMI NPs (Zhao *et al*., 2004).

The detection limit assay was repeated again, this time with 0.5 mg of NPs tested against bacteria concentrations between 10^2 and 10^5 cells/mL, while centrifuging at 24 276 x g for 30 seconds. A positive control (the entire mass of 0.5 mg centrifuged and resuspended for transfer to the 96-well plate) as well as a NP control (0.5 mg of NPs contacted with 1x PBS and treated similarly to the NP-bacteria samples) were included in the data set shown in Figure 51.

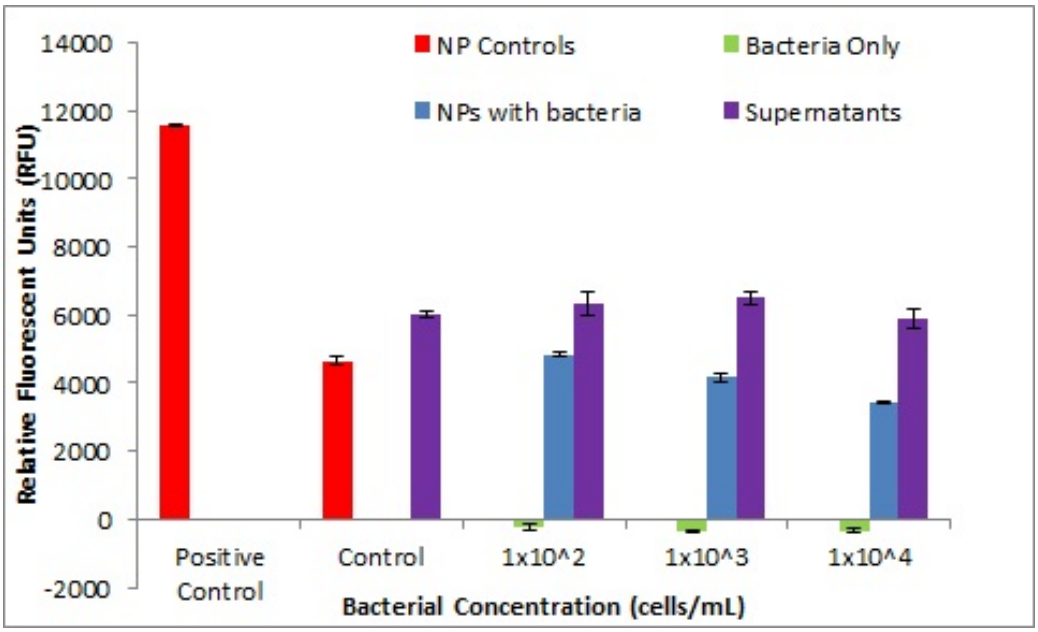

Figure 51: Detection limits of 0.5 mg of 5 mg dye-loaded 4C diamine-functionalised PSMI NPs against varying bacterial concentrations with a positive control and a negative control ('control') included.

The positive particle control showed a strong signal, while the data points in general showed less variation between the individual triplicate points than seen in Figure 49 and Figure 50.

The supernatants showed high intensity signals for all three bacteria concentrations tested, indicating high levels of unbound NPs.

The control consisting of NPs contacted with PBS and separated similarly to the bacteria-NP samples was still not significantly lower than the signals generated with NP-bound bacteria. Experimentation with various centrifuging times and speeds repeatedly facilitated the formation a visible pellet of unbound NPs. Zhao *et al*. (2004) originally published the centrifuge method as a means of separating unbound SiO_2 NPs from bacteria-NP conjugates, using NP with antibodies passively absorbed onto the NP surfaces. It was thus concluded that the avidin conjugated onto the PSMI NP surfaces (in order to facilitate directed antibody binding) caused an increase in the weight of the particles to such an extent that the difference in weight between bacteria-NP conjugates and unbound NPs was not sufficient to allow separation based on centrifuging.

4.3.3.3 Bacteria detection via fluorescence microscopy

Images of *E. coli* (not contacted with NPs) are given in Figure 52. Bright field emission of the bacteria showed the expected size and shape of *E. coli*, as seen in Figure 52a. The corresponding fluorescent image is shown in Figure 52b, and shows only a dark field, indicating that the bacteria did not fluoresce on their own.

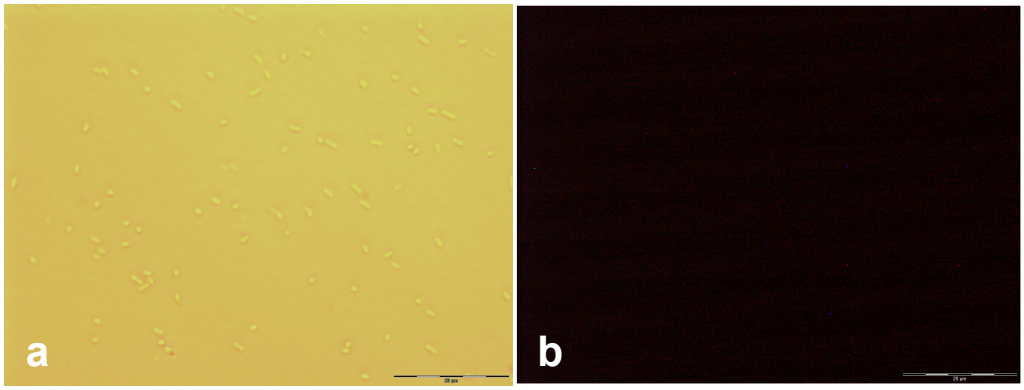

Figure 52: *E. coli* K-12 bacteria at a concentration of 1 X 10^8 cells/mL as viewed under a) bright field and the corresponding image shown under fluorescent filter b), at a magnification of 100X.

Fluorescence microscopy images were generated by contacting 50 µL of a range of bacteria concentrations with 0.06 mg of PSMI NPs. The results can be seen in Figure 53.

In Figure 53 a), b) and c) fluorescent dots could be observed similar in size and shape to bacteria. These dots also showed mobility when viewed directly under the microscope, indicating live bacteria. The control in Figure 53 d) showed NPs gathered in clumps. There was however no motion of these clumps when viewed directly under the microscope, indicating that the clumps consisted of NPs only and that the clustering of NPs were not due to bacteria being present in the control. Even though the control looks similar to the test images, differentiation between control and tests could be made based on evaluating the movement of the localised fluorescent dots as well as their shape and size, similarly to the interpretation of fluorescent images of dye-doped SiO_2 NPs attached to *Vibrio cholera* cells made by Thepwiwatjit *et al.* (2013).

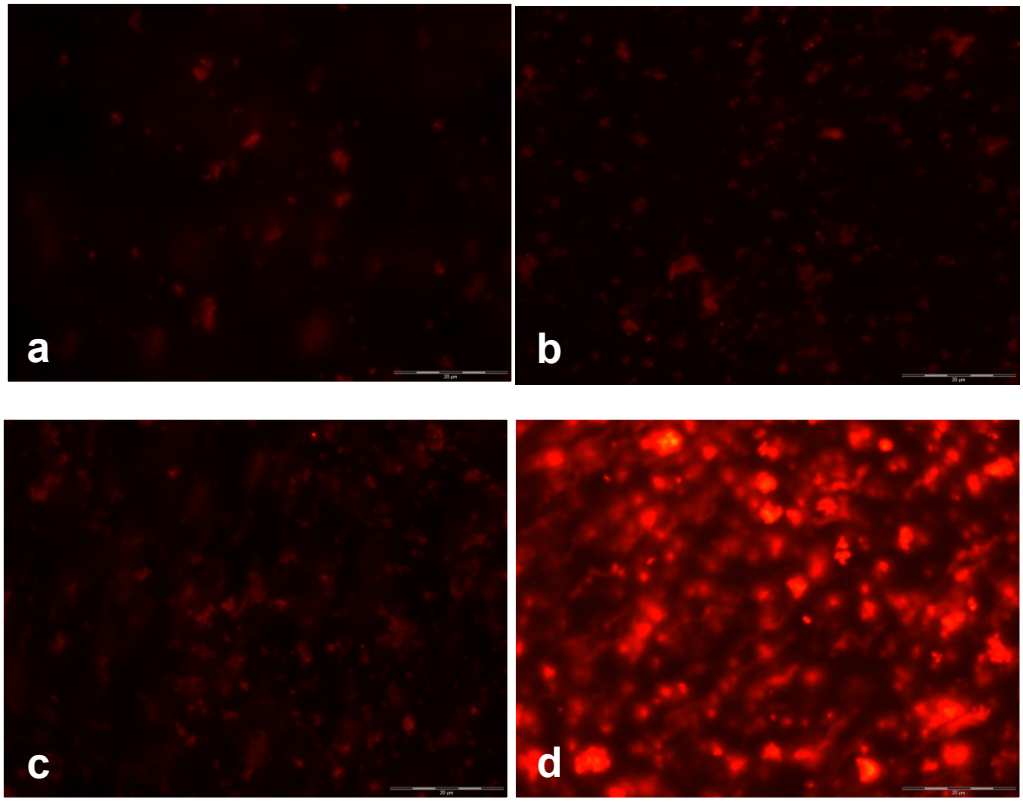

Figure 53: Fluorescence microscopy images of 0.06 mg PSMI NP dispersion contacted with 50 µl of a) a 1X10^2 cells/mL, b) a 1X10^3 cells/mL and c) a 1X10^4 cells/mL of *E. coli* K-12 bacteria, as well as d) NPs contacted only with PBS as a control and viewed at 100X magnification.

An additional control was prepared, consisting of PSMI NPs that were dispersed via sonication and vortexing, and not subjected to centrifuging. This meant that the entire control volume of 0.06 mg of NPs could not be concentrated into a smaller volume and that the resultant sample viewed under the fluorescence microscope would be at a lower concentration than the samples shown in Figure 53. The corresponding fluorescence image is shown in Figure 54.

A well-dispersed red fluorescence haze could be observed without any indication of localised increased signals. It could thus be argued that a well dispersed control was reliant on a sufficiently low NP concentration, and that the aggregation of particles in the control could be attributed to a particle concentration too excessive for the limited resuspension volume required for representative microscopy work.

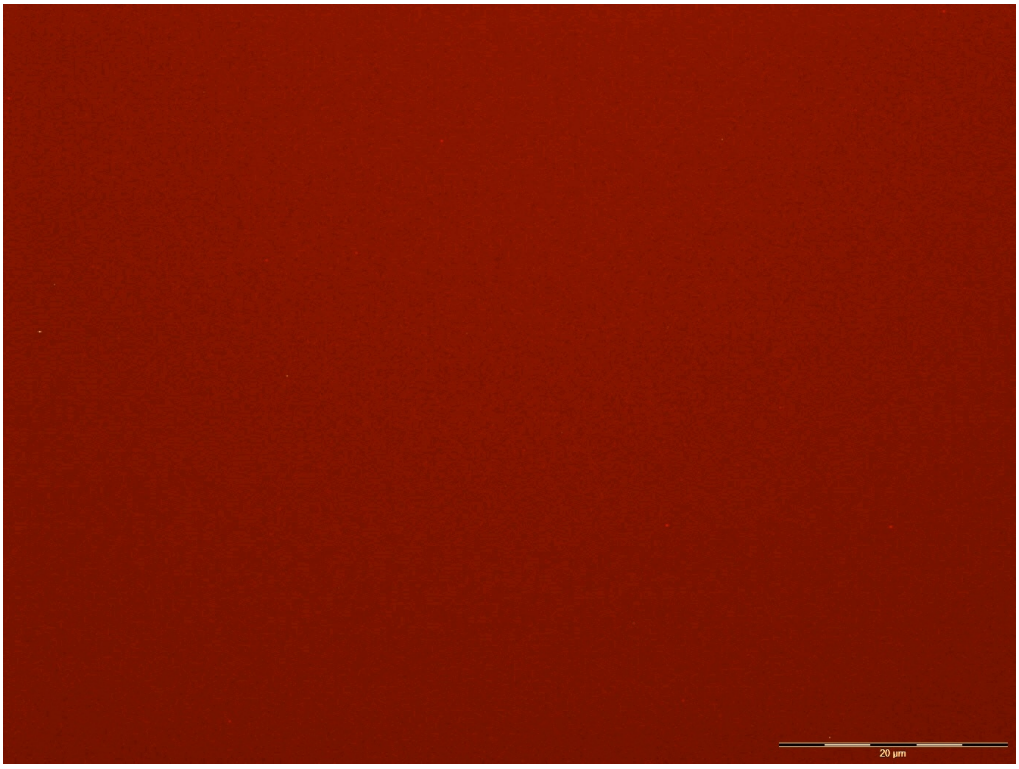

Figure 54: Fluorescence microscopy image of well-dispersed PSMI NPs viewed at 100X magnification.

The volume of bacteria used was increased from 50 µL to 1 mL and contacted with 0.06 mg, 0.04 mg, 0.03 mg and 0.02 mg NPs. Although general background haze could still be observed, localised increased signals in the shape and size of bacteria could be observed, as seen in Figure 55.

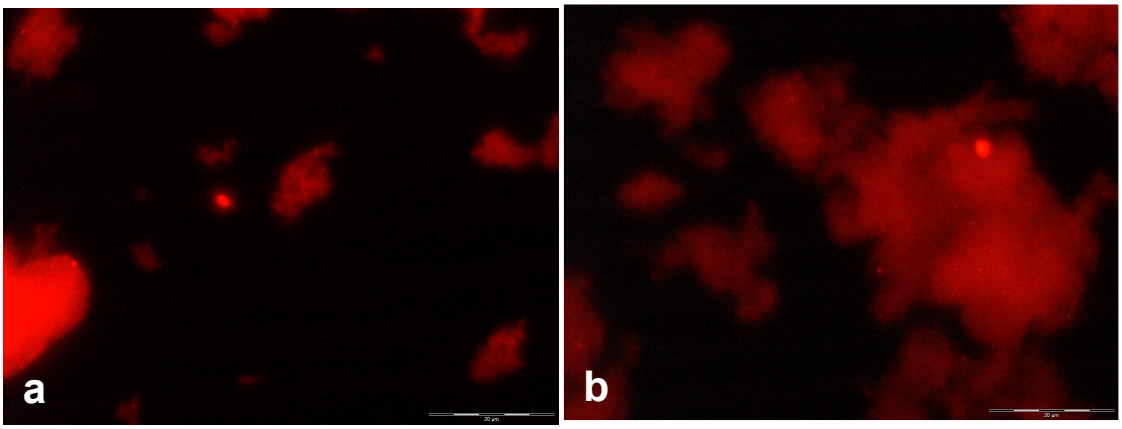

Figure 55: Fluorescent microscopy images showing increased localised fluorescent signals with background haze for a) 1X10^5 cells/mL contacted with 0.06 mg and b) 1X10^4 cells/mL contacted with 0.04 mg PSMI NPs viewed at 100X magnification.

In Figure 56 the localised fluorescent signal of what appeared to be two bacteria in close proximity to each other could be observed clearly with very little background signal seen.

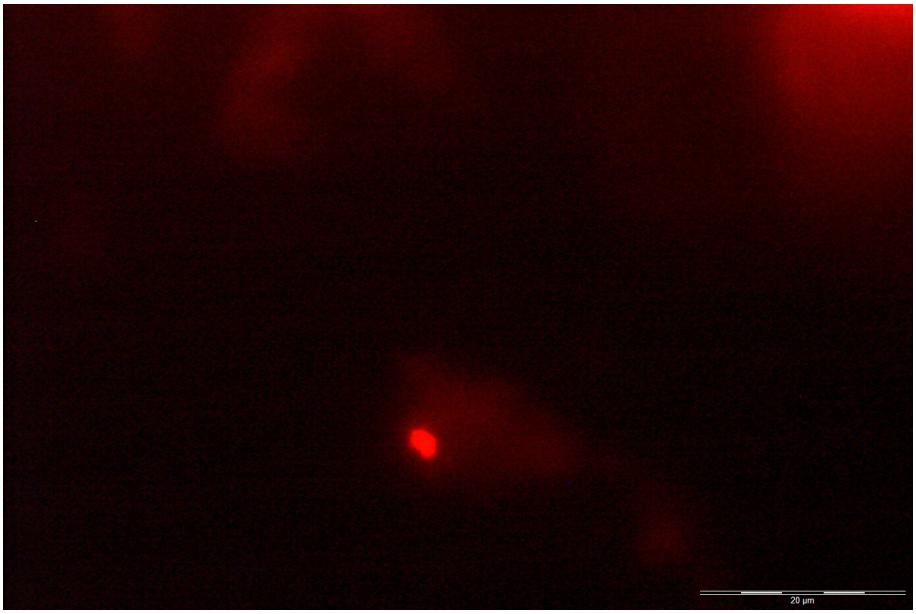

Figure 56: Fluorescent microscopy image of 1X10^5 cells/mL contacted with 0.06 mg PSMI NPs, showing localised fluorescent signal of what appeared to be two bacteria in close proximity to one another.

In Figure 57 a) and Figure 57 b) the fluorescent image and the corresponding image taken in bright field of 1X10^2 *E. coli* cells/mL contacted with 0.02 mg are shown. Bacteria visible in the bright field are encircled in red, and almost all of the bacteria encircled in red in Figure 57 b) can be seen highlighted by the dye-doped PSMI NPs in Figure 57 a). Not all of the bacteria highlighted in Figure 57 a) were accounted for in Figure 57 b), and the visible bacteria were also not in the exact same locations in the two images. This could be explained by the time taken to switch between bright field and fluorescent filters and the movement of the bacteria during that time. The images did illustrate that the PSMI NPs had a specific affinity for the bacteria, leading to the conclusion that antibodies had been successfully conjugated onto the NP surfaces. This then also proved that the concept of clustering of NPs around bacteria to cause a visible concentrated fluorescent signal could be performed using dye-doped bioconjugated PSMI NPs.

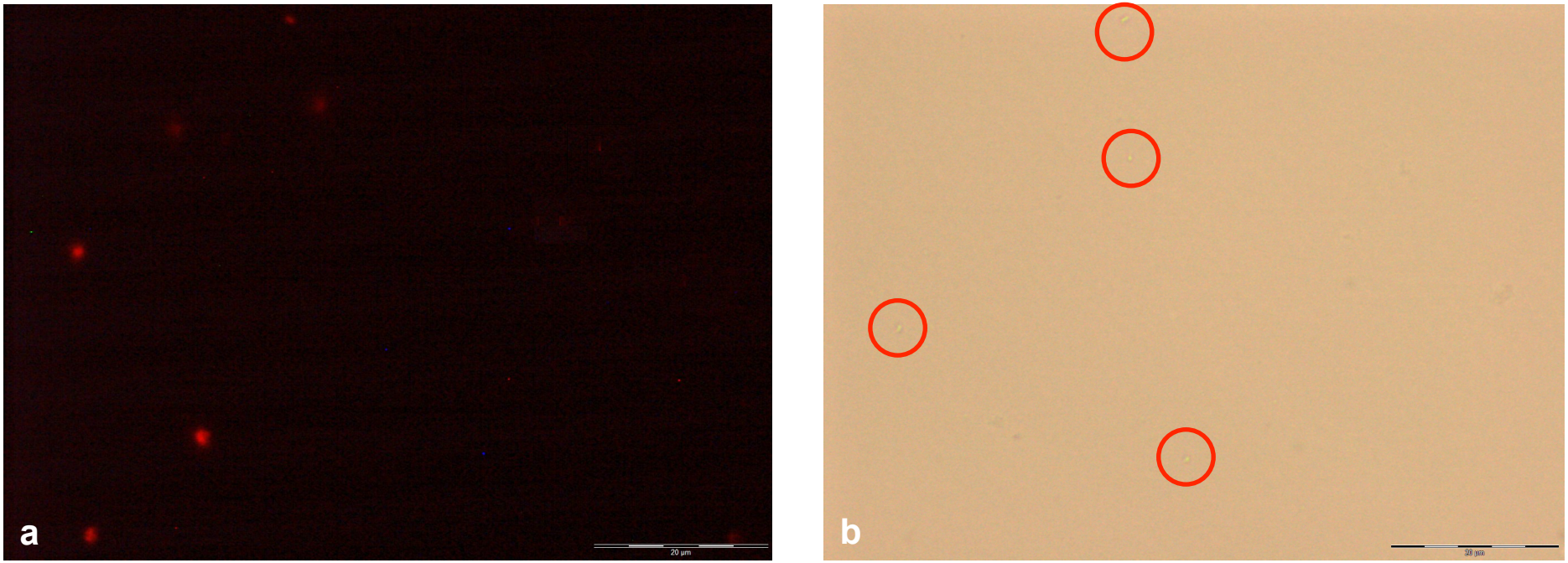

Figure 57: Fluorescent microscopy image of a) 1X10^2 cells/mL *E. coli* K-12 contacted with 0.02 mg PSMI NPs, showing localised fluorescent signals of bacteria, as well as b) the corresponding bright field image showing the bacteria responsible for the localised signal.

Chapter 5: Summary

Dye-doped PSMI NPs were functionalised and bioconjugated with avidin and biotinylated antibodies in order to develop a nanoprobe to detect *E. coli* in aqueous samples via signal amplification. The signal amplification caused by the dye-doped NPs eliminates the need for lengthy incubation periods associated with standard detection methods and enables rapid detection of *E. coli.*

The following conclusions could be made with regards to the synthesis, surface functionalisation and bioconjugation of dye-doped PSMI NPs:

From **Chapter 3** it could be concluded that PSMI NPs were successfully manufactured via imidisation of PSMA, as confirmed by FTIR analyses. Successful imidisation was concluded based on the appearance of imide characteristic peaks at 1709 cm^{-1}, 1345 cm^{-1} and 1177 cm^{-1}, coupled with the reduction of the anhydride peak at 1774 cm^{-1} and the disappearance of the characteristic anhydride peak at 1856 cm^{-1}. These observations were in accordance with what was found in literature (Samyn *et al*., 2010). Dye-doping of the PSMI NPs did not result in the appearance of any new characteristic FTIR peaks.

FTIR characterisation of formaldehyde and diamine surface-functionalised NPs indicated successful functionalisation based on the appearance (upon formaldehyde-functionalisation) and increase in intensity of (when functionalising with the diamine compounds) a characteristic peak at 1400 cm^{-1}, taken to be indicative of additional CH_2 linkages introduced onto the NPs after surface-functionalisation. Successful amine-functionalisation was characterised by the appearance of a characteristic peak at around 1555 cm^{-1} (seeing as primary N-H bending is characterised by peaks in the range between 1650 and 1580 cm^{-1}). FTIR analyses of PSMI NPs did not show significant differences in the degree of successful amine-functionalisation achieved when comparing NPs functionalised with three different diamine compounds of varying aliphatic chain lengths.

Variations in the molar excesses of formaldehyde and 2C, 4C and 6C diamine compounds used for surface-functionalisation did not indicate significant increases in amine surface-functionalisation when using higher molar excesses of the reagents. It could be concluded that as long as a sufficient excess of reagent was used to prevent crosslinking of the PSMI NPs, all possible reaction sites on the NPs would be saturated and that any increases in excesses of reagents would not be able to contribute to increased surface-functionalisation. The exact amounts of molar excesses to be used (as calculated based on the assumptions made in the appendix) would have to be determined for each batch of PSMI NPs synthesised as variations in particle size distributions between batches of NPs would influence the particle surface area available for functionalisation and thus also the amounts of reagents needed to saturate all possible surface sites.

The dye-loading of newly synthesised PSMI NPs was varied from 5 mg to include 7.5 mg and 10 mg of dye added per 20 g of PSMA to the particle formulation. Comparisons between the FTIR spectra of the initially synthesised and newly synthesised NPs showed increased intensity in the absorption region between 1560 cm^{-1} and 1510 cm^{-1} when compared to that of the 1710 cm^{-1} imide peak for especially the 7.5 mg and the 5 mg dye-loaded NPs. It was concluded that the increased absorption in this region was indicative of the formation of amic acid moieties at lower latex pH, as found by Samyn *et al*. (2010). Measurements of NP suspension pH values indicated a pH of around 7 for the initially synthesised dye-doped NPs. The newly synthesised 5 mg and 7.5 mg dye-loaded NP suspensions displayed lower pH values of around 6, with only the newly synthesised 10 mg dye-loaded NPs recording a pH value of around 7 similar to that of the initially synthesised NPs. Further comparisons between the FTIR absorption spectra showed that for the three newly synthesised PSMI samples, the 10 mg dye-loaded sample showed the lowest intensity in the absorption region between 1560 cm^{-1} and 1510 cm^{-1} with the 7.5 mg dye-loaded sample recording the highest intensity absorption in this region. Comparison of the intensities of the imide characteristic peaks at 1710 cm^{-1}, 1345 cm^{-1} and at 1177 cm^{-1} between the 3 samples showed that the 10

mg dye-loaded NPs displayed the highest absorption intensities, while the 7.5 mg dye-doped NPs recorded the lowest intensities for these characteristic peaks.

Based on the abovementioned FTIR information it can thus be concluded that the newly synthesised 5 mg and 7.5 mg dye-doped PSMI suspensions suffered from lower degrees of imidisation than the previously synthesised batches or the newly synthesised 10 mg dye-loaded NPs. The differences in imidisation could be attributed to deviations in reaction conditions (such as temperature or pressure regulation in the reactor) during synthesis of the individual batches.

Preliminary conclusions based on the FTIR data shown do seem to indicate that the 5 mg dye-loaded NP suspension display more functionalised amine groups to be used as handles for bioconjugation compared to the 7.5 mg and the 10 mg dye-loaded samples, based on increased absorption intensity in the primary amine absorption region between 1650 cm^{-1} and 1580 cm^{-1}. It was however difficult to conclude to what extent the differences in degree of imidisation between the different dye-loaded PSMI NP batches influenced the surface functionalisation of said PSMI NPs based on FTIR analysis alone.

TEM imaging of the initially synthesised NP batches showed the formation of regularly shaped particles with an average particle size estimated at between 20 and 50 nm. TEM imaging also showed no definite differences in size and morphology between pristine and dye-doped NPs, or between pure or surface-functionalised NPs. Imaging of the newly synthesised NPs suggested that the 7.5 mg dye-loaded NP suspension contained more irregularly shaped NPs than the 10 mg dye-loaded NPs, and it was assumed this could be attributed to the lower degree of imidisation achieved for the 7.5 mg dye-loaded NPs

Pristine PSMI NPs displayed highly negative zeta-potential measurements of approximately -68 mV, similar to what was reported in literature (Samyn *et al*., 2010). Similar zeta-potential values were recorded for dye-doped PSMI NPs. Zeta-potential measurements of diamine-functionalised PSMI NPs at in situ pH values showed decreases in the highly negatively

charge of PSMI NPs upon functionalisation to between -45 mV for the 2C diamine-functionalised PSMI NPs and -25 mV for the 6C diamine-functionalised NPs. The increasing reduction in negative zeta-potential with increasing chain length of compound used for amine surface-functionalisation could be explained by the differences in pKa values for the three diamine compounds. Analyses of the amine-functionalised NPs when resuspended in PBS buffer at an adjusted pH of 7.4 indicated that zeta-potential values of between -28 mV and -30 mV could be expected for the 2C, 4C and 6C diamine-functionalised NPs when suspended in PBS for bioconjugation. It was thus concluded that the surface-functionalised NPs would retain stability in suspension when bioconjugated.

A T_g of 179 °C for the pristine PSMI NPs was recorded via DSC analysis, and corresponded well with the T_g of 181 °C for PSMI NPs dried from aqueous suspension as reported by Samyn *et al*. (2010). The T_g for the initially synthesised dye-doped NPs was determined to be 183 ºC, similar to that of the pristine NPs. It could thus be concluded that dye-doping did not impact on the thermal properties of the NPs, and hence did not interfere with the imidisation process. T_g values measured for the newly synthesised dye-doped NPs varied between 175 ºC, 174 ºC and 183 ºC for the 5 mg, 7.5 mg and the 10 mg dye-loaded NPs respectively. The lower T_g values recorded for the 5 mg and the 7.5 mg dye-doped NPs than what was recorded for the initially synthesised samples supported the FTIR and pH results that indicated that these NP batches had not reached the same degrees of imidisation than the initial batches or the newly synthesised 10 mg dye-loaded NP batch.

Surface-functionalisation with formaldehyde increased the T_g of both the pristine and dye-doped NPs significantly ($p<0.05$) with between 7 and 11 degrees, for initially and newly synthesised NP batches. This could be explained by increased inter- and intramolecular interactions between the hydroxyl groups newly introduced to the NP surfaces. The increased T_g values of the NPs upon surface-functionalisation with formaldehyde could thus be taken as further proof of successful surface-functionalisation.

The increased T_g was maintained upon surface-functionalisation with the 2C and 4C diamine compounds. A significant decrease in T_g was observed upon surface-functionalisation of the pristine NPs with the 6C diamine compound from 191 ºC to 183 ºC. This decrease was attributed to the increased flexible aliphatic chain length introduced onto the NP surfaces via 6C diamine-functionalisation. Functionalisation of the newly synthesised 5 mg and 10 mg dye-doped NPs with the 6C diamine compound did not however result in reduced T_g values when compared to the corresponding formaldehyde-functionalised NPs. This could be as a result of fewer 6C diamine chains being functionalised onto the NP surfaces than for the pristine NPs.

The absorption and emission characteristics of Exalite 613 and the dye-doped PSMI NPs were measured via UV-Vis spectrophotometry and spectrofluorimetry. The free dye (dissolved in acetone) showed maximum absorption at 569 nm. The PSMI NPs doped with three different dye loadings all showed maximum emission at approximately 600 nm. Comparison of emission intensity between free dye molecules and dye-doped NPs indicated that the encapsulation of the Exalite 613 dye into the PSMI NPs did result in a slight enhancement in fluorescence emission intensity when loaded at a maximum weight% of 0.038% and when compared with the emission intensity of an equivalent amount of free dye. It was also concluded that for the synthesis of dye-loaded PSMI NPs a dye-loading of between 0.025% and 0.038% (w/w) represented the optimum dye-loading level.

The conclusions from **Chapter 4** were as follows:

Titration assays with biotin(5-fluorescein) showed that approximately 94% of the total avidin added initially was retained on the NP surfaces, independent of the diamine compound used for surface-functionalisation. This confirmed successful attachment of avidin to the particle surfaces (for both the control as well as the surface-functionalised NPs). The presence of residual avidin in the supernatant after avidin conjugation also indicated that the concentration of avidin added per mg of NPs was sufficient to saturate all the binding sites

available on the NPs. The avidin assays also showed a high level of passive adsorption of avidin onto the NPs, as indicated by the high retention of avidin onto the control NPs (pure NPs as well as formaldehyde-functionalised NPs).

Initial sandwich assay results indicated successful bacteria detection (and by implication successful antibody attachment to the NP surfaces), but could unfortunately not be repeated. An alternative centrifuge separation based assay was introduced. NPs contacted with bacteria showed significantly higher fluorescent signals than bacteria only controls, but no significant differences could be observed between NPs contacted with bacteria and the NP only controls. It was concluded that the addition of avidin onto the NP surfaces caused significant increases in the weight of the NPs, thus causing them to pellet at centrifuge settings at which pure NPs would not normally do, making the detection assay as described in literature not suitable for avidin functionalised NPs.

Fluorescence microscopy was utilised to demonstrate the utility of the bioconjugated dye-doped NPs in visualising (and thus detecting) *E. coli*. Localised fluorescent signals were generated when contacting *E. coli* K-12 with dye-doped PSMI NPs with similar sizes and shapes as that expected from *E. coli*. When switching between the fluorescent and bright field filters the bacteria labelled with fluorescent NPs could be distinguished in the bright field. This indicated that the NPs did bind successfully to the bacteria and in so doing created localised fluorescent signals.

The detection tests performed in this project were of a preliminary nature and used as a tool to provide proof of concept for the use of dye-doped PSMI NPs. Further development is still required in order to practically implement dye-doped PSMI NPs as a working detection method for *E. coli*.

Chapter 6: Outlook

Initial testing indicated the usefulness of dye-doped bioconjugated PSMI NPs for the visual detection of *E. coli* in aqueous suspensions. The dye-doped PSMI NPs are synthesised according to a simple method (when compared to dye-doped Si NPs) that can deliver large volumes of dye-doped NPs with reactive surfaces for functionalisation. The NPs, when kept in suspension, are easy to handle and retain stability during the proposed functionalisation process. At optimum dye loading the NPs provide enhanced emission intensity compared to what would have been suspected of the corresponding amounts of free dye molecules.

There are however additional points to be further investigated:

Firstly, consistency between NP batches should be ensured by better monitoring of the conditions in the reactor during imidisation. Characteristics such as suspension pH and T_g can also be routinely measured in order to quantify and/or compare the degree of imidisation achieved between different batches.

Variations in dye-loading of the PSMI NPs in small increments between a dye-loading of 5 mg and 7.5 mg should indicate the optimum dye-loading level associated with the current PSMI synthesis protocol.

As the pure PSMI NPs retained similar amounts of avidin onto the NP surfaces as the surface-functionalised NPs, investigation into the effectiveness of utilising pure PSMI NPs for bioconjugation and bacteria detection would verify if orientated bioconjugation via targeting of amine surface groups improved the efficacy of bioconjugation or not. This would require a quantitative or semi-quantitative detection method. As it was concluded that the centrifuge based assay for the determination of quantitative detection limits was not suitable for the NPs bioconjugated with avidin and biotinylated antibodies due to the increased weight of the NPs, an alternative detection method would have to be developed to accurately assess whether surface-functionalised NPs enable more efficient bioconjugation than pure PSMI NPs or not.

Additional sandwich assays could be performed using plates with larger wells to increase the surface area available for bacteria binding.

It could also be determined whether the centrifuge assay would be better suited to the NPs with antibodies passively absorbed onto the functionalised NP surfaces, without any avidin attached to the NPs.

Testing of *E. coli* with the dye-doped PSMI NPs also needs to be expanded to testing against samples containing other bacteria, e.g. *Salmonella,* in order to test the specificity of the NPs for *E. coli*. Testing with environmental water samples will also determine whether the NPs can function in sample matrices other than PBS.

References

ALLEN, D.J. and ISHIDA, H., 2006. Physical and mechanical properties of flexible polybenzoxazine resins: effect of aliphatic diamine chain length. *Journal of Applied Polymer Science,* **101**(5), pp. 2798-2809.

BAHADUR, K.C., SO, M.L., EUN, S.Y., JIN, H.C. and HAN, D.G., 2009. Glycoconjugated chitosan stabilised iron oxide nanoparticles as a multifunctional nanoprobe. *Materials Science and Engineering: C,* **29**(5), pp. 1668-1673.

BASCOMB, S., 1987. Enzyme tests in bacterial identification. *Methods in Microbiology*, **19**, pp. 105-160.

BEJ, A.K. STEFFAN, R.J., DICESARE, J., HAFF, L. & ATLAS, R.M., 1990. Detection of coliform bacteria in water by polymerase chain reaction and gene probes. *Applied and Environmental MIcrobiology*. **56**, pp. 307–314.

BITAR, A., AHMAD, N.M., FESSI, H. and ELAISSARI, A., 2012. Silica-based nanoparticles for biomedical applications. *Drug discovery today,* **17**(19–20), pp. 1147-1154.

BURTSCHER, C., FALL, P.A., WILDERER, P.A., WUERTZ, S., 1999. Detection of *Salmonella* spp. and *Listeria monocytogenes* in suspended organic waste by nucleic acid extraction and PCR. *Applied and Environmental MIcrobiology*. **65**, pp. 2235–2237.

BUSHON, R., BRADY, A., LIKIRDOPULOS, C. and CIREDDU, J., 2009. Rapid detection of Escherichia coli and enterococci in recreational water using an immunomagnetic separation/adenosine triphosphate technique. *Journal of Applied Microbiology,* **106**(2), pp. 432-441.

CAI, L., CHEN, Z., CHEN, M., TANG, H. and PANG, D., 2012. MUC-1 aptamer-conjugated dye-doped silica nanoparticles for MCF-7 cells detection. *Biomaterials,* **34**(2), pp. 371-381.

CHEN, Z., CAI, L., DONG, X., TANG, H. and PANG, D., 2012. Covalent conjugation of avidin with dye-doped silica nanopaticles and preparation of high density avidin nanoparticles as photostable bioprobes. *Biosensors and Bioelectronics,* **37**(1), pp. 75-81.

CHENG, Y., LIU, Y., HUANG, J., LI, K., ZHANG, W., XIAN, Y. and JIN, L., 2009. Combining biofunctional magnetic nanoparticles and ATP bioluminescence for rapid detection of Escherichia coli. *Talanta,* **77**(4), pp. 1332-1336.

CHILDRESS, E.S., ROBERTS, C.A., SHERWOOD, D.Y., LEGUYADER, C.L. and HARBRON, E.J., 2012. Ratiometric Fluorescence Detection of Mercury Ions in Water by Conjugated Polymer Nanoparticles *Analytical Chemistry,* **84**(3), pp. 1235-1239.

CLOETE, W.J. et al. 2011. *Facile immobilization of enzymes on electrospun poly(styrene-alt-maleic anhydride) nanofibres.* - The Royal Society of Chemistry. Available from: <-http://dx.doi.org/10.1039/C1PY00069A>.

COWLES, C.L., ZHU, X. and PAI, C., 2011. Using fluorescence measurement of zinc ions liberated from ZnS nanoparticle labels in bioassay for *Escherichia coli* O157: H7. *Journal of Nanoparticle Research,* **13**(10), pp. 5407-5413.

DE DIOS, A.S. and DÍAZ-GARCÍA, M.E., 2010. Multifunctional nanoparticles: analytical prospects. *Analytica Chimica Acta,* **666**(1), pp. 1-22.

DONATI, I. et al. 2002. - *Synthesis, Characterization, and Preliminary Biological Study of Glycoconjugates of Poly(styrene-co-maleic acid).* - American Chemical Society. Available from: <- http://dx.doi.org/10.1021/bm020018x>.

DÖRR, M., ZENTEL, R., DIETRICH, R., MEERHOLZ, K., BRÄUCHLE, C., WICHERN, J., ZIPPEL, S. and BOLDT, P., 1998. Reactions on Vinyl Isocyanate/Maleimide Copolymers: NLO-functionalized Polymers with High Glass Transitions for Nonlinear Optical Applications. *Macromolecules*, **31**, pp. 1454-1465.

DYER, M.A., OBERHOLTZER, J.A., MULLIGAN, D.C. and HANSON, W.P., 2009. New biosensors for food safety screening solutions, *Proc. of SPIE Vol,* 2009, pp73060G-1.

EDGAR, R., MCKINSTRY, M., HWANG, J., OPPENHEIM, A.B., FEKETE, R.A., GIULIAN, G., MERRIL, C., NAGASHIMA, K. and ADHYA, S., 2006. High-sensitivity bacterial detection using biotin-tagged phage and quantum-dot nanocomplexes. *Proceedings of the National Academy of Sciences of the United States of America,* **103**(13), pp. 4841-4845.

EL-BOUBBOU, K., GRUDEN, C. and HUANG, X., 2007. Magnetic glyco-nanoparticles: a unique tool for rapid pathogen detection, decontamination, and strain differentiation. *Journal of the American Chemical Society,* **129**(44), pp. 13392-13393.

FERNÁNDEZ-GARCÍA, M., CUERVO-RODRIGUEZ, R. and MADRUGA, E.L., 2000. Glass transition temperature of methyl methacrylate–ethyl α-benzoyloxymethylacrylate copolymers. *Polymer International,* **49**(4), pp. 377-381.

GENG, T., UKNALIS, J., TU, S. and BHUNIA, A.K., 2006. Fiber-optic biosensor employing Alexa-Fluor conjugated antibody for detection of *Escherichia coli* O157: H7 from ground beef in four hours. *Sensors,* **6**(8), pp. 796-807.

GODARD, M. and SAITER, J., 1998. Fragility and non-linearity in polymethyl(α-n-alkyl)acrylates. *Journal of Non-Crystalline Solids*, **235-237**, pp 635-639.

GOODRIDGE, L., CHEN, J. and GRIFFITHS, M., 1999. Development and characterization of a fluorescent-bacteriophage assay for detection of Escherichia coli O157: H7. *Applied and Environmental Microbiology,* **65**(4), pp. 1397-1404.

GRABOW, W.O.K & DU PREEZ, M., 1979. Comparison of m-Endo LES, MacConkey, and Teepol Media for Membrane Filtration Counting of Total Coliform Bacteria in Water. *Applied and Environmental Microbiology*, **38**(3), pp. 351-358.

HE, X., ZHOU, L., HE, D., WANG, K. and CAO, J., 2011. Rapid and ultrasensitive *E. coli* O157: H7 quantitation by combination of ligandmagnetic nanoparticles enrichment with fluorescent nanoparticles based two-color flow cytometry. *Analyst,* **136**(20), pp. 4183-4191.

HEREDIA, K.L. & MAYNARD, H.D. 2007. *Synthesis of protein-polymer conjugates.* - The Royal Society of Chemistry. Available from: <- http://dx.doi.org/10.1039/B612355D>.

HERZ, E., OW, H., BONNER, D., BURNS, A. & WIESNER, U., 2009. Dye structure-optical property correlations in near-infrared fluorescent core-shell silica nanoparticles. *Journal of Materials Chemistry*. Available from: <-http://dx.doi.org/10.1039/B902286D>.

HO, H.A., DORÉ, K., BOISSINOT, M., BERGERON, M.G., TANGUAY, R.M., BOUDREAU, D. and LECLERC, M., 2005. Direct Molecular Detection of Nucleic Acids by Fluorescence Signal Amplification. *Journal of the American Chemical Society,* **127**(36), pp. 12673-12676.

HOLZAPFEL, V., MUSYANOVYCH, A., LANDFESTER, K., LORENZ, M.R. and MAILÄNDER, V., 2005. Preparation of Fluorescent Carboxyl and Amino Functionalized Polystyrene Particles by Miniemulsion Polymerization as Markers for Cells. *Macromolecular Chemistry and Physics,* **206**(24), pp. 2440-2449.

HUANG, X., AGUILAR, Z.P., LI, H., LAI, W., WEI, H., XU, H. and XIONG, Y., 2013. Fluorescent Ru $(phen)_3^{2+}$-doped silica nanoparticles-based ICTS sensor for quantitative detection of enrofloxacin residues in chicken meat. *Analytical Chemistry,* **85**(10), pp. 5120-5128.

HUANG, Y.F., WANG, Y.F. and YAN, X.P., 2010. Amine-Functionalized Magnetic Nanoparticles for Rapid Capture and Removal of Bacterial Pathogens. *Environmental science & technology,* **44**(20), pp. 7908-7913.

IGNATOVA, M., STOILOVA, O., MANOLOVA, N., MITA, D.G., DIANO, N., NICOLUCCI, C. and RASHKOV, I., 2009. Electrospun microfibrous poly(styrene-alt-maleic anhydride)/poly(styrene-co-maleic anhydride) mats tailored for enzymatic remediation of waters polluted by endocrine disruptors. *European Polymer Journal,* **45**(9), pp. 2494-2504.

KADA, G., FALK, H. and GRUBER, H.J., 1999a. Accurate measurement of avidin and streptavidin in crude biofluids with a new, optimized biotin–fluorescein conjugate. *Biochimica et Biophysica Acta (BBA)-General Subjects,* **1427**(1), pp. 33-43.

KADA, G., KAISER, K., FALK, H. and GRUBER, H.J., 1999b. Rapid estimation of avidin and streptavidin by fluorescence quenching or fluorescence polarization. *Biochimica et Biophysica Acta (BBA)-General Subjects,* **1427**(1), pp. 44-48.

KELL, A.J., STEWART, G., RYAN, S., PEYTAVI, R., BOISSINOT, M., HULETSKY, A., BERGERON, M.G. and SIMARD, B., 2008. Vancomycin-modified nanoparticles for efficient targeting and preconcentration of Gram-positive and Gram-negative bacteria. *Acs Nano,* **2**(9), pp. 1777-1788.

KILIAN, M. & BULOW, P., 1976. Rapid diagnosis of Enterobacteriaceae:I. Detection of bacterial glycosidases. *Acta Pathologica et Microbiologica Scandinavica Section B,* **84**, pp 245–251.

KIM, G. and SON, A., 2010. Development and characterization of a magnetic bead-quantum dot nanoparticles based assay capable of< i> Escherichia coli</i> O157: H7 quantification. *Analytica Chimica Acta,* **677**(1), pp. 90-96.

KIM, G., WANG, X. and SON, A., 2011a. Inhibitor resistance and in situ capability of nanoparticle based gene quantification. *Journal of Environmental Monitoring,* **13**(5), pp. 1344-1350.

KIM, S., LU, L., CHUNG, J., LEE, K., LI, Y. and JUN, S., 2011b. A microwire sensor for rapid detection of Escherichia coli K-12 in fresh produce. *Innovative Food Science & Emerging Technologies,* **12**(4), pp. 617-622.

KUO, Y., WANG, Q., RUENGRUGLIKIT, C., YU, H. and HUANG, Q., 2008. Antibody-conjugated CdTe quantum dots for Escherichia coli detection. *The Journal of Physical Chemistry C,* **112**(13), pp. 4818-4824.

LANGE, R.F.M. and MEIJER, E.W., 1995. Supramolecular polymer interactions based on the alternating copolymer of styrene and maleimide. Macromolecules, **28**, pp. 782-783.

LARSEN, M.U., SEWARD, M., TRIPATHI, A. and SHAPLEY, N.C., 2009. Biocompatible nanoparticles trigger rapid bacteria clustering. *Biotechnology progress,* **25**(4), pp. 1094-1102.

LAZCKA, O., CAMPO, F. and MUNOZ, F.X., 2007. Pathogen detection: a perspective of traditional methods and biosensors. *Biosensors and Bioelectronics,* **22**(7), pp. 1205-1217.

LEE, J.Y. and DEININGER, R.A., 2004. Detection of *E. coli* in beach water within 1 hour using immunomagnetic separation and ATP bioluminescence. *Luminescence,* **19**(1), pp. 31-36.

LEE, C.M., GRIFFITH, J.F., KAISER, W. and JAY, J.A., 2010. Covalently linked immunomagnetic separation/adenosine triphosphate technique (Cov-IMS/ATP) enables rapid, in-field detection and quantification of *Escherichia coli* and *Enterococcus spp*. in freshwater and marine environments. *Journal of applied microbiology,* **109**(1), pp. 324-333.

LESKINEN, S.D., SCHLEMMER, S.M., KEARNS, E.A. and LIM, D.V., 2009. Detection of *E. coli O157: H7* in complex matrices under varying flow parameters with a robotic fluorometric assay system, *Proceedings of SPIE,* 2009, pp. 71670J.

LIN, Y.S., TSAI, P.J., WENG, M.F. and CHEN, Y.C., 2005. Affinity capture using vancomycin-bound magnetic nanoparticles for the MALDI-MS analysis of bacteria. *Analytical Chemistry,* **77**(6), pp. 1753-1760.

LIU, H., CAO, K., HUANG, Y., YAO, Z., LI, B. and HU, G., 2006. Kinetics and simulation of the imidisation of poly (styrene-co-maleic anhydride) with amines. *Journal of Applied Polymer Science*, **100**(4), pp. 2744-2749.

LU, B., SMYTH, M.R. and O'KENNEDY, R., 1996. Tutorial review. Oriented immobilization of antibodies and its applications in immunoassays and immunosensors. *Analyst,* **121**(3), pp. 29R-32R.

MANAFI, M., KNEIFEL, W. & BASCOMB, S., 1991. Fluorogenic and chromogenic substrates used in bacterial diagnostics. *Microbiological Reviews*, 55, pp. 335–348.

MATSUYA, T., TASHIRO, S., HOSHINO, N., SHIBATA, N., NAGASAKI, Y. and KATAOKA, K., 2003. A Core-Shell-Type Fluorescent Nanosphere Possessing Reactive Poly(ethylene glycol) Tethered Chains on the Surface for Zeptomole Detection of Protein in Time-Resolved Fluorometric Immunoassay *Analytical Chemistry,* **75**(22), pp. 6124-6132.

MAZUMDER, S., SARKAR, J., DEY, R., MITRA, M., MUKHERJEE, S. and DAS, G., 2010. Biofunctionalised quantum dots for sensing and identification of waterborne bacterial pathogens. *Journal of Experimental Nanoscience,* **5**(5), pp. 438-446.

MOSIER-BOSS, P., LIEBERMAN, S., ANDREWS, J., ROHWER, F., WEGLEY, L. and BREITBART, M., 2003. Use of fluorescently labeled phage in the detection and identification of bacterial species. *Applied Spectroscopy,* **57**(9), pp. 1138-1144.

NAPP, J., BEHNKE, T., FISCHER, L., WURTH, C., WOTTAWA, M., KATSCHINSKI, D.M., ALVES, F., RESCH-GENGER, U. and SCHAFERLING, M., 2011-last update, targeted luminescent near-infrared polymer-nanoprobes for in vivo imaging of tumor hypoxia - analytical chemistry (ACS publications) . Available: http://pubs.acs.org/doi/abs/10.1021/ac201870b?prevSearch=%2527polymer+nanoparticles%2527&searchHistoryKey= [12/10/2012, 2012].

NOBLE, R.T. and WEISBERG, S.B., 2005. A review of technologies for rapid detection of bacteria in recreational waters. *Journal of water and health,* **3**(4), pp. 381-392.

QIN, D., HE, X., WANG, K. and TAN, W., 2008. Using fluorescent nanoparticles and SYBR Green I based two-color flow cytometry to determine *Mycobacterium tuberculosis* avoiding false positives. *Biosensors and Bioelectronics,* **24**(4), pp. 626-631.

QIN, D., HE, X., WANG, K., ZHAO, X.J., TAN, W. and CHEN, J., 2007. Fluorescent nanoparticle-based indirect immunofluorescence microscopy for detection of Mycobacterium tuberculosis. *BioMed Research International,* **2007**.

QIU, G., ZHU, B. and XU, Y., 2005. α-Amylase immobilized by Fe_3O_4/poly(styrene-*co*-maleic anhydride) magnetic composite microspheres: Preparation and characterization. *Journal of Applied Polymer Science,* **95**(2), pp. 328-335.

RAVINDRANATH, S.P., MAUER, L.J., DEB-ROY, C. and IRUDAYARAJ, J., 2009. Biofunctionalized magnetic nanoparticle integrated mid-infrared pathogen sensor for food matrixes. *Analytical Chemistry,* **81**(8), pp. 2840-2846.

ROMPRÉ, A., SERVAIS, P., BAUDART, J., DE-ROUBIN, M.R. and LAURENT, P., 2002. Detection and enumeration of coliforms in drinking water: current methods and emerging approaches. *Journal of microbiological methods,* **49**(1), pp. 31-54.

SAHA, K., AGASTI, S.S., KIM, C., LI, X. and ROTELLO, V.M., 2012. Gold nanoparticles in chemical and biological sensing. *Chemical reviews,* **112**(5), pp. 2739-2779.

SAMYN, P., DECONINCK, M., SCHOUKENS, G., STANSSENS, D., VONCK, L. and VAN DEN ABBEELE, H., 2010. Synthesis and characterization of imidized poly(styrene-maleic anhydride) nanoparticles in stable aqueous dispersion. *Polymers for Advanced Technologies,* **23**(3), pp. 311-325.

SAUER, R., TURSHATOV, A., BALUSCHEV, S. and LANDFESTER, K., 2012. One-Pot Production of Fluorescent Surface-Labeled Polymeric Nanoparticles via Miniemulsion Polymerization with Bodipy Surfmers. *Macromolecules,* **45**(9), pp. 3787-3796.

SHAN, Z., WU, Q., WANG, X., ZHOU, Z., OAKES, K.D., ZHANG, X., HUANG, Q. and YANG, W., 2010. Bacteria capture, lysate clearance, and plasmid DNA extraction using pH-sensitive multifunctional magnetic nanoparticles. *Analytical Biochemistry,* **398**(1), pp. 120-122.

SKOTTRUP, P.D., NICOLAISEN, M. and JUSTESEN, A.F., 2008. Towards on-site pathogen detection using antibody-based sensors. *Biosensors and Bioelectronics,* **24**(3), pp. 339-348.

SOCRATES, G., 2001. Infrared and Raman characteristic group frequencies (3rd ed.). John Wiley & Sons, LTD.

SOTO, C.M., BLUM, A.S., VORA, G.J., LEBEDEV, N., MEADOR, C.E., WON, A.P., CHATTERJI, A., JOHNSON, J.E. and RATNA, B.R., 2006. Fluorescent Signal Amplification of Carbocyanine Dyes Using Engineered Viral Nanoparticles. *Journal of the American Chemical Society,* **128**(15), pp. 5184-5189.

STOILOVA, O., IGNATOVA, M., MANOLOVA, N., GODJEVARGOVA, T., MITA, D.G. and RASHKOV, I., 2010. Functionalized electrospun mats from styrene–maleic anhydride copolymers for immobilization of acetylcholinesterase. *European Polymer Journal,* **46**(10), pp. 1966-1974.

SUN, H., SCHARFF-POULSEN, A.M., GU, H. and ALMDAL, K., 2006. Synthesis and Characterization of Ratiometric, pH Sensing Nanoparticles with Covalently Attached Fluorescent Dyes. *Chemistry of Materials,* **18**(15), pp. 3381-3384.

TAYLOR, J.R., FANG, M.M. and NIE, S., 2000. Probing Specific Sequences on Single DNA Molecules with Bioconjugated Fluorescent Nanoparticles. *Analytical Chemistry,* **72**(9), pp. 1979-1986.

THEPWIWATJIT, N., THATTIYAPHONG, A., LIMSUWAN, P., TUITEMWONG, K. and TUITEMWONG, P., 2013. Antibody-Conjugated Rubpy Dye-Doped Silica Nanoparticles as Signal Amplification for Microscopic Detection of Vibrio cholerae O1. Journal of Nanomaterials. Available from: <- http://www.hindawi.com/journals/jnm/2013/274805/>

TSENG, Y., CHANG, H., CHEN, C., CHEN, C. and HUANG, C., 2011. Preparation of highly luminescent mannose–gold nanodots for detection and inhibition of growth of *Escherichia coli. Biosensors and Bioelectronics,* **27**(1), pp. 95-100.

USA. Environmental Protection Agency. Microbiological methods for monitoring the environment [document on the Internet]. Cincinatti: Environmental Monitoring and Suport Laboratory; 1978 [cited 2014 Nov 11]. Available from http://nepis.epa.gov/EPA/html/DLwait.htm.

VAN DORST, B., MEHTA, J., BEKAERT, K., ROUAH-MARTIN, E., DE COEN, W., DUBRUEL, P., BLUST, R. and ROBBENS, J., 2010. Recent advances in recognition elements of food and environmental biosensors: A review. *Biosensors and Bioelectronics,* **26**(4), pp. 1178-1194.

VIKESLAND, P.J. and WIGGINTON, K.R., 2010. Nanomaterial Enabled Biosensors for Pathogen Monitoring-A Review. *Environmental science & technology,* **44**(10), pp. 3656-3669.

WANG, X., DU, Y., LI, Y., LI, D. and SUN, R., 2011. Fluorescent identification and detection of Staphylococcus aureus with carboxymethyl chitosan/CdS quantum dots bioconjugates. *Journal of Biomaterials Science, Polymer Edition,* **22**(14), pp. 1881-1893.

XUE, X., PAN, J., XIE, H., WANG, J. and ZHANG, S., 2009. Fluorescence detection of total count of *Escherichia coli* and *Staphylococcus aureus* on water-soluble CdSe quantum dots coupled with bacteria. *Talanta,* **77**(5), pp. 1808-1813.

YANG, L., WU, L., ZHU, S., LONG, Y., HANG, W. and YAN, X., 2009. Rapid, absolute, and simultaneous quantification of specific pathogenic strain and total bacterial cells using an ultrasensitive dual-color flow cytometer. *Analytical Chemistry,* **82**(3), pp. 1109-1116.

YILUN LUO, NARTKER, S., WIEDERODER, M., MILLER, H., HOCHHALTER, D., DRZAL, L.T. and ALOCILJA, E.C., 2012. Novel Biosensor Based on Electrospun Nanofiber and Magnetic Nanoparticles for the Detection of *E. coli O157:H7*. *Nanotechnology, IEEE Transactions on,* **11**(4), pp. 676-681.

ZHANG, Z., ZHAO, M. and JIANG, Q., 2001. Glass transition thermodynamics of organic nanoparticles. *Physica B: Condensed Matter,* **293**(3), pp. 232-236.

ZHAO, Y., YE, M., CHAO, Q., JIA, N., GE, Y. and SHEN, H., 2008. Simultaneous detection of multifood-borne pathogenic bacteria based on functionalized quantum dots coupled with immunomagnetic separation in food samples. *Journal of Agricultural and Food Chemistry,* **57**(2), pp. 517-524.

ZHAO, X., HILLIARD, L.R., MECHERY, S.J., WANG, Y., BAGWE, R.P., JIN, S. and TAN, W., 2004. A rapid bioassay for single bacterial cell quantitation using bioconjugated nanoparticles. *Proceedings of the National Academy of Sciences of the United States of America,* **101**(42), pp. 15027-15032.

Appendix

1. Calculation of molar excesses for surface-functionalisation

The following assumptions were made when calculating the molar excesses of formaldehyde and diamine compound used for surface-functionalisation of the NPs:

1. A 100% conversion of maleic anhydride to maleimide groups is achieved. The SMA used to synthesise the NPs had a maleic anhydride content of 26%, and thus it was assumed that the NPs formed would have a 26 wt% maleimide content.

2. All of the maleimide groups formed would be available for surface-functionalisation. This is of course not true as only a certain percentage of the actual weight of PSMI formed would constitute the outer surfaces of the NPs. However, since molar excesses were required for reaction it was decided to use this assumption as it would represent the most conservative estimate to be made. If the economic viability of the process were to be investigated these assumptions would most likely be changed to assuming the availability of a percentage of the converted maleimide groups for surface-functionalisation.

Measured volumes of NP suspensions, after dialysis, were dried and the solid content was determined via drying and weighing the dried product. It was then assumed that 26% of this dried product represented maleimide groups available for functionalisation. The weight of maleimide was converted to a molar amount by using the molecular weight of maleimide (97.07 g/mol), and the amount of moles available for surface-functionalisation per ml of NP suspension was thus calculated. A certain volume of NP suspension thus equated a certain amount of moles of maleimide to be reacted with formaldehyde. An arbitrary molar excess of formaldehyde was chosen (that would be enough not to cause cross-linking) and this information, along with the moles of maleimide represented by a chosen volume of NP suspension, was used to determine the volume of formaldehyde solution required for functionalisation.

This process was repeated for the diamine-functionalisation step.

2. Sample Calculations for the determination of avidin content in NP supernatans after avidin conjugation

Table 16: Sample calculations for determining the percentage of avidin retained in NP supernatants after avidin conjugation.

	PSMI-Formaldehyde Control	PSMI-2C Diamine	PSMI-4C Diamine	PSMI-6C Diamine
1. Minimum on intensity graph	4 019	3 787	4 616	4 998
2. Max fluorescence intensity (no avidin)	30 305	30 305	30 305	30 305
3. Difference in fluorescence intensity **=(2-1)**	26 286	26 518	25 689	25 307
4. Regression coefficients				
i)slope	17 224	17 224	17 224	17 224
ii)constant	-1591.5	-1591.5	-1591.5	-1591.5
5. Avidin intercept (µg/ml) **=(3-4ii)/4i**	1.619	1.632	1.584	1.562
6. Total volume of supernatant (ml)	12	12	12	12
7. Avidin in supernatant (µg) **=5X6**	19.42	19.58	19.01	18.74
8. Total avidin added (mg)	0.3	0.3	0.3	0.3
9. % avidin in Supernatant **=7/1000/8X100**	6.47	6.53	6.34	6.25